3-11-2011

Tension-Compression Fatigue of Hi-Nicalon/SiC Ceramic Matrix Composite at 1200°C in Air and Steam

Tyler P. Jones

Follow this and additional works at: https://scholar.afit.edu/etd

Part of the Aerospace Engineering Commons

TENSION-COMPRESSION FATIGUE OF Hi-NICALON/SiC CERAMIC MATRIX COMPOSITE AT 1200 °C IN AIR AND IN STEAM

THESIS

Jones Tyler, 2nd Lieutenant, USAF
AFIT/GA/ENY/11-M09

**DEPARTMENT OF THE AIR FORCE
AIR UNIVERSITY**

AIR FORCE INSTITUTE OF TECHNOLOGY

Wright-Patterson Air Force Base, Ohio

AFIT/GA/ENY/11-M09

TENSION-COMPRESSION FATIGUE OF Hi-NICALON/SiC CERAMIC MATRIX COMPOSITE AT 1200 °C IN AIR AND IN STEAM

THESIS

Presented to the Faculty

Department of Aeronautics and Astronautics

Graduate School of Engineering and Management

Air Force Institute of Technology

Air University

Air Education and Training Command

In Partial Fulfillment of the Requirements for the

Degree of Master of Science in Astronautical Engineering

Tyler Jones, B.S.

2nd Lieutenant, USAF

March 2011

TENSION-COMPRESSION FATIGUE OF Hi-NICALON/SiC CERAMIC MATRIX

COMPOSITE AT 1200 °C IN AIR AND IN STEAM

Tyler Jones, B.S.

2nd Lieutenant USAF

Approved:

_____   _____

Marina Ruggles-Wrenn, PhD (Chairman)   Date

_____   _____

Geoff Fair, PhD (Member)   Date

_____   _____

Thomas Eason, PhD (Member)   Date

Abstract

The tension-compression fatigue of a Hi-Nicalon /Silicon Carbide ceramic matrix composite (CMC) was studied at 1200°C in laboratory air and in steam environment. The CMC investigated in this effort consisted of an oxidation inhibited HyprSiC matrix reinforced with laminated woven Hi-Nicalon fibers. Fiber preforms had pyrolytic carbon fiber coating with boron carbide overlay applied were then densified with the HyprSiC oxidation inhibited matrix through chemical vapor infiltration (CVI). The tensile stress-strain behavior was evaluated and the tensile properties measured at 1200°C. Tension-compression fatigue tests were conducted at a frequency of 1.0 Hz with a ratio of minimum stress to maximum stress of R = -1.0. Tension-compression fatigue behavior was studied for fatigue stresses ranging from 80 to 300 MPa in air and in steam. Fatigue run-out was defined as $2x10^5$ cycles. Fatigue limit (based on a run-out condition of $2x10^5$ cycles) was 80 MPa in air and in steam. The presence of steam decreased the fatigue life of specimens tested above the fatigue limit. Specimens that achieved fatigue run-out were subjected to tensile tests to failure to characterize the retained tensile properties. The material retained 100% of its tensile strength. Reduction in tensile modulus was 68% while the change in compressive modulus was negligible.

Acknowledgements

I would like to thank Captains Joseph Whalquist and Mike Knauf for taking time from their work to share their wisdom. I would also like to acknowledge Jay Anderson, Barry Page, and Sean Miller for their expertise in taming the laboratory equipment. Brian Crabtree provided the best machine shop support any student could ask for. Lieutenant Garrett Kurtz was a great lab partner and companion in our quest for CMCs knowledge. Of course I am extremely grateful for the guidance and mentoring provided by Dr. Marina Ruggles-Wrenn.

Table of Contents

List of Figures

List of Tables

EFFECTS OF TEMPERATURE AND STEAM ENVIRONMENT ON FULLY REVERSED FATIGUE BEHAVIOR OF SiC/SiC CERAMIC MATRIX COMPOSITE AT ELEVATED TEMPERATURE

Introduction

Future warfighter demands on aerospace platforms are outstripping the capabilities of current aircraft systems. The demand for aerospace vehicles that can fly faster, longer, higher, and on less fuel will not diminish. For example responsive strike aircraft should have twice the range at half the aircraft unit cost of current systems. Certain Unmanned Combat Air Vehicle (UCAV) concepts require 2.5 times the mission radius or 3 times the loiter time. For access to space, a fuel efficient, on-demand turbine engine accelerator up to Mach 4+ is required. Such capability does not exist today [1].

Weight savings in aerospace structures through the use of new materials is the most apparent advantage of new material development. There are also many synergistic effects that occur when stronger more resilient materials are incorporated in aerospace structures. Table 1 lists many of these incentives.

Table 1: Drivers for Improved Materials for Aerospace Applications [3].

• Weight Reduction	• Improved Performance
– increased range	– smoother, more aerodynamic form
– reduced fuel cost	– special aeroelastic properties
– higher pay load	– increased temperature capability
– increased maneuverability	– improved damage tolerance
• Reduced Acquisition Cost	– reduced detectability
– reduced fabrication cost	• Reduced Through-Life Support Cost
– improved "fly-to-buy" ratio	– resistance to fatigue and corrosion
– reduced assembly costs	– resistance to mechanical damage

An issue that is not addressed in Table 1 is the economic impacts of a new material. With the demands for less expensive and higher performing aerospace systems cost of new material development and integration cannot be ignored. These costs include procurement and life support cost. Therefore the benefits of weight savings must be balanced against cost. Table 2 gives a comparison of weight savings and cost impacts.

Table 2: Approximate Actual (US\$/Kg) Values of Saving One Unit of Weight [3].

• small civil \$80	• advanced fighter \$500
• civil helicopter \$80–\$200	• VTOL \$800
• military helicopter \$400	• SST \$1500
• large transport \$300	• Space Shuttle \$45,000
• large commercial \$500	

Aerospace propulsion systems must operate under severe environmental conditions such as high temperature, high pressure, and water vapor. Components used in propulsion systems are required to maintain mechanical properties while subject to the extreme environmental conditions. Improvements to gas-turbine efficiencies can reduce cost and provide weight savings to the aircraft system. The working fluid in the engine is "heated" by an internal combustion process,to keep engine space small, the intensity of combustion must be as high as possible. [8]. Much attention has been directed at using ceramic matrix composites (CMCs) in aerospace engines due to their high strength and fracture toughness at elevated temperatures. [17] Reductions on cooling requirements and higher engine operation temperatures are advantages of using CMCs in engine components. [8] With a higher intensity of combustion brought on by high combustion temperatures the length of the combustor and overall weight and complexity of the engine is reduced. While exposed to severe engine environments ceramic matrix composites

must maintain their structural integrity as well as long-term environmental durability. Characterization of the mechanical behavior of the CMCs in relevant engine environments is required before these materials can be used in aerospace structural applications.

II. Background

2.1 Ceramics Matrix Composites

A ceramic matrix composite (CMC) is a material that utilizes a ceramic continuous phase or matrix and a physically distinct reinforcement phase such as fibers, wiskers or particles. The reinforcement in any phase can be polymeric, metallic, or ceramic.

Advanced ceramic materials such as SiC, Al_2O_3 and Si_3N_4 have unusually high resistance to heat, chemicals, abrasion and wear. These very characteristics however, make them difficult to fabricate in a simple and economical way [6]. Figure 1 shows the comparative advantage of CMC's over other common materials used in aerospace applications [21]. While CMCs do not have the highest strength to weight ration they retain their properties at much greater temperatures than carbonfiber reinforced plastics or nickel based super alloys.
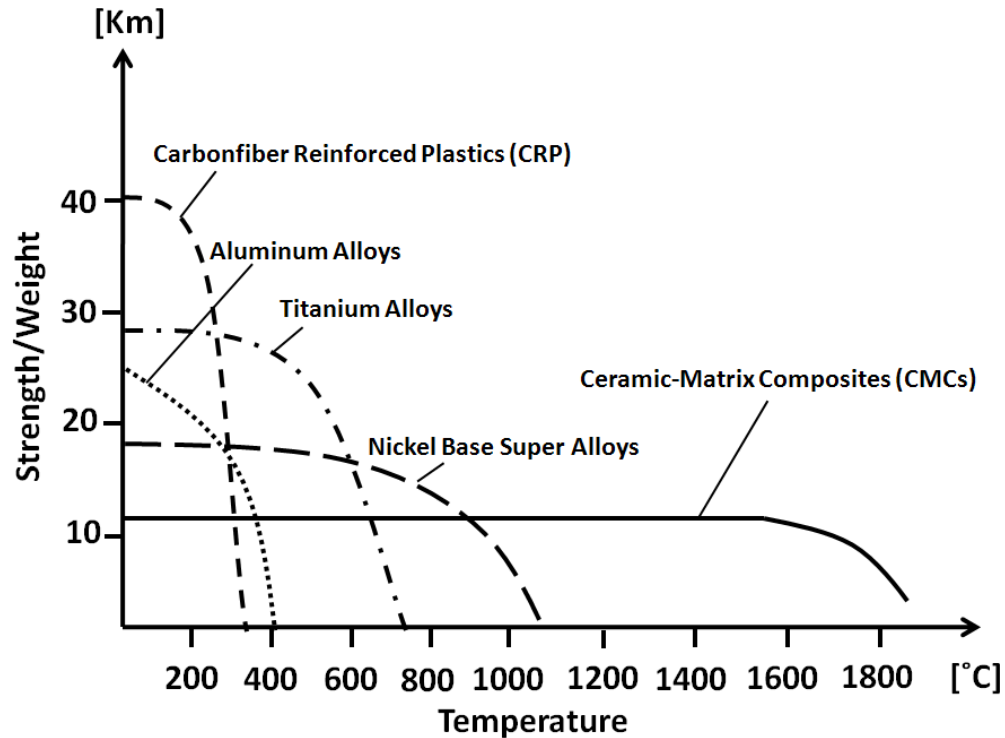
Figure 1: **Strength to weight ratio vs. operating temperature for various materials [21].**

Monolithic high performance ceramics combine some very desirable characteristics, e.g. high strength and hardness, excellent high-temperature capability, chemical inertness, wear resistance and low density. They are however, not very good under tensile and impact loading, and, unlike metals, they do not show any plasticity and are prone to catastrophic failure under mechanical or thermal loading (thermal shock) [6]. For this reason monolithic ceramics are not commonly used. So far, high-temperature ceramic structures have not proved sufficiently durable for practical use [8]. However CMCs offer superior toughness to monolithic ceramics. They exhibit tolerance to the presence of cracks and defects, and non-catastrophic modes of failure. This key advantage is achieved through a proper design of a fiber/matrix interphase, which serves to deflect matrix cracks and prevent early failures of the fibrous reinforcement [20,13].

5

This is achieved by decoupling the fibers from the matrix during cracking by   allowing gradual

load transfer to the fibers with the addition of a fiber matrix interphase.

A typical stress-strain curve and associated failure mechanisms are given for a CMC in

Figure 2. The difference in strong and weak matrix fiber interfaces is shown. Strong fiber matrix

bonds lead to premature failure compared to a weaker fiber matrix bond. In ceramic fiber

composites the failure strain of the reinforcing fiber ($\varepsilon \sim$ 1-1.5%) is much greater than that of the

matrix (0.1-0.2%). Therefore, under an applied tensile stress the matrix will always fail first [13].

The unreinforced ceramic matrix exhibits catastrophic brittle failure at low strain. The CMC

exhibits linear stress-strain until the matrix starts to crack. This initial matrix micro-cracking is

treated by the ACK theory of matrix strain enhancement [2]. ACK theory is derived from an

energy criterion where the fiber strength is large enough to support the load with a matrix crack

transversing the fibers.
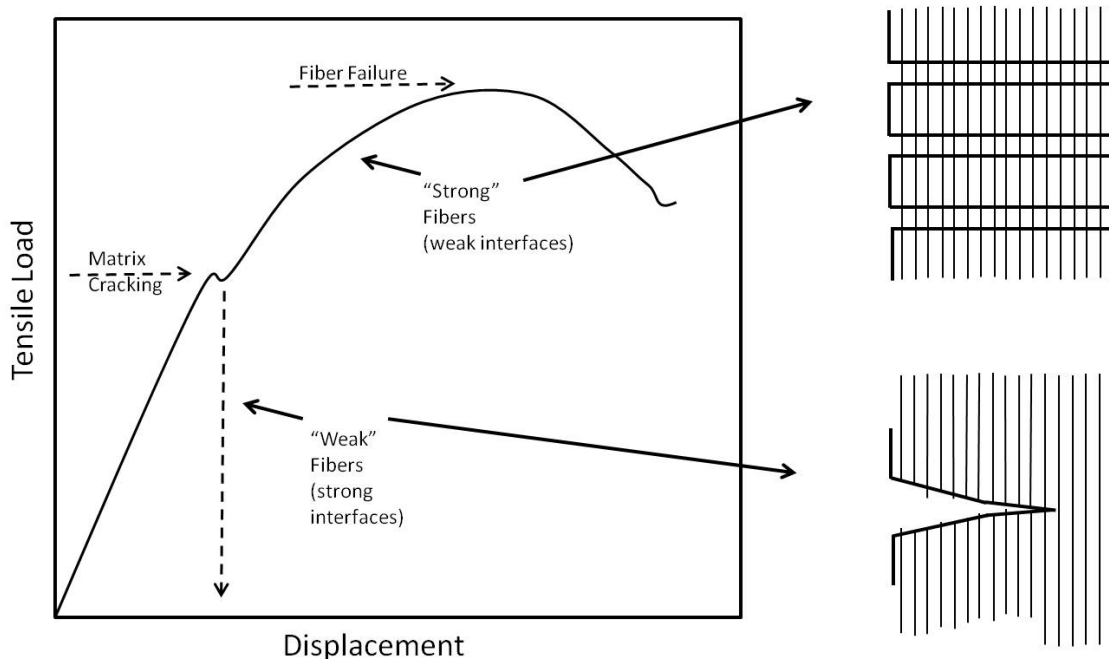
Figure 2: Tensile stress-strain curve for a "tough" ceramic matrix composite.

The carbon layer provides the weak interface necessary for fiber pullout and toughness. The fundamental problem is that in a high temperature thermostructural environment when the strain is higher than the proportional limit the air environment is permitted to penetrate to interfacial regions. This leads to (1) removal of the carbon rich interface, (2) oxidation of the fiber (increasing notch sensitivity), and (3) accelerated fiber-matrix bonding with associated return to brittle behavior. This phenomenon is commonly referred to as the oxidation embrittlement problem [13].

2.2 SiC/SiC Ceramic-Matrix Composites Prior Research

Previous research on the material tested in this effort at high temperature showed a reduction in fatigue life due to the presence of steam. In work done by Delapasse the same Hi-Nicalon/PyC/HyperSiC material was used. Tension-tension fatigue and tensile tests were performed at 1200°C. Fatigue testing was done in both laboratory air and steam enviriomnts at frequencies of 0.1Hz, 1.0Hz, and 10Hz with max stress ranging from 100-140 MPa. For testing at 1Hz the fatigue limit for both laboratory air and steam enviriements was 100 MPa (67% of UTS). Fatigued specimens exhibited strain ratcheting accompanied by strain accumulations of up to 2%. Specimens subjected to prior fatigue retained 42% and 59% of their ultimate tensile strength for air and steam environments respectively. Figure 3 shows accumulated strain vs. cycles and Figure 4 shows retained stress-strain properties for work done by Delapasse [7].
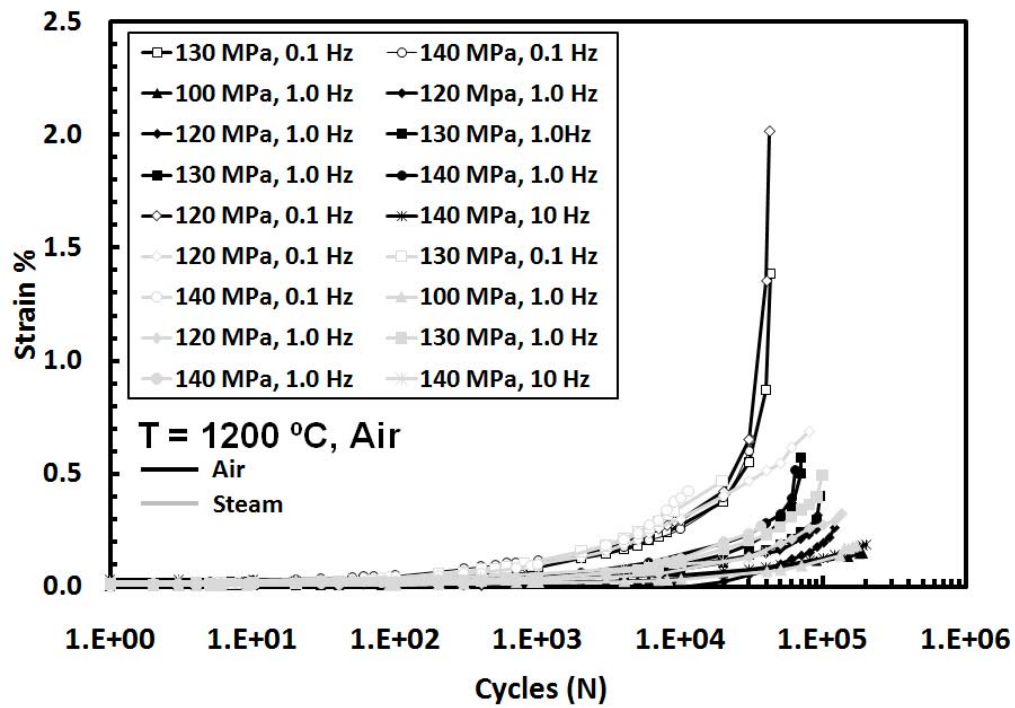
Figure 3: Accumulated strain vs. fatigue cycles for the Hi-Nicalon/PyC/HyprSiC ceramic composite at 1200°C in laboratory air and steam [7].
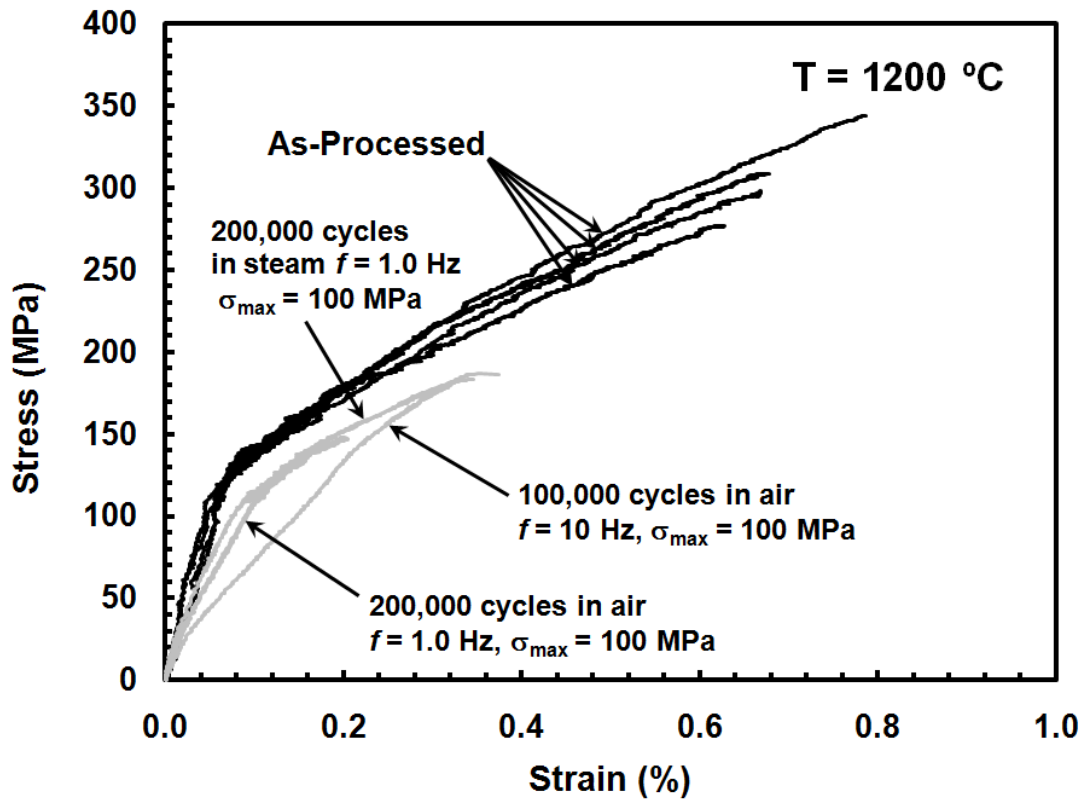
Figure 4: Tensile stress-strain curves obtained for the Hi-Nicalon/ PyC/HyprSiC specimens subjected to prior fatigue at 1200°C. Tensile stress-strain curves for the as-processed specimens are shown for comparison [7].

2.2 Tension-Compression Fatigue

Before extensive use of CMC's in gas turbine engine applications can occur, their response to the various loading and environmental conditions must be understood. Work has been done to investigate the tension-tension fatigue and tensile response at 1200°C in air and steam. However these are not the only load conditions experienced during nominal operation of gas turbine engines. Tension-compression fatigue loading is one such unique load. Work done by Rotem demonstrated that for meaningful fatigue conditions, the tension compression case is the dominant one [19]. Temperature and stress analysis of turbine sections showed that the surface of a gas turbine blade is subjected to a biaxial tensile-compressive fatigue loading during a start-

stop operation [16]. Further, the failure of a laminated composite under tension-compression fatigue is unique and cannot be predicted from a simple tension-tension or compression-compression fatigue test [19]. Tension-compression testing on a silicon carbide fiber-reinforced glass ceramic matrix SiC/1723 with a circular hole was investigated at room temperature by Mall. Compared to tension-tension or compression-compression testing at equal maximum stresses, the tension-compression cycling was found to considerably reduce fatigue life [12].

Tension-compressive fatigue is often investigated in polymeric materials through the use of a bend test. Brittle materials such as ceramics and glasses are frequently tested in flexure (three-point or four-point). Although flexure tests are easy to do, results generally do not reflect randomly occurring defects in highly stressed parts. In a bend test only a small material volume of the test piece experiences the maximum load. the strength values obtained from a bend test are considerably higher than those from a tensile test [6]. The effects of environmental attack on specimens tested in flexure fatigue cannot be accurately determined for the same reason. Load and test environment effects are best characterized by axial tension-compression fatigue.

The operating environment inside a gas turbine engine is characterized by high temperatures and the presence of oxidizing constituents such as steam. Effects such as increased oxidization embitterment due to the presence of steam have been shown to reduce the fatigue life of CMCs [7,15]. Below the point of matrix microcracking, ceramic composites are generally thought to exhibit no (or at least minimal) fatigue effects and environmental interaction and degredation [13,14]. Signifigant matrix cracking occurs at stress levels greater than the proportional limit for the ceramic composite in question. Previous work by Delapasse showed that tension-tension fatigue tests conducted at maximum stress levels below the proportional limit of 116 MPa did not demonstrate appreciable reductions in fatigue life.

III. Material and Test Specimen

3.1 Material

The SiC/SiC composite investigated in this research was manufactured by Hyper-Therm High-Temperature Composites, Inc., Huntington Beach CA. A HyprSiC oxidation inhibited matrix was reinforced with woven Hi-Nicalon fiber performs by chemical vapor infiltraion (CVI). Three 5.0 mm thick panels were supplied for this effort. Each panel consisted of 12 plies of 8 harness satin weave (8HSW) laid-up symmetric about the mid-plane with warp and fill plies alternated. To toughen the CMC by promoting weak interfaces a pyrolytic carbon (~0.40μm) with boron carbide (~1.0μm) overlay was applied to the fibers before matrix CVI densification. Fiber volume fraction for the composite was on average 36.0%, and its density was 2.40 g/cm^3. After machining, the specimens were given a seal coat of HyprSiC by chemical vapor deposition (CVD). Properties of the as-processed Hi-Nicalon/PyC/HyprSiC panels are summarized in Table 3.

Table 3: Specifications for Hi-Nicalon 8HS/PyC/HyprSiC Material

Panel ID	Density (g/cm3)	Fiber volume (%)
10C362-05	2.43	36.1
10C362-07	2.41	36.7
10C362-10	2.37	35.2

Average Density : 2.40 (g/cm3)
Average Fiber Volume: 36.0%

3.2 Test Specimen

Eight test specimens were cut from each panel by the AFIT machine shop using diamond grinding resulting in 24 specimens. The specimens were cut in accordance with the specification in Figure 5. The length and width of the specimens were cut in the direction of the fibers.
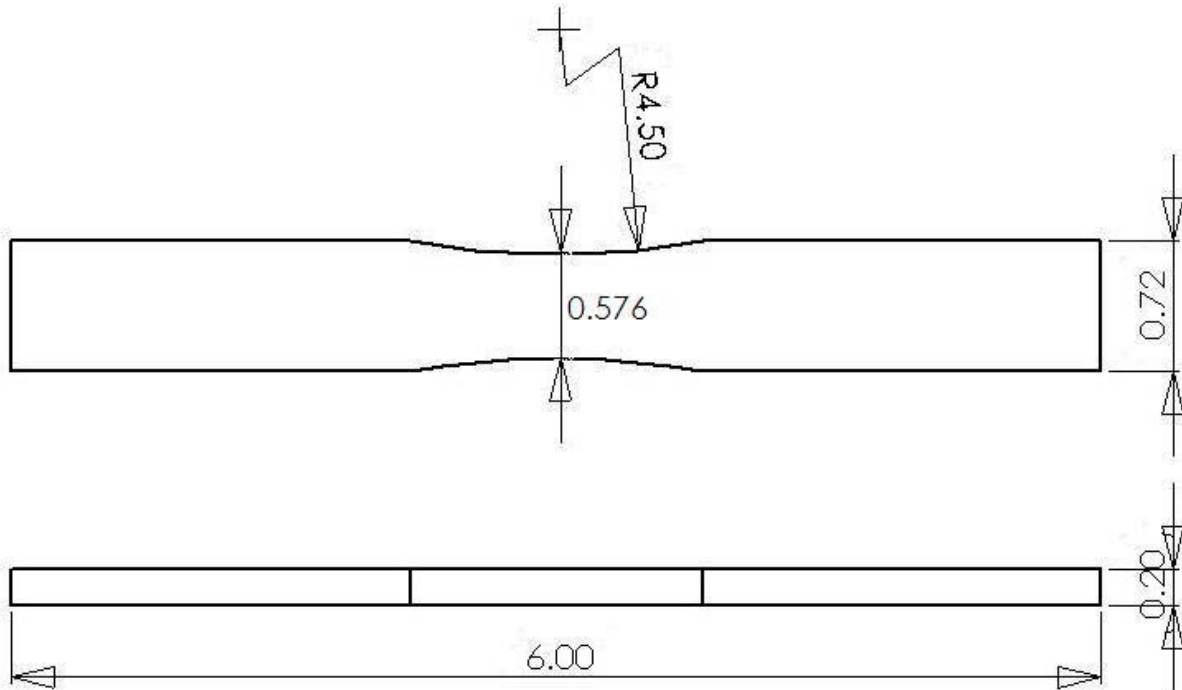
Figure 5: Test Specimen Specifications, all dimensions in inches.

A common mode of failure during fatigue tests with negative R ratios is buckling of the specimen while under compressive loads. This mode of failure is undesirable, and avoided by using an hourglass shaped specimen. The hourglass shape concentrates the maximum stress in the gauge section of the specimen while providing support to prevent buckling. Finite-element analyses of the hourglass specimen show that an axial stress at the edges in the middle of the hourglass section is 3.5% higher than the average axial stress [10]. Hourglass specimens have

been used successfully in fatigue tests of glass strand composites with a negative R ratio [18]. To

ensure that the CMC material in this research would not buckle geometry test specimens were

machined using excess CMC material from work done by Knauf [11]. These specimens were

tested to demonstrate the mode of failure would be compressive or tensile for this family of

material. After the specimens were cut the width and thickness of the gauge area were measured

using a Mitutoyo Corporation Digital Micrometer. The dimensions and the identification of each

test specimen can be seen in Table 4 through Table 6.The largest variation between specimens

was in the thickness due to the weave of the fibers. All dimensions are in millimeters.

Table 4: Dimensions for Specimens from Panel 5

Identification	Width (mm)	Thickness (mm)	Area (mm^2)
P5-1	5.00	14.76	73.80
P5-2	5.00	14.70	73.50
P5-3	4.95	14.93	73.90
P5-4	4.95	14.70	72.77
P5-5	5.00	14.69	73.45
P5-6	5.00	14.72	73.60
P5-7	5.00	14.63	73.15
P5-8	5.00	14.75	73.75

Table 5: Dimensions for Specimens from Panel 7

Identification	Width (mm)	Thickness (mm)	Area (mm^2)
P7-1	5.14	14.67	75.40
P7-2	5.15	14.70	75.71
P7-3	5.18	14.68	76.04
P7-4	5.18	14.68	76.04
P7-5	5.07	14.72	74.63
P7-6	4.92	14.69	72.27
P7-7	5.08	14.67	74.52
P7-8	5.04	14.68	73.99

Table 6: Dimensions for Specimens from Panel 10

Identification	Width (mm)	Thickness (mm)	Area (mm^2)
P10-1	5.08	14.65	74.42
P10-2	5.05	14.60	73.73
P10-3	5.01	14.60	73.15
P10-4	5.15	14.64	75.40
P10-5	5.15	14.47	74.52
P10-6	5.15	14.53	74.83
P10-7	5.15	14.51	74.73
P10-8	5.15	14.67	75.55

Before testing each specimen was fitted with aluminum tabs to protect the specimen from the MTS machine grips. The 6061-T6 aluminum tabs are ductile enough to form a sufficient mechanical bond between the specimen and the grips, while also able to transfer the high loading conditions without failing. Care was taken to keep the tab-specimen surface free of adhesive. This was accomplished with bonding a piece of paper to the end of the specimen, and bonding the aluminum tabs to the paper. This held the tabs in place prior to gripping in the MTS machine and provided a suitable tab-specimen interface. The presence of adhesive in the gripping surface was found to cause slippage of the specimen in the grips under the loads experienced in this effort. The final specimen before testing can be seen in Figure 6. Detail of aluminum tabs is given in Figure 7.
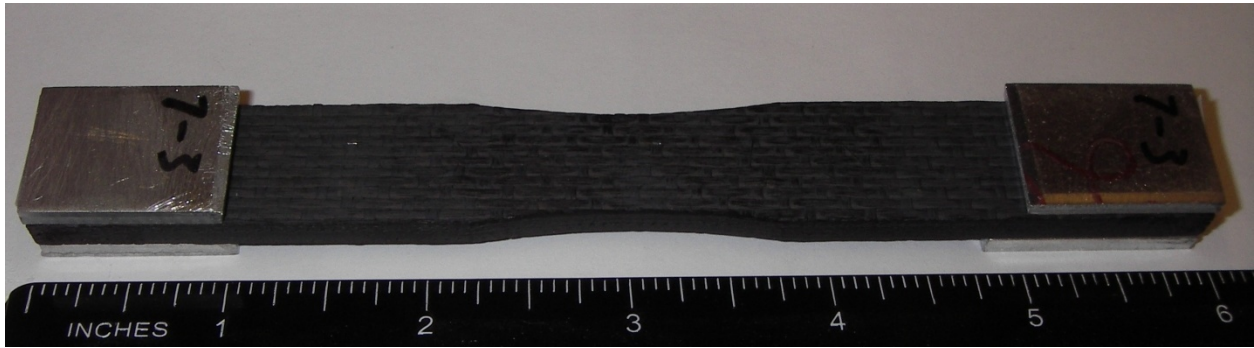
Figure 6: Final Test Specimen shown with aluminum tabs attached.
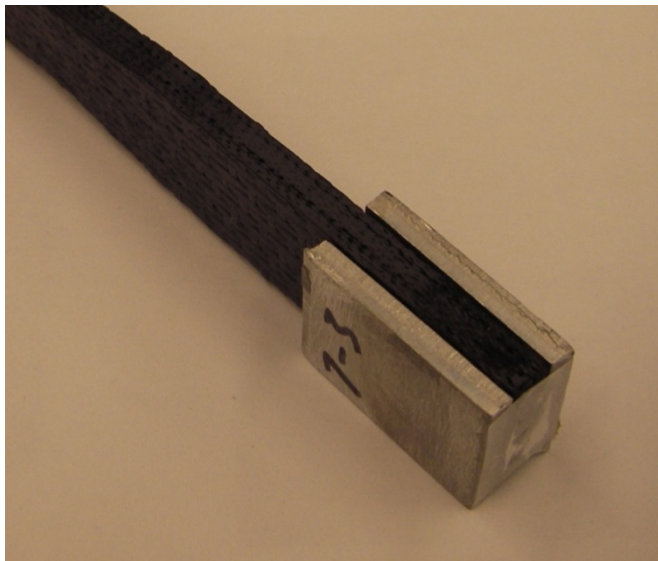
Figure 7: Detail of Aluminum tabs and bonding surface.

IV. Experimental Arrangements and Procedures

4.1 Test Equipment and Setup

Mechanical testing was performed with a MTS 810 Material Test System 5,000 lb capacity servo-hydraulic machine MTS Station run by a Flextest 40 digital controller and Manager/Multipurpose Testware software, as pictured in Figure 8. An MTS Model 632.53 E-14 uniaxial low contact force, high temperature extensometer was employed for strain measurement. The gauge section of the extensometer was 12.7mm. Water cooled wedges with Surfalloy grip treatments were used to grip the specimens. Cooling water was supplied to the wedges at 15°C by a Neslab Coolflow Refrigerated Recirculator, Model HX-7. A purpose built compact two-zone resistance-heater furnace using an MTS 409 temperature controller was used for elevated temperature testing. For tests that required steam an Amteco Chromalox 2110 Steam Generator supplied with distilled water was used.

To ensure testing of the specimens occurred at 1200°C the temperature controller set points were calibrated for both steam and air environments. Two R-Type thermocouples were held against the specimen in the gauge section to measure specimen temperature on an Omega CL3515A digital hand, thermometer. Furnace temperatures were slowly increased until the specimen temperature reached 1200°C. Once specimen temperature was maintained at 1200°C for two hours the set point on the temperature controller was recorded for steam and air.

Specimens were loaded into a small ceramic cylinder called a susceptor before being placed in the MTS grips.

Figure 8: MTS 5 Kip Machine

The wedge grip pressure was raised to 20MPa to prevent slippage without crushing the test specimen.

4.2 Microstructural Characterization

The fracture surfaces of test specimens were evaluated with a Zeiss Stemi SV II optical microscope equipped with a Zeiss AxioCam HRc digital camera and the Quanta 200 scanning electron microscope (SEM).

Figure 9: Zeiss Stemi SV II optical microscope (left) and Quanta 200 scanning electron microscope (right).

Sections of the lower portion of the specimen were cut transverse to the loading direction with a diamond dicing saw. These samples were then mounted in phenolic resin and polished on a Buehler AutoMet Specimen polisher using progressively finer Metadi Diamond Suspension polishing fluids. The steps are outlined in Table 7.

Table 7: Polishing sample process.

Disk/Cloth	Sandpaper	Sandpaper	Ultra Pad	Ultra Pad	Texmet 2500	Texmet 2500	Chemomet
Abrasive Type	SiC Sandpaper	Sic Sandpaper	Dia, susp	Dia, susp	Dia, susp	Dia, susp	Dia, susp
Grit or Grain Size (µm)	400	600	15	9	6	3	0.05
Lubricant Type	Water	Water					
Rotation Disk/ Holder rpm/rpm	300/150	150/150	150/150	150/150	150/150	150/150	150/150
Comp/ Contra	Contra	Comp	Comp	Comp	Comp	Comp	Comp
Force per Specimin (lb)	7	7	7	7	7	5	2
Time (min)	5	5	10	10	20	40	6

4.3 Test Procedures

4.3.1 Monotonic Tensile Testing

Randomly chosen specimens from each panel were tested under monotonic tensile loading to determine as processed mechanical properties. Each specimen was heated to 1200°C at a constant rate of 1.0°C/s while held at zero load condition. After a 20-minute dwell period at 1200°C with no temperature perturbation greater than five degrees the specimen was loaded to failure. The specimens were loaded using a displacement command of 0.05mm/s until failure. For all portions of the test strain, load, oven temperature, displacement, displacement command, and time data were recorded.

4.3.2 Fatigue Testing

Tension-compression fatigue testing was conducted at 1 Hz with a load ratio (R) equal to -1.0 in air and steam environments. Each specimen was heated to 1200°C at a constant rate of 1.0°C/s while held at zero load condition. After a 20-minute dwell period at 1200°C with no temperature perturbation greater than five degrees the fatigue cycles began. Fatigue run-out condition was specified as 2×10^5 cycles. During fatigue testing strain, load, load command cycle number, displacement, temperature, and time data were recorded. Four separate data files were created for each test. Data collected during initial heating was stored in the "Specimen" file. The "Peak and Valley" file reported data values at each peak and valley of all recorded cycles. Data for a full cycle loop was collected during the following cycles: i) cycles 1 to 25, ii) every tenth cycle from cycle 30 to 100, iii) every 100th cycle from cycle 100 to 1000, iv) every 1000th cycle from cycle 1000 to 10000, and v) every 10000th cycle from cycle 10000 to run-out.

19

4.3.3 Monotonic Compression-Tensile Testing

A remaining specimen with no loading history was tested under monotonic compression then tensile loading to determine as processed mechanical properties. The specimen was heated to 1200˚C at a constant rate of 1.0˚C/s while held at zero load condition. After a 20-minute dwell period at 1200˚C with no temperature perturbation greater than five degrees the specimen was loaded first in compression then in tension to failure. The specimen was loaded in compression using a load rate command of 200 lbf/s to a compressive stress of 250 MPa, then in displacement command of 0.05mm/s the specimen was loaded in tension until failure. Load control for compression was selected to ensure that MTS machine limits were not exceeded. The transition to displacement control for the tensile loading was done to maintain experimentally similar conditions to those obtained for tensile to failure loads for subsequent comparison of the results. For all portions of the test strain, load, oven temperature, displacement, displacement command, and time data were recorded.

V. Results and Discussion

5.1 Chapter Overview

The results of all testing are presented in the following chapter. Thermal strain and coefficient of thermal expansion for each specimen is presented in section 5.2. Monotonic tension to failure results are presented in section 5.3. Tension-compression fatigue test results in laboratory air are presented in section 5.4. Tension-compression fatigue test results in steam are presented in section 5.5. Results of tension to failure testing carried out on specimens that achieved run-out are presented in section 5.6. Compression to tension loading results are presented in section 5.7. Specimen microscopy results are presented in section 5.8. Comparison to test results obtained from tension-tension fatigue are obtained from Delepasse[7], and are denoted by their R ratio as being R = 0.05.

Each specimen was assigned a number according to its panel of origin to differentiate between panels. Panels tested in this effort were panel 5,7, and 10. Each of eight specimens from the panels were assigned numbers such as P10-5, to identify specimen five from panel ten. Fatigue run-out was defined at $2x10^5$ cycles. Table 8 summarizes all test data for this effort.

Table 8: Summary of Hi-Nicalon/PyC/HyperSiC specimen data. All tests conducted at 1200°C.

Specimen	Fatigue Frequency (Hz)	Test Environment	Maximum Stress (Mpa)	Elastic Modulus (Gpa)	Cycles to Failure (n)	Time to Failure (h)	Failure Strain (%)
Tensile Test							
P5-7	-	Air	296.3	159.12	-	-	0.56
P7-7	-	Air	406.9	179.19	-	-	0.83
P10-8	-	Air	391.9	93.94	-	-	0.78
Compression - Tension Test							
P7-3	*Compression*	Air	250	176.76	-	-	-
	Tension	Air	385.5	168.23	-	-	0.86
Tension - Compression Fatigue Tests							
P10-6	1	Air	80	-	200000	55.56	-
P10-3	1	Air	100	-	161110	44.75	-
P10-5	1	Air	120	-	83799	23.28	-
P10-2	1	Air	140	-	23277	6.47	-
P5-3	1	Air	160	-	29988	8.33	-
P7-1	1	Air	160	-	6914	1.92	-
P7-8	1	Air	200	-	10656	2.96	-
P5-5	1	Air	200	-	9612	2.67	-
P7-6	1	Air	300	-	541	0.15	-
P5-2	1	Steam	80	-	200000	55.56	-
P10-7	1	Steam	100	-	144519	40.14	-
P10-1	1	Steam	120	-	50499	14.03	-
P5-4	1	Steam	140	-	12784	3.55	-
P7-2	1	Steam	160	-	2214	0.62	-
P7-4	1	Steam	200	-	948	0.26	-

5.2 Thermal Expansion

All testing in this effort was conducted with a specimen temperature of 1200°C. Heat up of the specimen for all tests was conducted at 1°C/s while maintaining zero load. During the heat up and 20 min dwell period after heating, the specimen's thermal strain was recorded. For each specimen the coefficient of thermal expansion (CTE) was calculated using the following formula:

$$\alpha_t = \frac{\varepsilon_t}{\Delta T}$$

where ε_t is the measured thermal strain (m/m) and ΔT is the change in temperature (°C) of the specimen. The thermal strain measured for each specimen and its corresponding coefficient of thermal expansion are summarized in Table 9. Specimen's thermal strain ranged from 0.43% to 0.55%. The average coefficient of thermal expansion was 4.15 x 10^{-6} 1/°C, which is 14% lower than the average reported by Delapasse[7] in Table 10. Panel seven has the highest and lowest measured thermal strains.

Table 9: Thermal strains produced by Hi-Nicalon/PyC/HyperSiC due to temperature rise from 23°C to 1200°C and corresponding coefficients of linear thermal expansion.

Specimen	Thermal Strain (%)	Coefficient of Linear Thermal Expansion, a (10^{-6}/C)
P5-1	0.47	4.02
P5-2	0.45	3.85
P5-3	0.49	4.16
P5-4	0.44	3.71
P5-5	0.54	4.58
P5-6	-	-
P5-7	0.54	4.56
P5-8	-	-
Average		4.15
Standard Deviation		0.36
P7-1	0.43	3.62
P7-2	0.44	3.70
P7-3	0.49	4.18
P7-4	0.46	3.90
P7-5	0.55	4.67
P7-6	0.51	4.36
P7-7	0.49	4.15
P7-8	0.53	4.52
Average		4.14
Standard Deviation		0.38
P10-1	0.44	3.75
P10-2	0.50	4.29
P10-3	0.52	4.45
P10-4	-	-
P10-5	0.52	4.45
P10-6	0.52	4.42
P10-7	0.43	3.62
P10-8	0.50	4.24
Average		4.17
Standard Deviation		0.35

5.3 Monotonic Tension

To determine the initial tensile properties at 1200°C, one specimen from each panel was tested in monotonic tension to failure. The measured results and corresponding properties for each specimen are given in Table 10. The tensile stress strain curves are given in Figure 10. An average ultimate tensile strength (UTS) of 365.03 MPa, the average elastic modulus was144.08 GPa, and the average failure strain was 0.72%. The point at which the stress strain curve transitions from linear to non linear behavior is the proportional limit. The average proportional limit was 123.33 MPa, or approximately 34% of the average UTS. This value is similar to Delapasse[7] Table 12. However unlike the previous work a distinct "knee" in the stress strain curve is not seen. This would indicate that the fibers are carrying a significant portion of the load before extensive matrix micro cracking occurs. This comparison is shown in Figure 11with the tensile stress strain curves for this effort plotted with those of Delapasse[7].

Table 10: Tensile properties obtained for Hi-Nicalon/PyC/HyperSiC at 1200°C in laboratory air at a constant displacement rate of 0.05 mm/s.

Specimen	Elastic Modulus (GPa)	Proportional Limit (MPa)	Ultimate Strength (MPa)	Failure Strain (%)
P5-7	159.12	120	296.3	0.56
P7-7	179.19	120	406.9	0.83
P10-8	93.94	130	391.9	0.78
Average	144.08	123.33	365.03	0.72
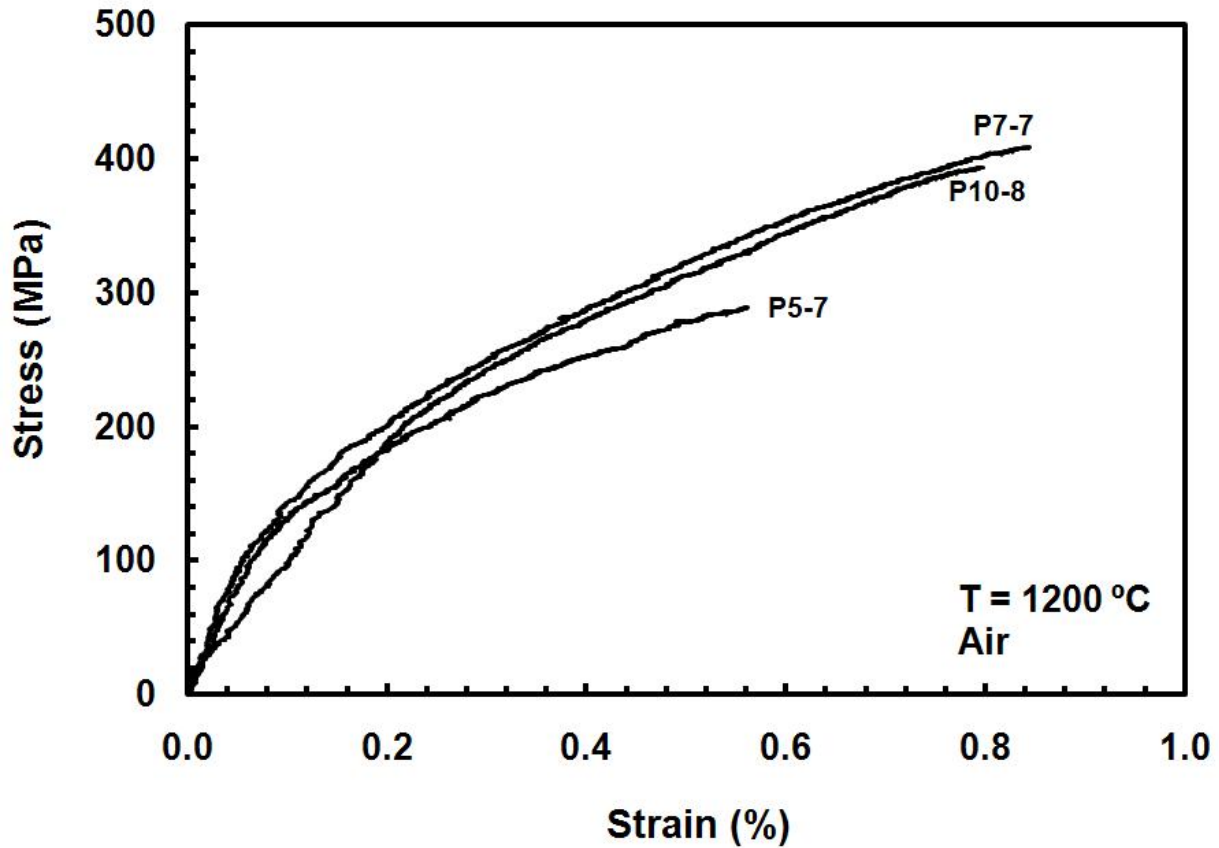
Figure 10: Tensile stress-strain curves for Hi-Nicalon/PyC/HyprSiC Ceramic composite at 1200°C in air.

The specimens tested in this effort averaged about a cross sectional area of about 7.5×10^{-5} m², about twice the area of specimens tested in tension-tension [7]. For composites that are manufactured with the chemical vapor infiltration process the increasing of thickness tends to lead to more voids within the specimen and a less dense matrix. More voids between fiber tows and a less dense matrix would lead to poor performance in tension for the CMC. However this is not the case for specimens tested in this work. Figure 11 shows the comparison of the stress strain properties of the smaller specimens and larger hourglass specimens. No loss of strength is

observed for the larger hourglass specimens, conversely they perform better in tensile loading. This can be due to better control of the fiber perform weaving and CVI process.
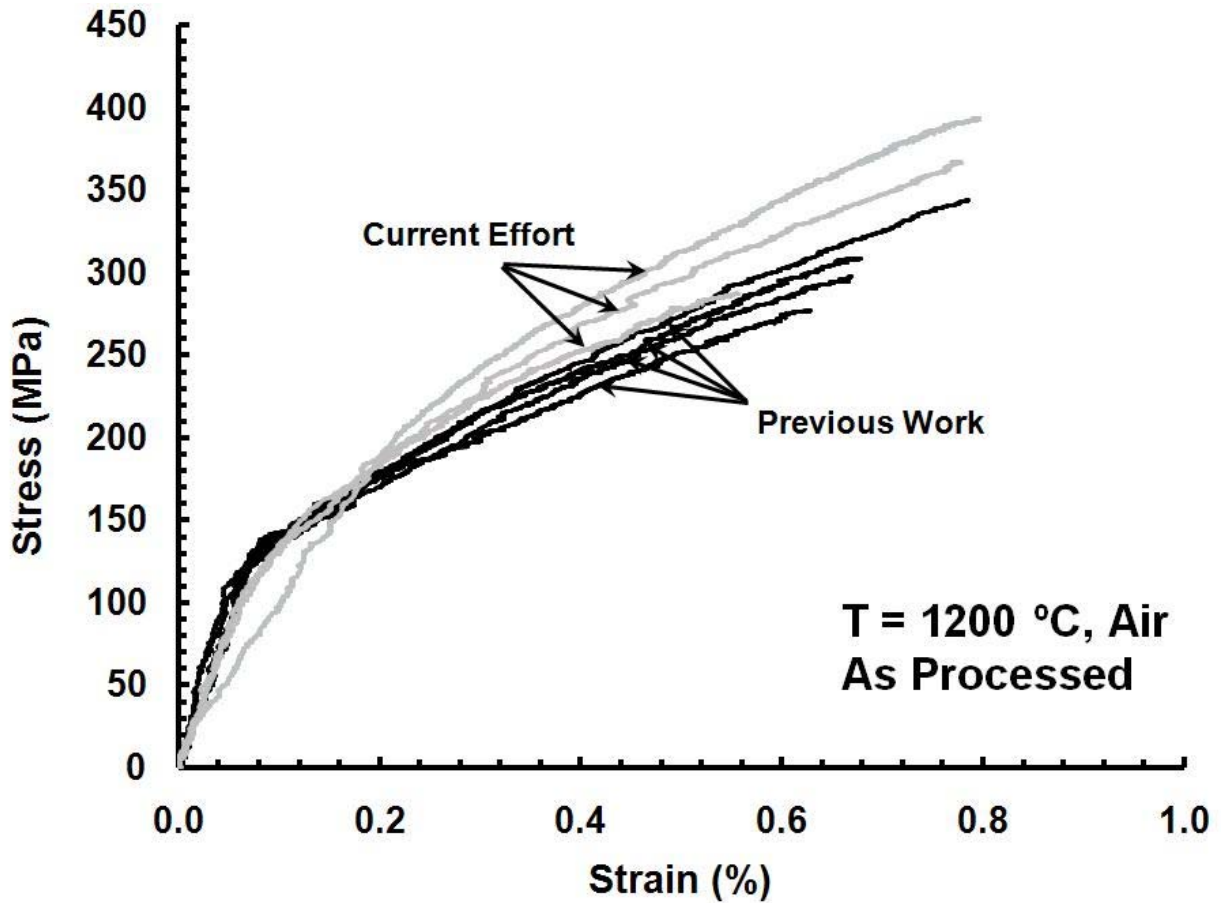
Figure 11: Tensile stress-strain curves for Hi-Nicalon/PyC/HyprSiC Ceramic composite at 1200°C in air compared to work by Delapasse[7].

5.4 Tension-Compression Fatigue Test at 1200°C in Air

In laboratory air, nine tension-compression fatigue tests were conducted with an R ratio (minimum to maximum stress) of -1.0 at 1200°C and 1.0 Hz. The fully reversed stress levels ranged from

80 to 300 MPa. The run-out condition of 200,000 cycles was achieved at a stress of 80 MPa. Table 11 summarizes the results of fatigue testing in air. A stress vs. cycles to failure plot is given in Figure 12.

Table 11: Summary of fatigue results for Hi-Nicalon/PyC/HyperSiC at 1200°C in laboratory air.

Specimen	Fatigue Frequency (Hz)	Maximum Stress (Mpa)	Cycles to Failure (n)	Time to Failure (h)
P10-6	1	80	200000	55.56
P10-3	1	100	161110	44.75
P10-5	1	120	83799	23.28
P10-2	1	140	23277	6.47
P5-3	1	160	29988	8.33
P7-1	1	160	6914	1.92
P7-8	1	200	10656	2.96
P5-5	1	200	9612	2.67
P7-6	1	300	541	0.15
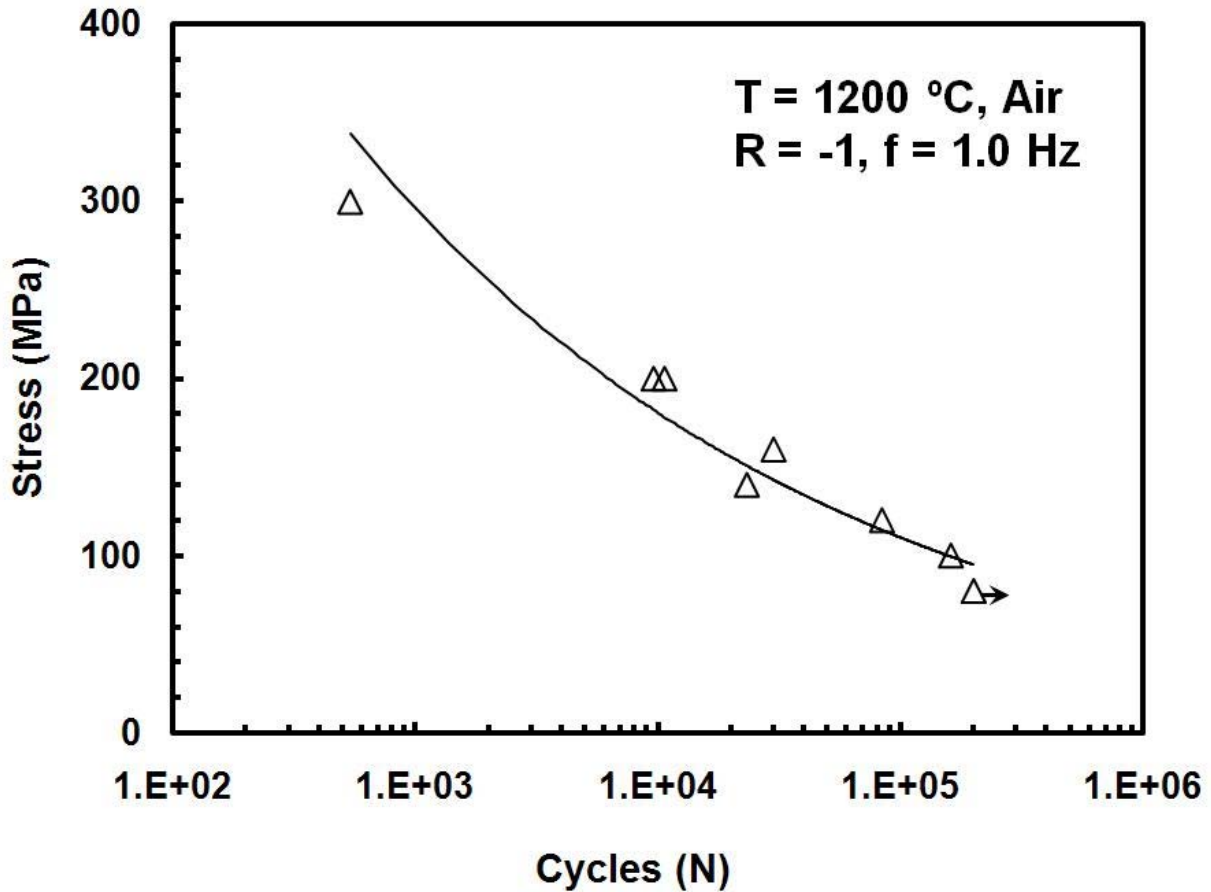
Figure 12: Fatigue S-N diagram for the Hi-Nicalon/PyC/HyprSiC composite at 1200°C in laboratory air.

The data in Table 11 shows that as the stress is increased the fatigue performance decreases. This expected decrease in cycles to failure is also shown in Figure 12. The stress level of 80 MPa at which run-out was achieved is below the proportional limit of the material found from tensile testing. Fatigue run-out is depicted in Figure 12 with an arrow on the data point.

The results from tension-compression testing are compared to tension-tension fatigue testing [7] in Table 12. Stress vs. cycle data is displayed for both R ratios in laboratory air in Figure 13. Tension-tension fatigue testing was done at 1.0 Hz with an R ratio of 0.05, at 1200°C in laboratory air. Reduction in life due to the presence of a compressive portion of the fatigue cycle ranged from 19.4% for a max

stress of 100 MPa to 63.3% for a max stress of 140 MPa. When the maximum stress exceeded the

approximate proportional limit of 120 MPa the reduction in cycles to failure doubled to 63.3%. Past the

proportional limit where matrix cracking occurs the presence of a compressive load in the fatigue cycle

significantly reduces life.

Table 12: Reduction in fatigue life for Hi-Nicalon/PyC/HyprSiC CMC due to R ratio, in laboratory air.

Max Stress (Mpa)	Fatigue at R = 0.05	Fatigue at R = -1	Reduction in Fatigue Life (%)
100	200000	161110	19.4
120	119530	83799	29.9
140	63458	23277	63.3

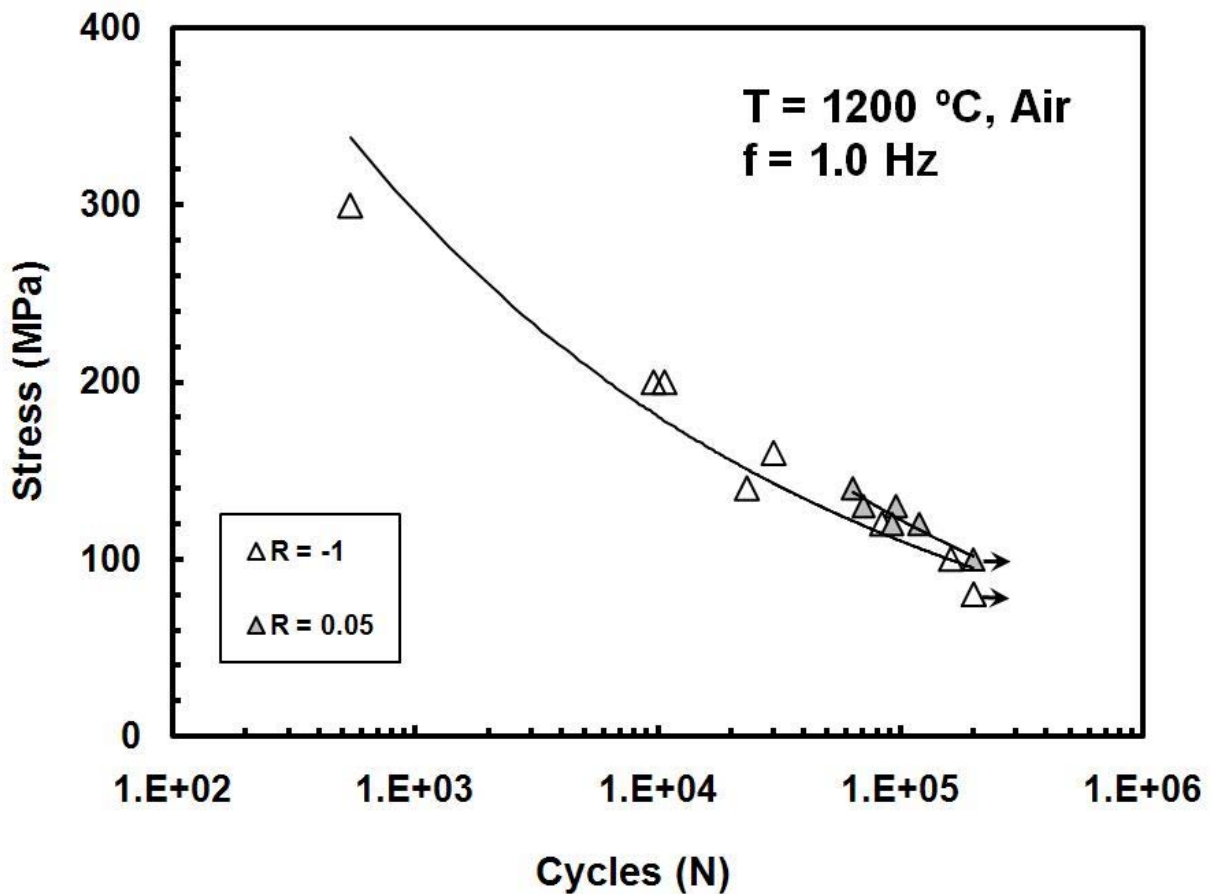**Figure 13: Fatigue S-N diagram for the Hi-Nicalon/PyC/HyprSiC CMC at 1200°C in laboratory air. Data for R ratio = 0.05 from Delapasse [7].**

Figure 13 shows the shift in the stress vs. cycles curve from tension-tension fatigue to tension-compression fatigue. Run-out in laboratory air was accomplished at 80 MPa for fully reversed testing compared to run-out at 100 MPa for R = 0.05 fatigue.

During cyclic fatigue the extent of damage development in the composite can be investigated by observing the reduction in stiffness over time. The tensile and compressive stiffness of the composite or, hyseresis modulus for a cycle is determined from the corresponding maximum and minimum stress-strain points. The tensile modulus evolution with fatigue cycles is shown in Figure 14. In Figure 14 the modulus is normalized for each cycle to the second cycle to show a relative change and plotted vs. fatigue cycle number. All specimens tested in Air showed a decrease in the normalized modulus with increasing cycle numbers. This indicates that damage such as matrix cracks are forming in the specimen. As these cracks grow the modulus of the composite decreases due to progressively less matrix contribution to stiffness. Comparing to work done by [7] the modulus loss in fully reversed fatigue did not exhibit a high dependence on stress levels.
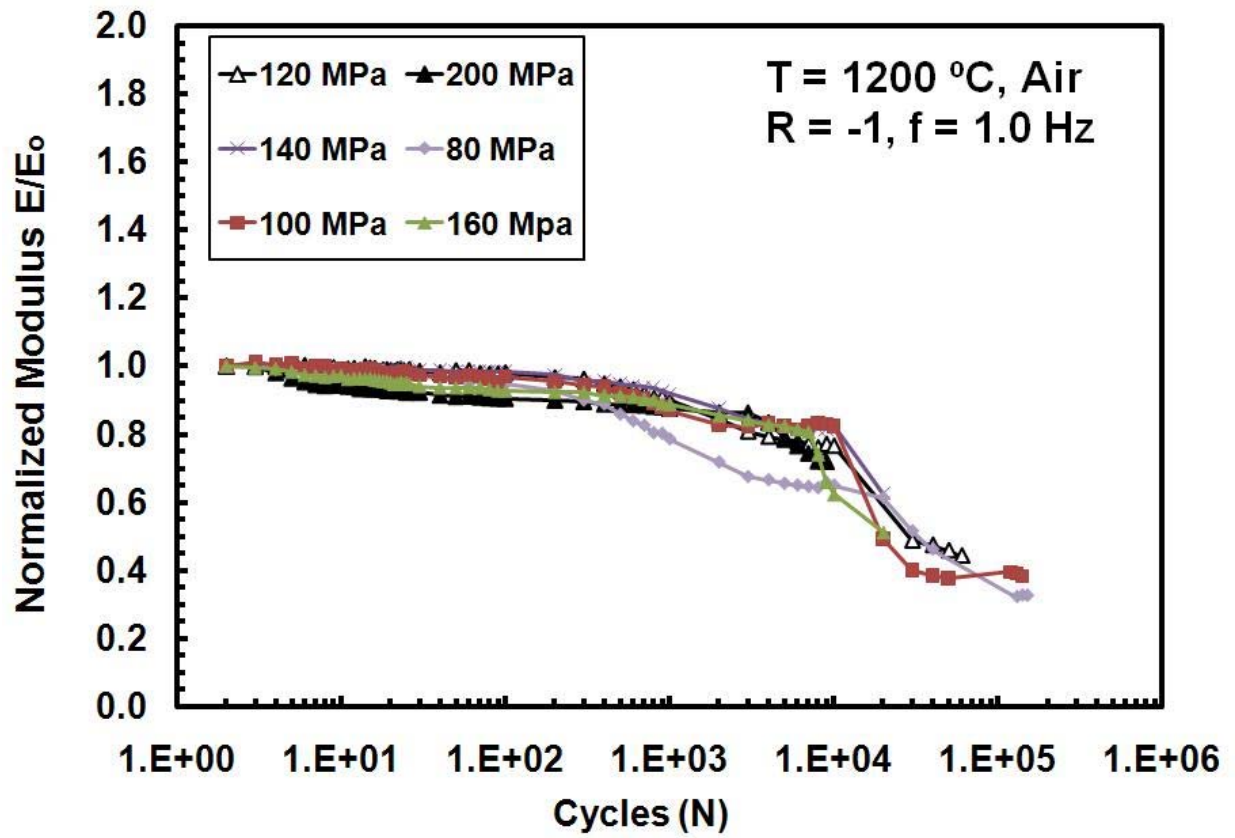
Figure 14: Normalized tensile modulus vs. fatigue cycles for the Hi-Nicalon/PyC/HyperSiC ceramic composite at 1200°C in laboratory air.
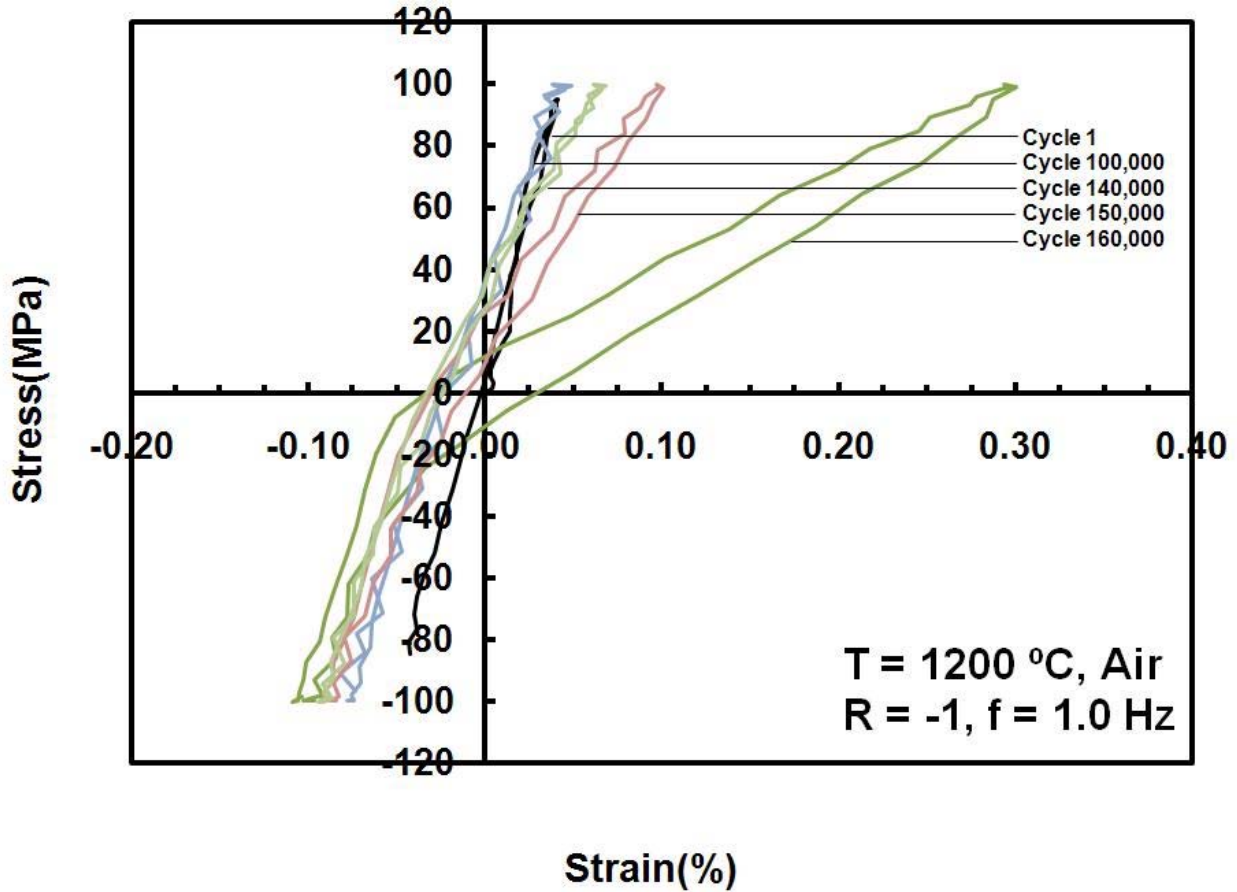
Figure 15: Evolution of stress-strain hysteresis response of Hi-Nicalon/PyC/HyperSiC with fatigue cycles in laboratory air at 1200°C.

Figure 15 shows the stress-strain curves for selected cycles of Hi-Nicalon/PyC/HyperSiC tested in air at 1200°C. The decrease in the tensile modulus of the material as the cycles increase is observed. Also the compressive modulus remains constant when compared to the relative change in the tensile modulus. This would suggest that the damage development is more apparent under tensile load. No strain accumulation is observed for tension-compression fatigue, compared to accumulated strains of 2% observed in tension-tension [7]. The presence of a compressive load in the fully reversed cycle removes the strain ratcheting effect that is common in testing with positive R ratios.

The maximum and minimum cyclic strains as a function of cycle number for fatigue tests conducted at 1200°C in laboratory air at 100 MPa are shown in Figure 16. The compressive strain as

33

well as the tensile strains remains nearly constant throughout the lifetime. This is due in part to the fact that the testing conditions are below the proportional limit of about 120 MPa. At this level little damage development will take place. Towards the end of the test maximum strain values begin to increase as the hysteretic tensile modulus decreases.

Figure 16: Maximum and minimum strains vs. fatigue cycles for the Hi-Nicalon/PyC/HyperSiC ceramic composite at 1200°C in laboratory air and $\sigma_{max} = 100$ MPa.

To observe the difference in the maximum and minimum strain behavior for tension-compression fatigue, stress values past the proportional limit are needed. Testing conducted at 200 MPa is presented in Figure 17. Throughout the duration of the test the maximum strain

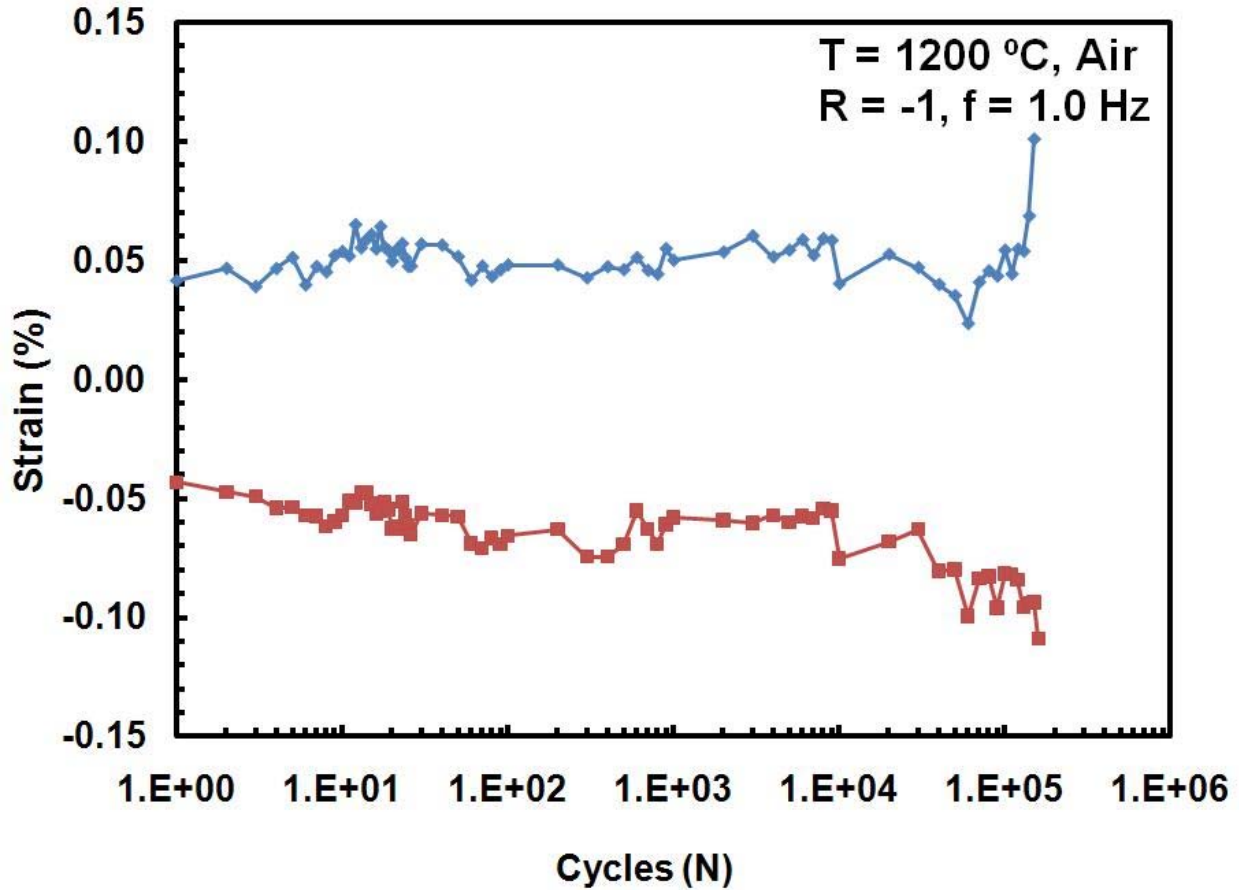gradually increases about 0.15% while the minimum strain remains fairly constant at about -0.10%.
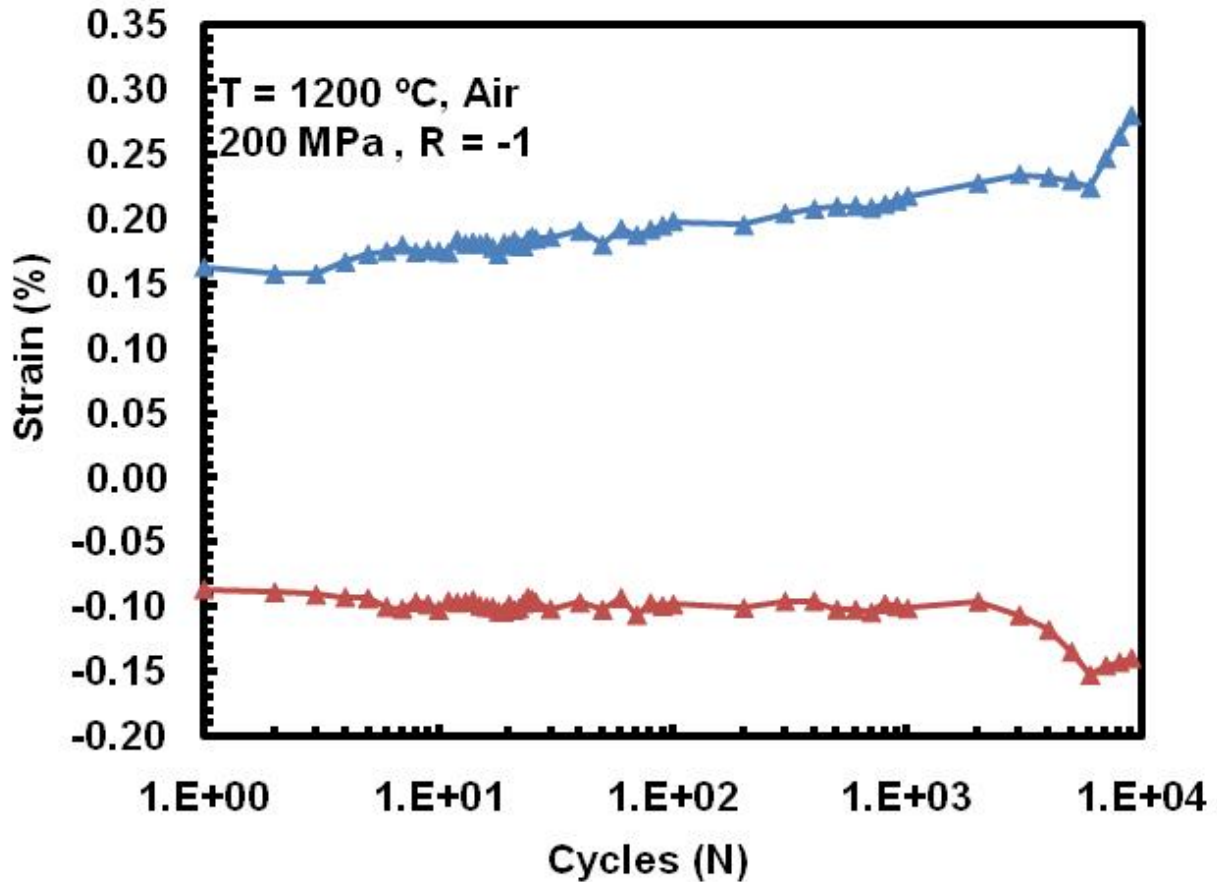
Figure 17: Maximum and minimum strains vs. fatigue cycles for the Hi-Nicalon/PyC/HyperSiC ceramic composite at 1200°C in laboratory air and $\sigma_{max} = 200$ MPa

The gradual increase in the tensile strain corresponds to continuously developing damage beginning at the initiation of loading cycles. There is some damage development apparent in the compressive loading that is reflected in the slight decrease of the minimum strains.

5.5 Tension-Compression Fatigue Test at 1200°C in Steam

Testing at 1200°C in a steam environment was completed for six randomly chosen specimens at a loading frequency of 1.0 Hz. The tension-compression testing used an R ratio of -1.0 with stresses ranging from 80 to 200 MPa. Fatigue run-out condition was set to 2 x 10^5 cycles. The results of testing in a steam environment are summarized in Table 13 which also includes results for testing in air at 1200°C for comparison. Figure 18 shows the stress vs. cycles for testing in steam. Fatigue run-out is denoted with an arrow.

Table 13: Summary of fatigue results for Hi-Nicalon/PyC/HyperSiC. At 1200°C in laboratory air and steam environment.

Specimen	Fatigue Frequency (Hz)	Test Environment	Maximum Stress (Mpa)	Cycles to Failure (n)	Time to Failure (h)
Tension - Compression Fatigue Tests					
P10-6	1	Air	80	200000	55.56
P10-3	1	Air	100	161110	44.75
P10-5	1	Air	120	83799	23.28
P10-2	1	Air	140	23277	6.47
P5-3	1	Air	160	29988	8.33
P7-1	1	Air	160	6914	1.92
P7-8	1	Air	200	10656	2.96
P5-5	1	Air	200	9612	2.67
P7-6	1	Air	300	541	0.15
P5-2	1	Steam	80	200000	55.56
P10-7	1	Steam	100	144519	40.14
P10-1	1	Steam	120	50499	14.03
P5-4	1	Steam	140	12784	3.55
P7-2	1	Steam	160	2214	0.62
P7-4	1	Steam	200	948	0.26

The results from Table 13 show that as the stress increases the effect of the test environment on fatigue life increases. Figure 19 shows results of tension-compression fatigue testing in both air and steam.
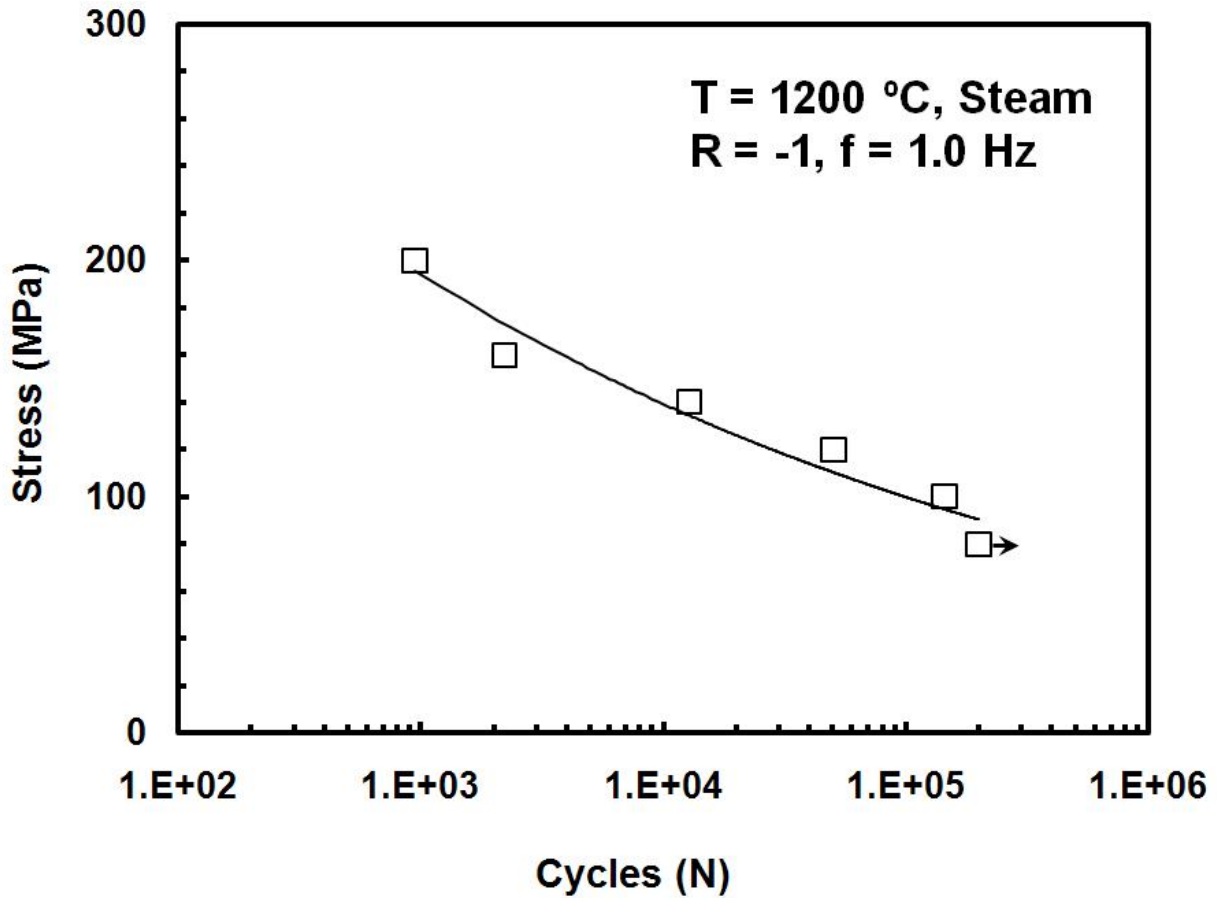

Figure 18: Fatigue S-N diagram for the Hi-Nicalon/PyC/HyprSiC CMC, R ratio of -1 composite at 1200°C in steam.
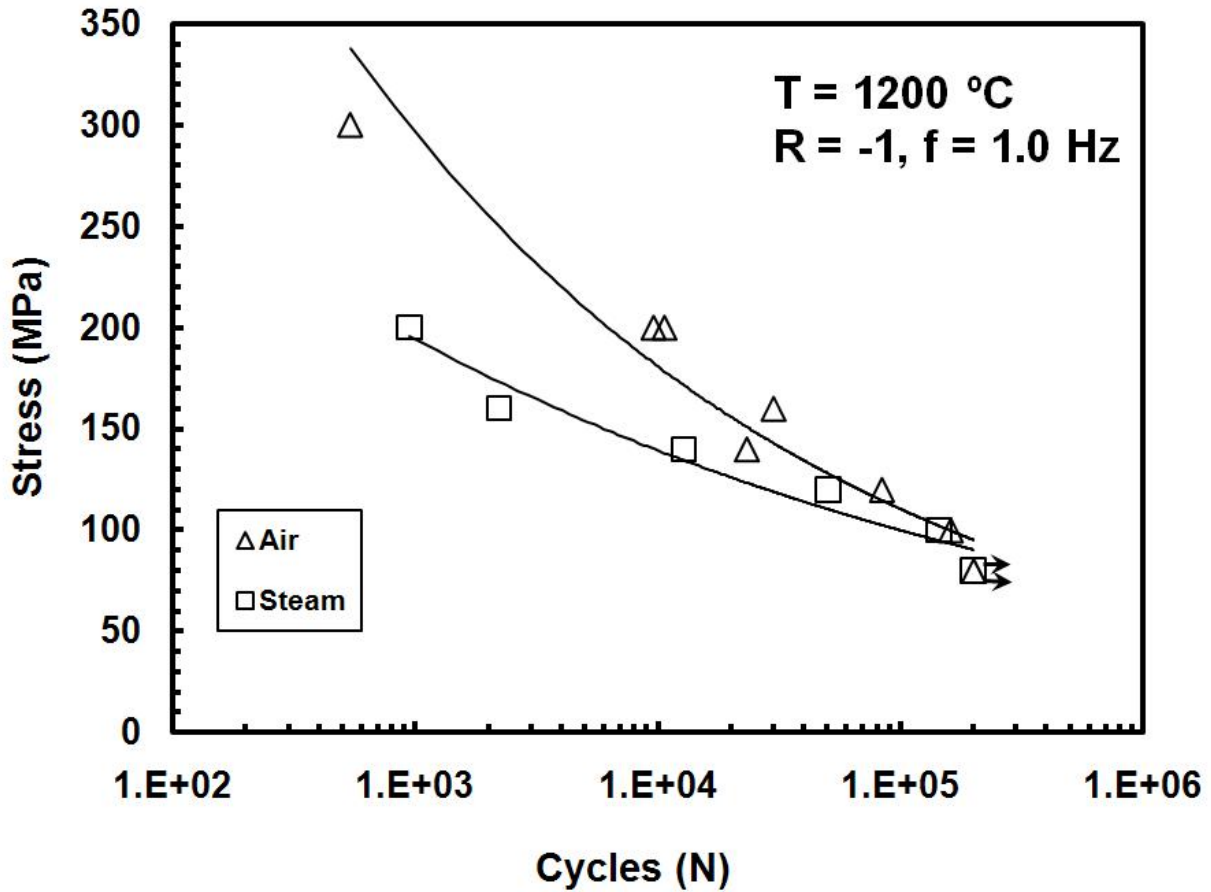
Figure 19: Fatigue S-N diagram for the Hi-Nicalon/PyC/HyprSiC composite at 1200°C in laboratory air and steam.

Figure 19 further illustrates that as the magnitude of the minimum and maximum stress is increased in testing in steam the fatigue life rapidly decreases. Table 14 shows the reduction in life due to the presence of steam for R ratios of -1.0 and 0.05. At fatigue stresses higher than the proportional limit of the composite significant reductions in fatigue life were observed. At 100 MPa the presence of steam reduced the tension-compression fatigue life by 10.3%, compared to the reduction of 91.1% for fatigue at 200 MPa. Compared to tension-tension with R ratio equal to 0.05 and maximum stress of 140 MPa the reduction in life for fully reversed fatigue at 140 MPa was 1.9% greater. A comparison to testing done at an R ratio of 0.05 [7] to testing in this effort is

given in Figure 20. Data presented in Figure 20 shows the loss of fatigue life for testing in fully

reversed fatigue shown in Table 14.

Table 14: Reduction in life cycles due to the presence of steam for Hi-Nicalon/PyC/HyperSiC for R ratios of -1 and 0.1 at frequency of 1.0 Hz. Data for R ratio = 0.05 from Delapasse [7].

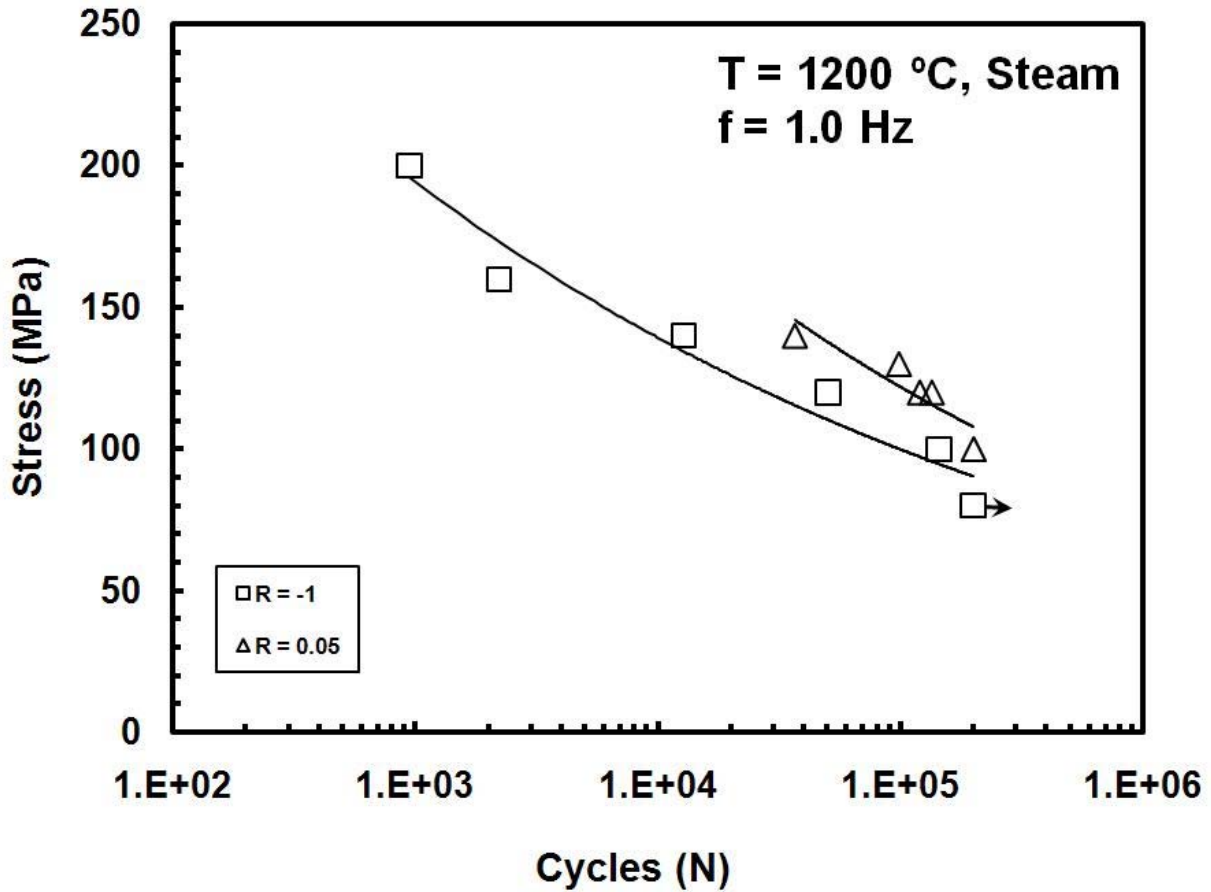| Max Stress (Mpa)	Cycles to Failure (n) Air	Steam	Reduction in Fatigue Life (%)
Fatigue at R = -1			
80	200000	200000	None
100	161110	144519	10.3
120	83799	50499	39.7
140	23277	12784	45.1
160	29988	2214	92.6
200	10656	948	91.1
Fatigue at R = 0.05			
100	200000	200000	None
120	119530	119931	None
140	63458	36679	42.2

Figure 20: Fatigue S-N diagram for Hi-Nicalon/PyC/HyprSiC composite at 1200°C in steam. Data for R ratio = 0.05 from Delapasse [7].

For fatigue cycling in steam at 1200°C, the hysteresis tensile modulus was determined for each cycle. Figure 21 shows the normalized hysteretic tensile modulus vs. fatigue cycle for each of the six specimens tested in steam. Figure 22 presents a comparison of the evolution of the hysteresis modulus for tension-compression testing with an R ratio of -1.0 in both air and steam environments at 1200°C.
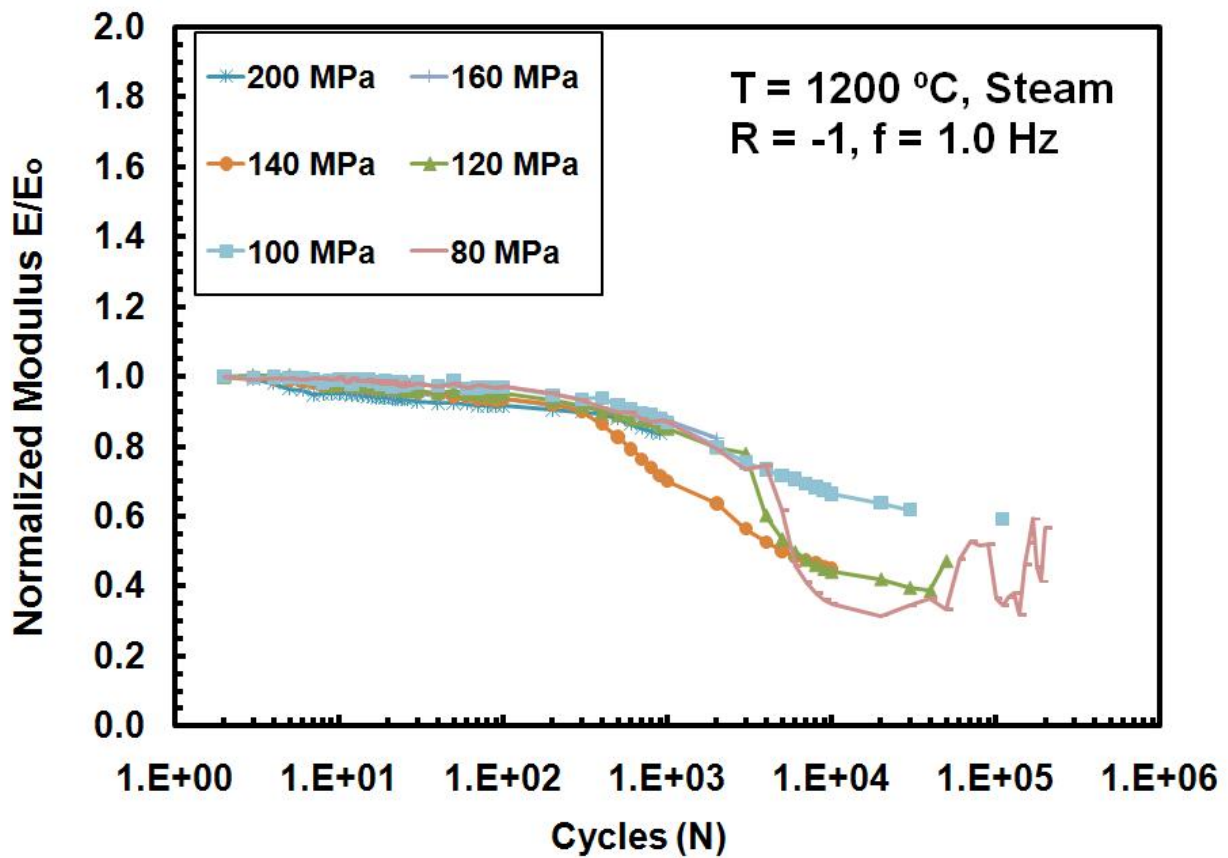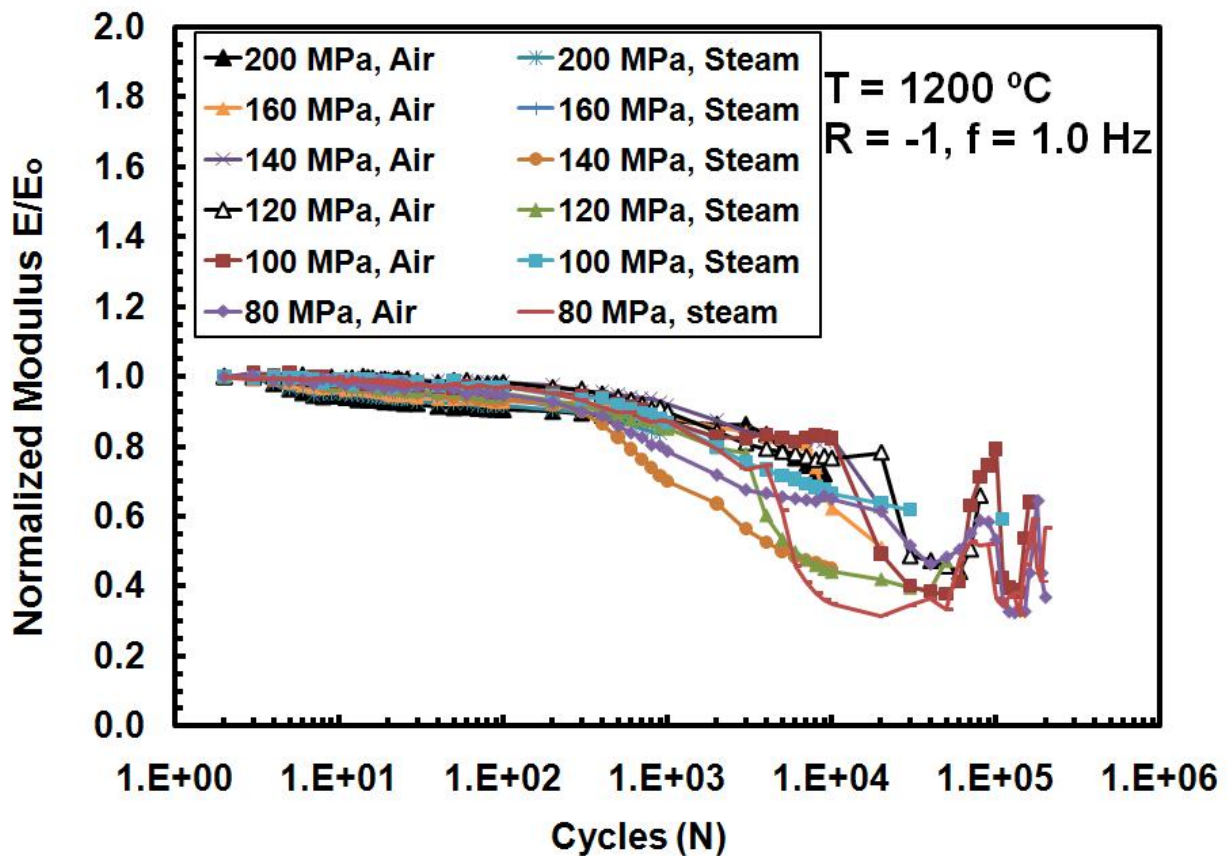
Figure 21: Normalized tensile modulus vs. fatigue cycles for the Hi-Nicalon/PyC/HyperSiC ceramic composite at 1200°C in steam.

The evolution of the tensile modulus in steam shows little dependence on the magnitude of the fatigue stress. Figure 22 shows that the normalized hysteresis modulus evolution is not dependent on test environment. For example, specimens tested at a fully reversed stress of 80 MPa experienced a decrease in tensile modulus for steam of 68.4% compared to 64.7% for air.

Figure 22: Normalized tensile modulus vs. fatigue cycles for the Hi-Nicalon/PyC/HyperSiC ceramic composite at 1200°C in laboratory air and steam.

Figure 23 presents the evolution of the hysteresis response of the composite with fatigue cycles for tension-compression stress of 100 MPa in steam at 1200°C. The response of the modulus of the hysteresis loop in steam closley follows that of specimens tested in an air enviroment. The trends seen in testing conducted in air are also presnt. The tensile modulus of the hysteresis loop decreases with increaseing cycle number. Also there is no progressive accumulation of strain with increasing cycle number. Also the presence of steam does not effect the response of the CMC in compression. There is no signifigant change in the compressive modulus of the hysteresis loop throughout the duration of the test.
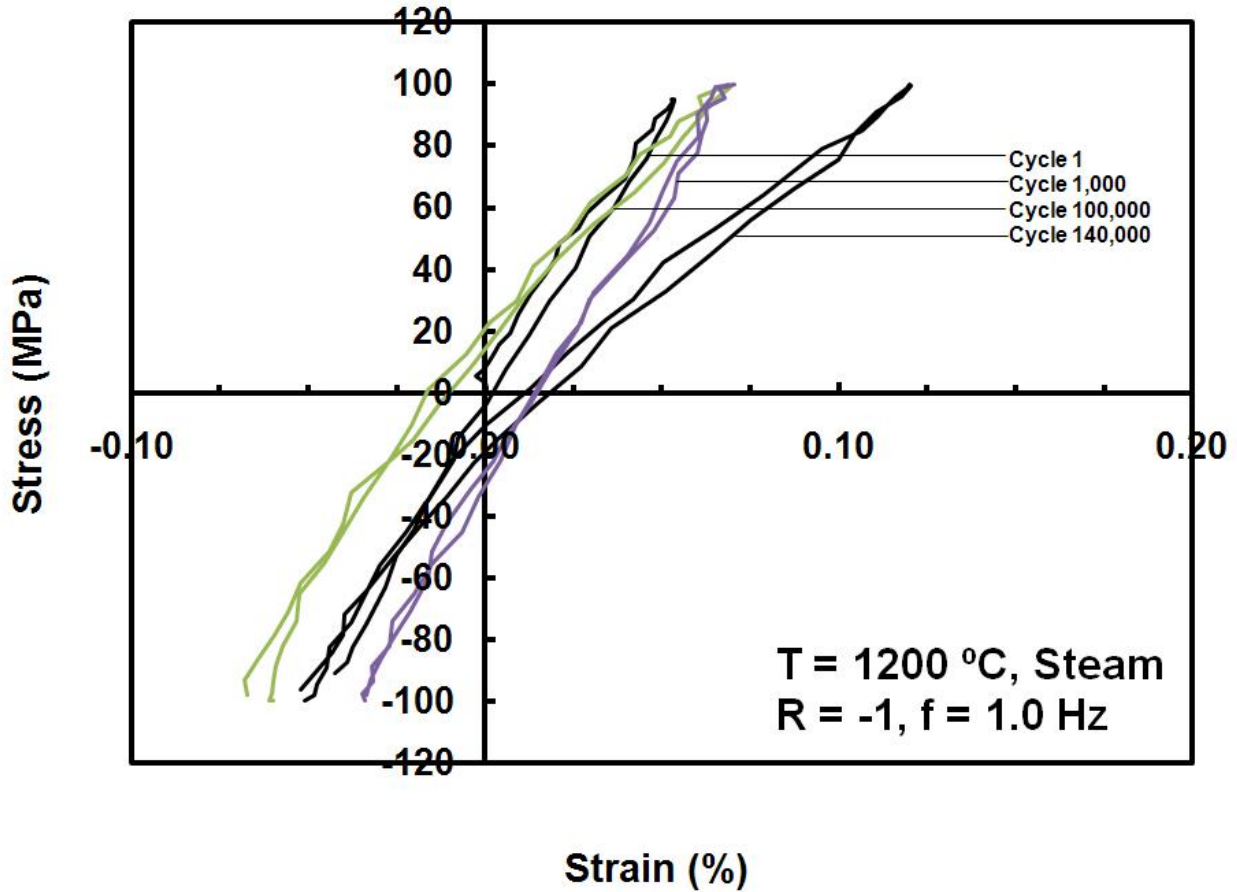
42

Figure 23: Evolution of stress-strain hysteresis response of Hi-Nicalon/PyC/HyperSiC with fatigue cycles in steam at 1200°C.

Figure 24 shows the maximum and minimum cyclic strains for tension-compression fatigue at 100 MPa, R ratio of -1.0 at 1200°C in steam. This plot typifies the cyclic strain response of Hi-Nicalon/PyC/HyperSiC in steam at stress levels below the proportional limit. The tensile strain gradually increases with increasing cycle, while the compressive strains remain relatively constant. The increase in the tensile strain is due to the development of matrix cracks and slow fiber failure.
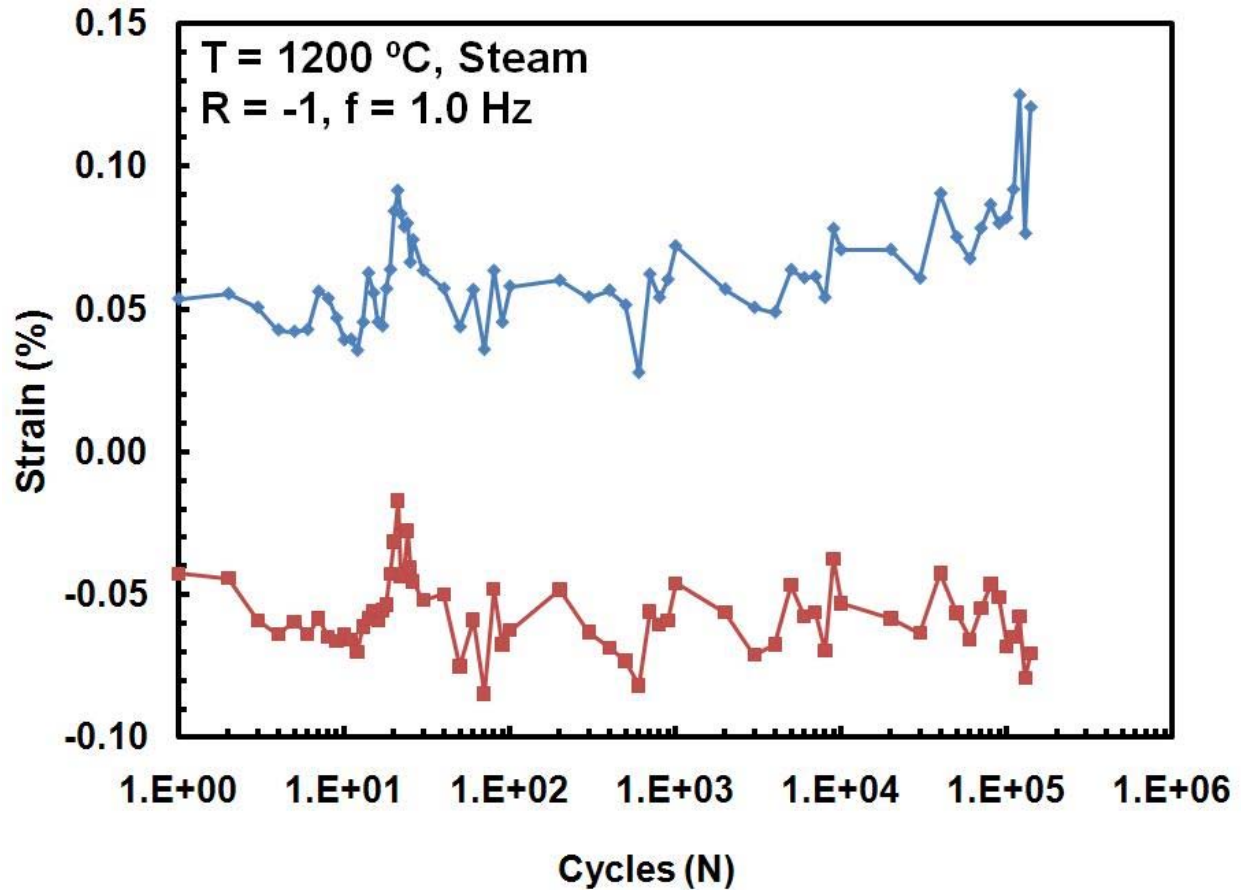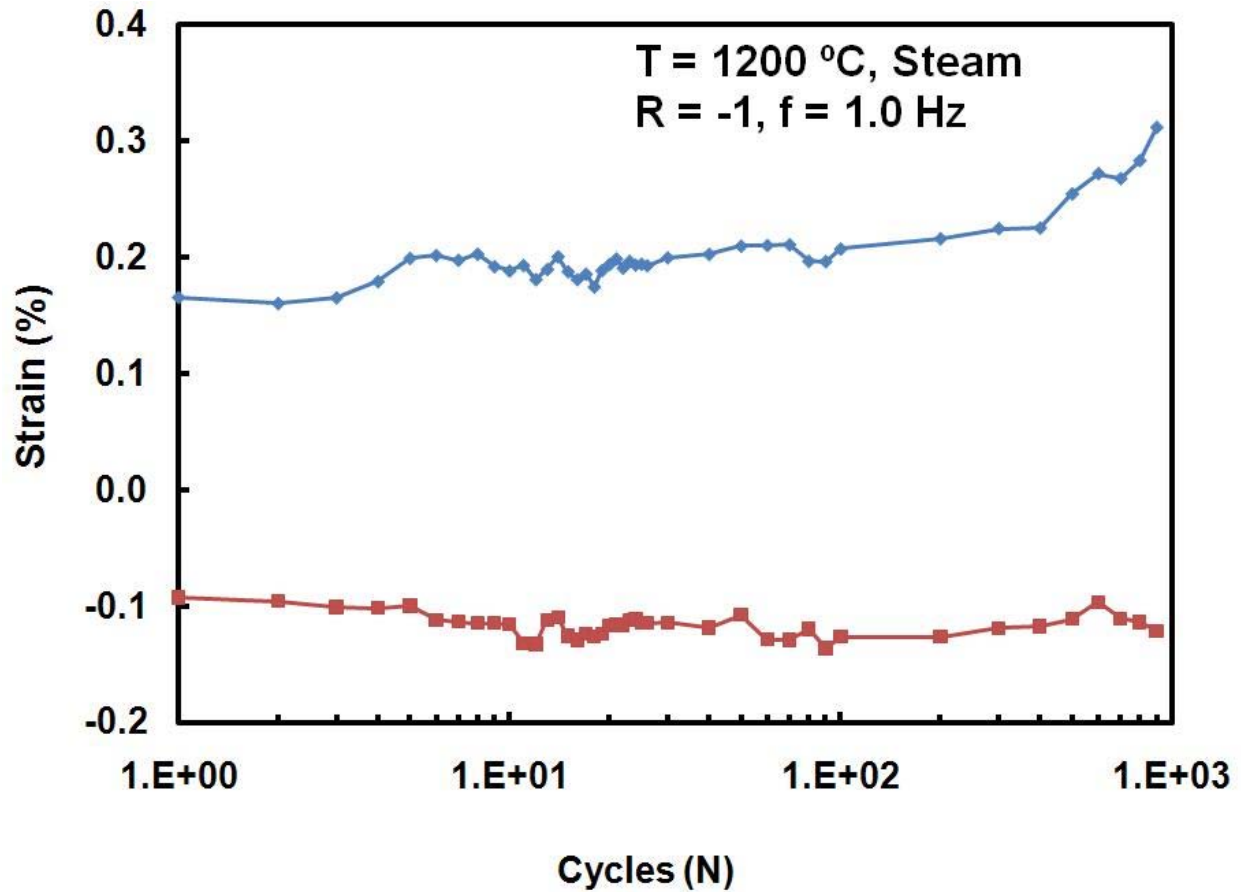
Figure 24: Maximum and minimum strains vs. fatigue cycles for the Hi-Nicalon/PyC/HyperSiC ceramic composite at 1200°C in steam and σ_{max} = 100 MPa.

Figure 25 shows the evolution of maximum and minimum strains with increasing cycles characteristic of stresses above the proportional limit in a steam environment. The maximum and minimum strain trends are similar to those recorded for tests performed in air at the same stress level in Figure 16. The maximum strains brought on by tensile loading increase with increasing cycle number, showing damage development in the form of transverse cracks forming. The compressive loads which cause minimum cycle strains cause only slight damage development over the course of the test.

Figure 25: Maximum and minimum strains vs. fatigue cycles for the Hi-Nicalon/PyC/HyperSiC ceramic composite at 1200°C in steam and σ_{max} = 200 MPa.

5.6 Effect of Prior Fatigue on Tensile Properties and Tensile Stress-Strain Behavior

To determine retained tensile properties specimens that achieved run-out of 2 x 10^5 cycles were subjected to tensile tests to failure. The tensile tests on the run-out specimens were performed at 1200°C in the fatigue test environment of air or steam. The retained ultimate strength and stiffness, as well as the strain and failure results are summarized in Table 15 for all run-out specimens.

Table 15: Retained properties of the Hi-Nicalon/PyC/HyperSiC subjected to prior fatigue in laboratory air and in steam at 1200°C at 1.0 Hz.

Fatigue Stress (MPa)	Fatigue Environment	Retained Strength (MPa)	Strength Retention (%)	Retained Modulus (GPa)	Modulus Retention (%)	Strain at failure (%)
80	Air	413.8	105.59	178.9	190.44	0.721
80	Steam	301.2	101.65	171.04	107.49	0.565

The results of Table 15 show that for specimens subjected to prior fatigue no loss of strength occurred. The retained strength of each specimen was compared to specimens tested in tension from the same panel. In both cases the retained ultimate strength was greater than initial tensile testing, 5.59% and 1.65% for air and steam respectively. The fiber matrix interface was maintained throughout fatigue and sub critical crack growth in the fibers did not occur. These results contrast to tension-tension fatigue testing where retained strengths were 42.2% and 58.7% shown in Table 16, for air and steam respectively [7].

Stress-strain curves for pre-fatigued specimens are presented in Figure 26 with stress-strain curves for the initial as-processed material. The behavior of the stress-strain curves for the original and pre-fatigued Hi-Nicalon/PyC/HyperSiC are similar. The specimens exhibit a linear elastic stress-strain response, followed by a non-linear to failure response. For all specimens the elastic modulus is within 1.9% of the original. Past the proportional limit the pre-fatigued specimens exhibit a slightly higher stress response, leading to the higher ultimate strengths. A comparison of the retained stress-strain behavior for tensile loading given prior fatigue with R values of -1.0 and 0.05 is given in Figure 27.
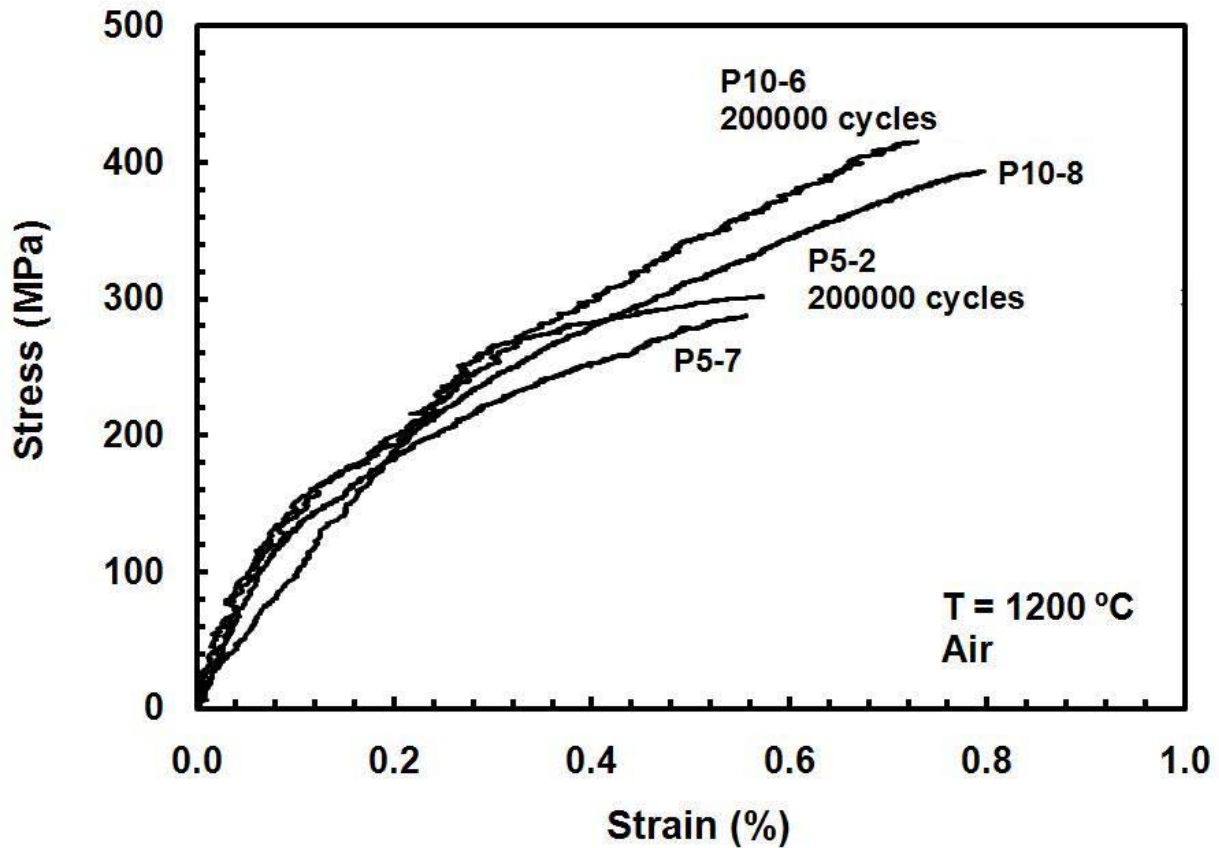
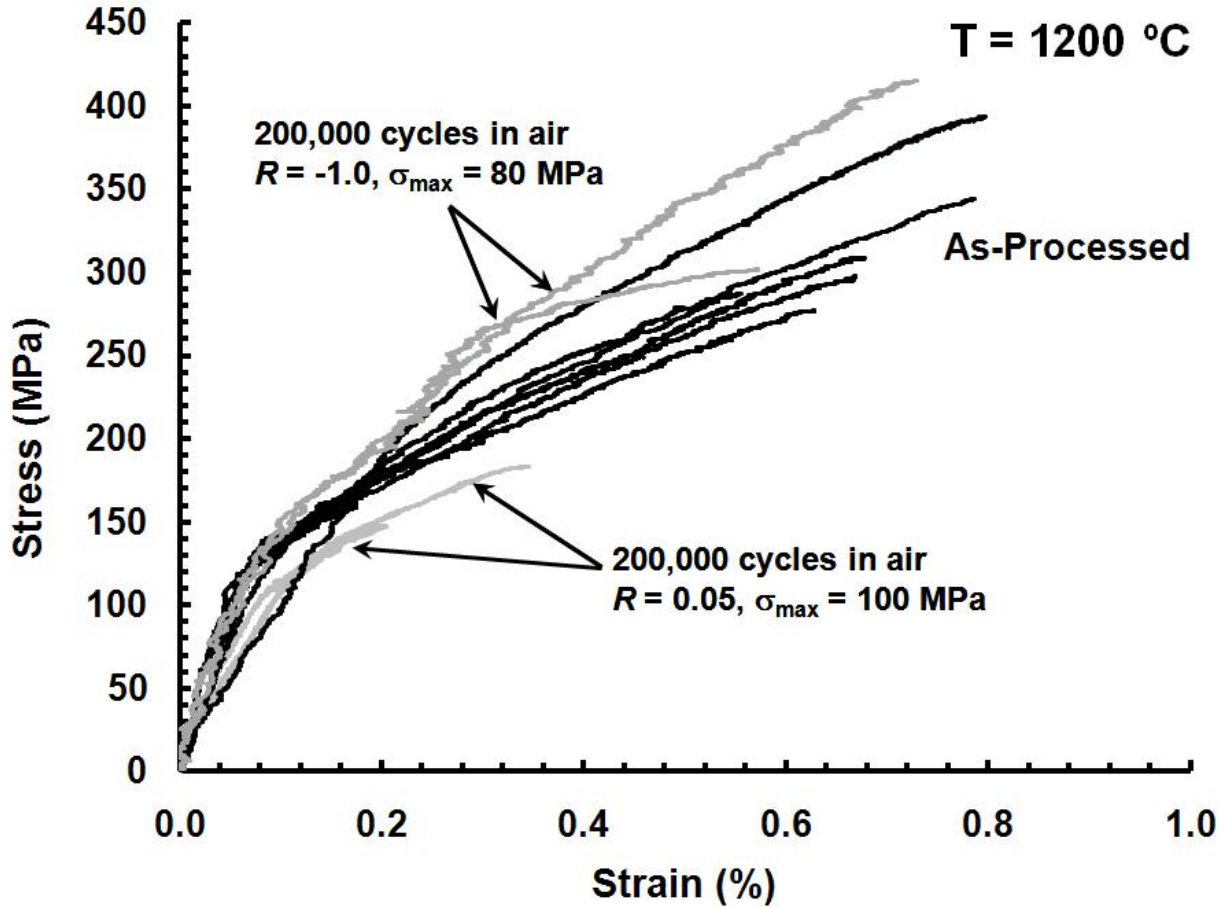**Figure 26: Tensile stress-strain curves for Hi-Nicalon/PyC/HyprSiC Ceramic subjected to prior fatigue at 1200°C. Tensile stress-strain curves for the as-processed specimens are shown for comparison.**

The calculated value of the modulus retention for specimen P10-6 is an artifact of the anomalous behavior of specimen P10-8 tested in tension to failure. Specimen P10-8 experienced some degree of slipping in the grips during initial loading. This reduction in measured load for the applied displacement at the rate of 0.05mm/s resulted in a below average modulus for the specimen. When compared to specimens tested in tension to failure from other panels the retained modulus is within 10% of those values.

Figure 27: Tensile stress-strain curves for Hi-Nicalon/PyC/HyprSiC Ceramic subjected to prior fatigue at 1200°C at R = -1.0 and 0.05 [delapasse]. Tensile stress-strain curves for the as-processed specimens are shown for comparison.

Table 16: Retained properties of the Hi-Nicalon/PyC/HyperSiC subjected to prior fatigue in laboratory air and in steam at 1200°C at 1.0 Hz. Data for R ratio = 0.05 from Delapasse.

Fatigue Stress (MPa)	Fatigue Environment	Retained Strength (MPa)	Strength Retention (%)	Retained Modulus (GPa)	Modulus Retention (%)	Strain at failure (%)
Prior Fatigue at R = -1						
80	Air	413.8	105.59	178.90	190.44	0.721
80	Steam	301.2	101.65	171.04	107.49	0.565
Prior Fatigue at R = 0.05						
100	Air	130	42.4	171.5	83.1	0.196
100	Steam	183.1	59.7	141.6	68.6	0.345

Fatigue failure envelopes are a convenient way of presenting fatigue data for a material. The fatigue envelope is a plot with the mean of the cyclic stress on the abscissa and the extremum of the cyclic stress (maximum and minimum) on the ordinate [19]. Figure 28 presents a typical fatigue envelope for the failure of a material after some number of cycles N_s. For this figure the failure mode will change from tension to compression when the mean stress passes through zero. For this effort as the failure mode observed for all specimens was in tension. Fatigue failure envelopes reveal fatigue behavior for all types of loading (tension-tension, compression-compression and tension-compression) [19].
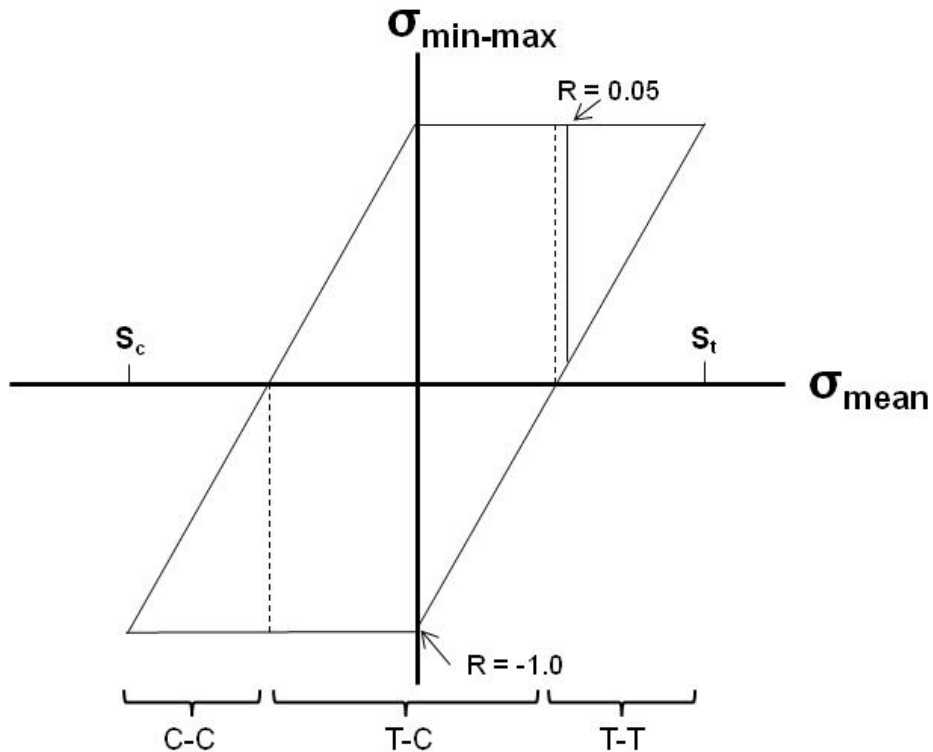
Figure 28: Fatigue failure envelope for N_s.

Figure 29 displays fatigue stress amplitude, mean stress, and cycles to failure data for Hi-Nicalon/PyC/HyprSiC at 1200°C in air and steam as a three-dimensional fatigue failure

49

envelope. Tension-tension fatigue data was taken from [7]. Data points corresponding to testing in laboratory air are given as triangles and connected with the two maximal and minimal surfaces. Test data points for testing in a steam environment are designated with squares and the two interior surfaces connect these points.

There currently is no available compression-compression fatigue data for Hi-Nicalon/PyC/HyprSiC at 1200°C in air and steam. Therefore Figure 29 shows only data for mean stresses greater than or equal to zero. From Figure 29 the reduction in cycle life at higher stress amplitudes due to the presence of steam is seen for tension-tension and tension-compression fatigue. For a given cycle life there is a tradeoff between increasing mean stress and decreasing stress amplitude.
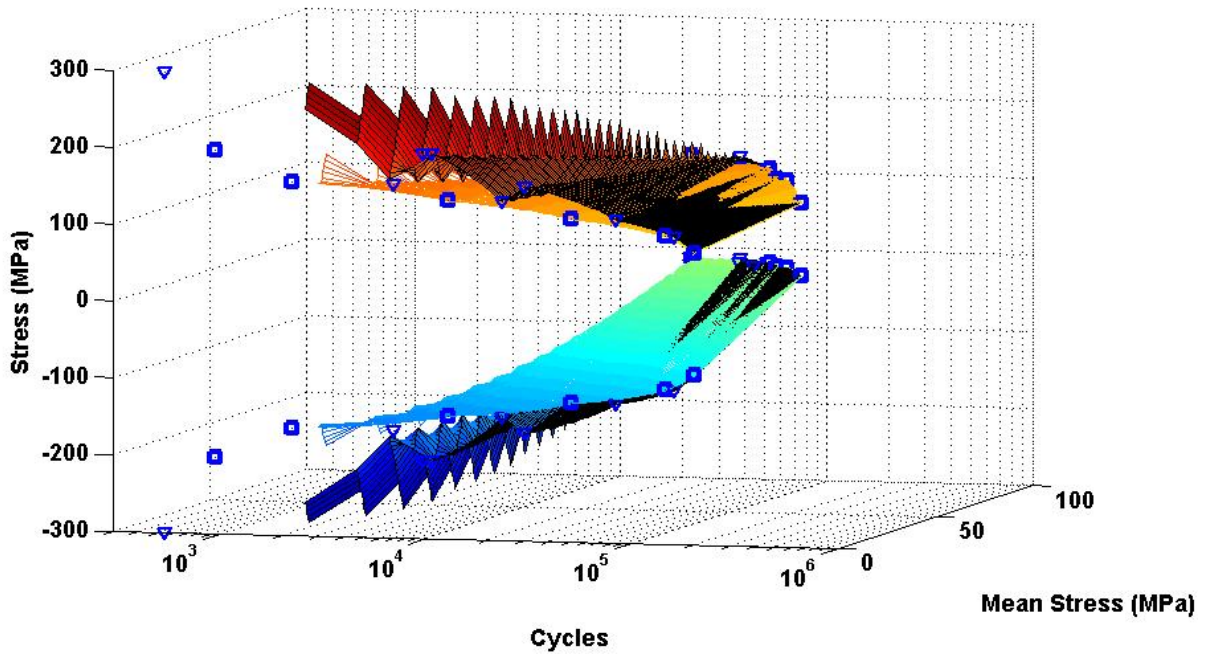
Figure 29: Fatigue failure envelope for Hi-Nicalon/PyC/HyprSiC tested at 1200°C in laboratory air and steam.

50

Failure envelopes combined on a three-dimensional plot reveal behavior over a range of fatigue testing conditions. The fatigue envelope shows areas of interest in the material behavior such as at larger stresses where the presence of steam has a greater effect. Such a procedure will significantly reduce test time and enhance the understanding of the overall fatigue process [19].

5.7 Compression-Tension Loading

Figure 30 shows the results of the compressive characterization of Hi-Nicalon/PyC/HyprSiC followed by a tensile loading to failure. Also displayed is the hysteresis loop for specimen P10-3, characteristic of specimens tested in tension-compression fatigue in air at stress levels below the proportional limit of 120 MPa. Performing a compression loading on an as processed specimen would highlight the effects of prior load history if any on the compressive response. The compressive modulus for the as processed material was found to be 176.7 GPa indicating that the CMC has a symmetric stress strain behavior in the linear region of response. When compared to specimens that underwent prior tensile loading and associated damage development the compressive response of the two are nearly identical. The compression-tension to failure test results were compared to results for pure tension to failure to assess the impact of prior compressive loading on the tensile behavior of the CMC in Figure 31. The dense matrix CMC tested in this effort the compressive response sees no effect from prior tensile loading. As seen in the stress-strain history for specimen's tested in tension-compression fatigue the compressive modulus undergoes very little change throughout the fatigue life of the specimen. After the initial compressive loading the specimen's ultimate tensile strength was found to be 385.5 MPa, within 5% of the UTS found for specimen P7-7 suggesting that the small amounts of

damage that do occur in compression do not adversely affect the tensile response in a short

duration test where oxidation effects are not present.
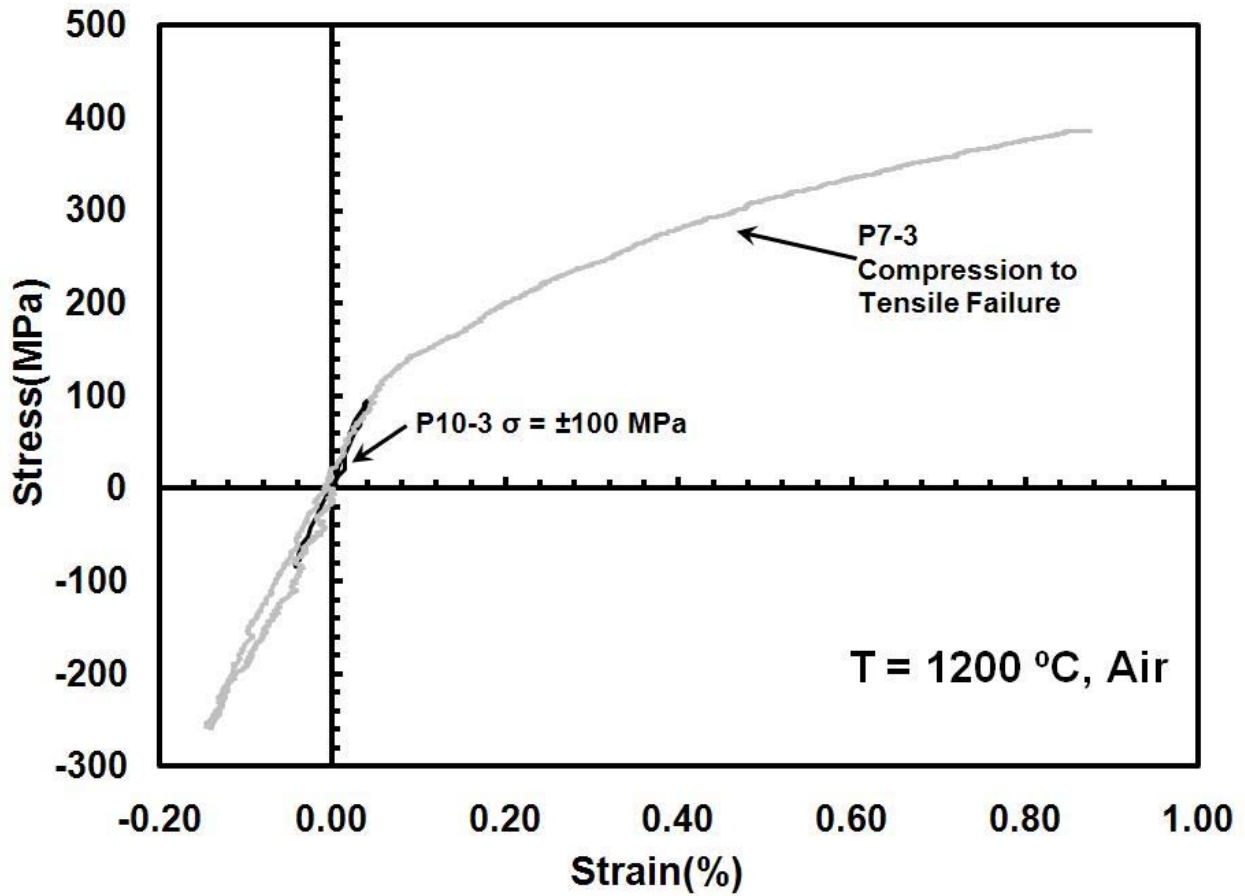
Figure 30: Stress-strain curve for as processed material loaded in compression-tension to failure compared to hysteresis curve of P10-3.
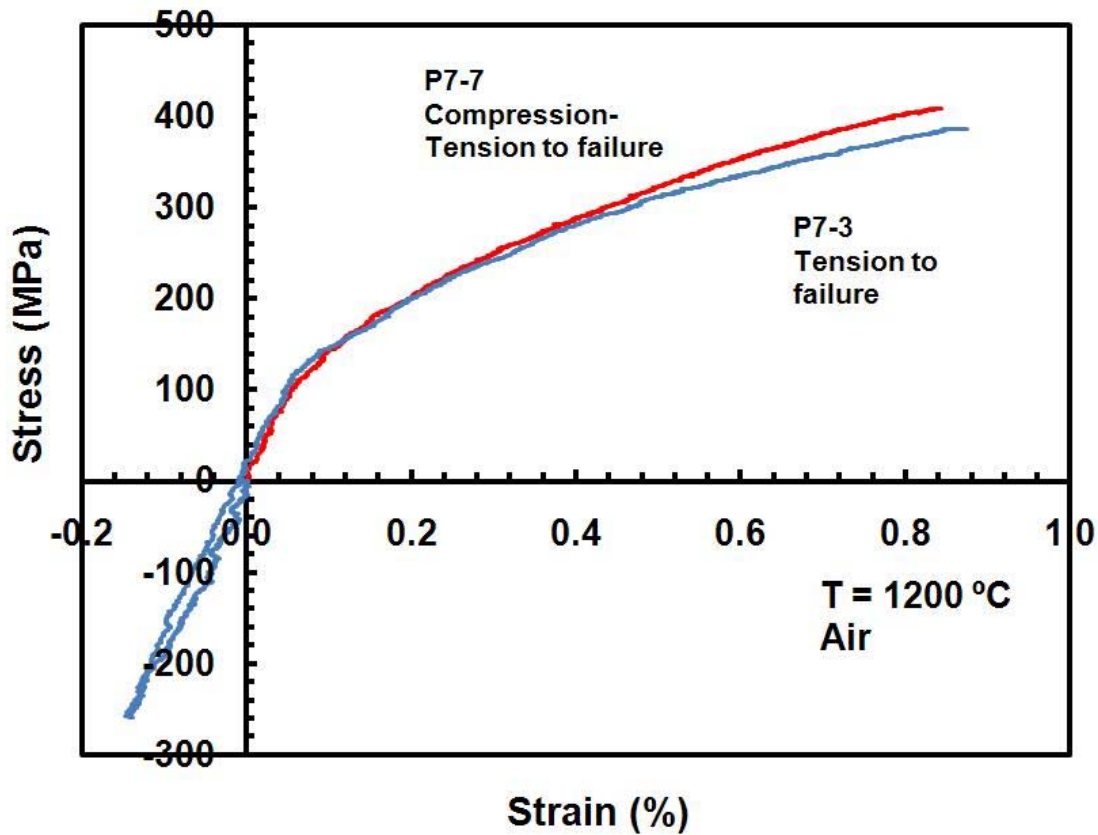
Figure 31: Stress-strain curve for as processed material tested in compression-tension to failure compared to tension to failure.

5.8 Microstructural Charaterization

Microstructural characterization of fracture surfaces tested to failure reveal the internal processes that affected failure mechanisms. Non oxidized specimens that maintained their fiber matrix interface coatings retained higher fracture toughness characteristics and overall better mechanical performance. SEM micrographs of characteristic non-oxidized and oxidized fracture surfaces are presented in Figure 32 and Figure 33 respectively. An optical micrograph of a specimen fracture surface showing oxidization and glass deposits is given in Figure 34.
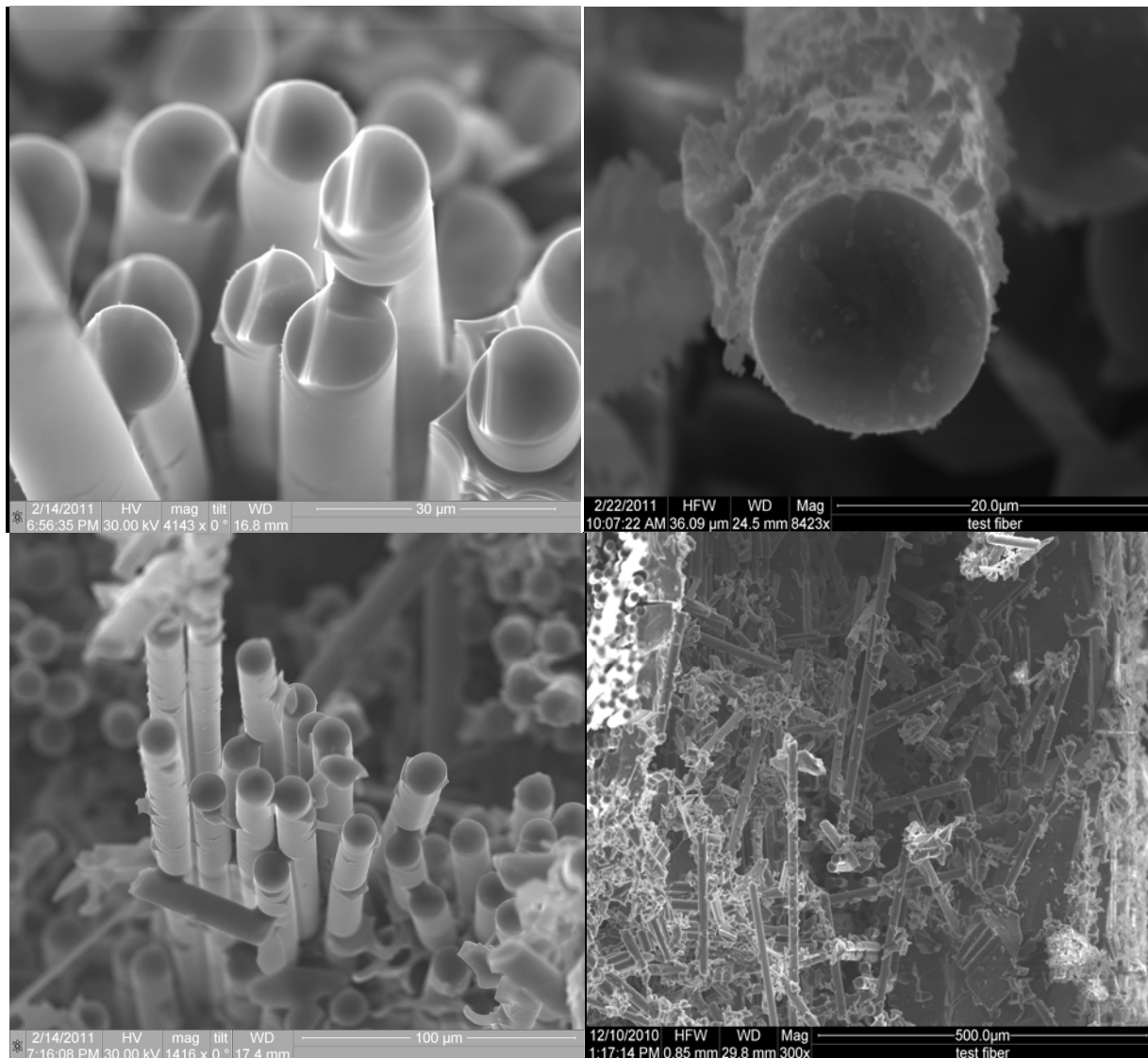
Figure 32: SEM micrograph of non oxidized fracture surface for 0.05mm/s tension to failure test at 1200°C in air on specimen P7-7.
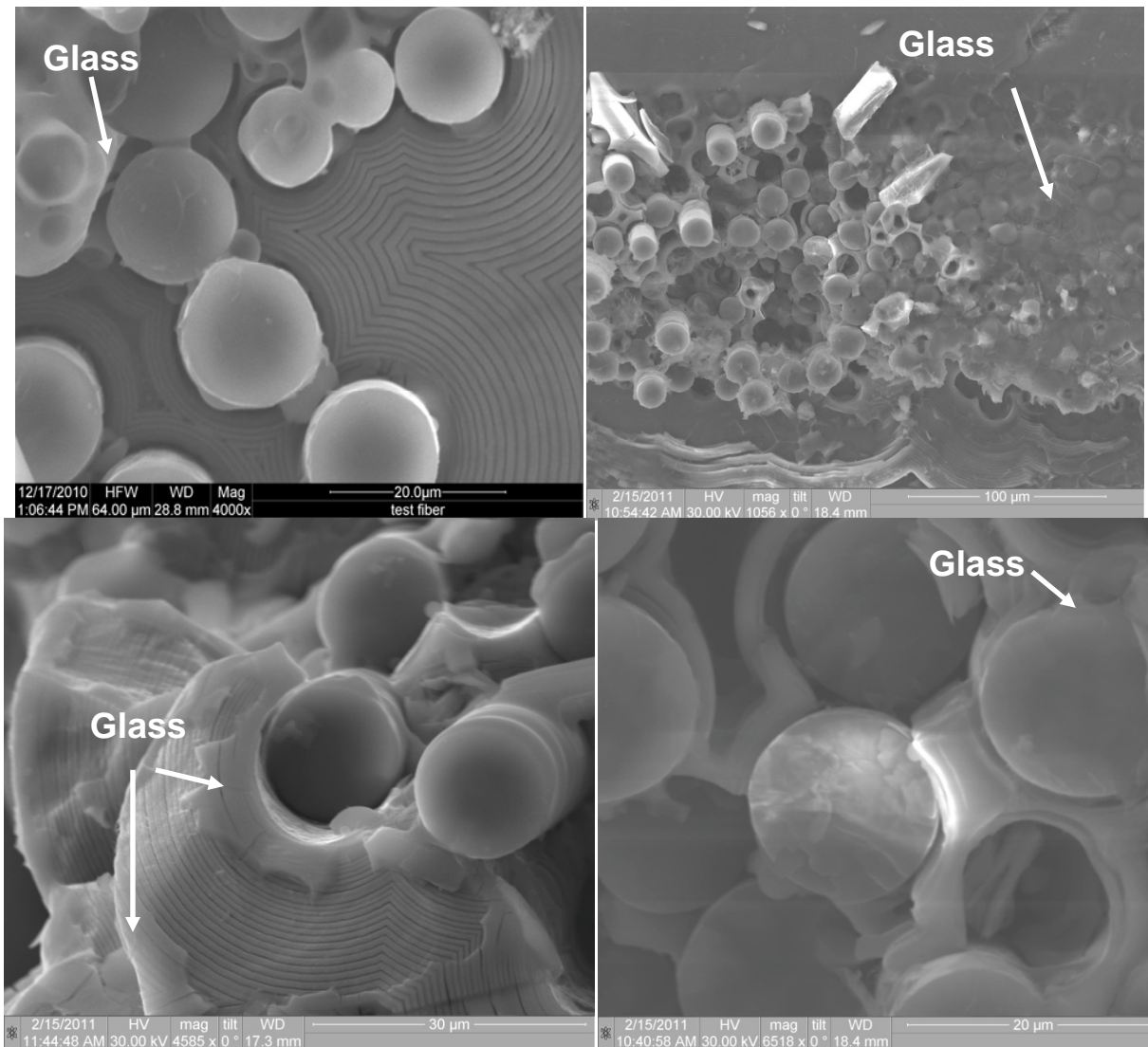
Figure 33: SEM micrograph of oxidized fracture surface for P5-2 tested in fatigue at 1200°C in steam. σ = 80 MPa, N_f =200000.

Non oxidized fracture surfaces as characterized by Figure 32 display high degrees of fiber pull out and almost no glass formation. The fiber pull out is facilitated by the PyC and boron fiber matrix interface. Boron and carbon are highly susceptible to oxidation and are chosen as fiber coatings to provide adequate debonding to increase fracture toughness [13]. Compared to the irregular and fibrous nature of a non-oxidized failure surface, oxidized fracture surfaces are

typically flat with little evidence of fiber pull out. This is commonly due to the formation of a

SiO$_2$ layer across the exposed surface. The environment degrades the fiber matrix interface

coating allowing cracks to propagate directly from the matrix to the fiber. Oxidation can be

considered to progress at the same rate as the growing cracks as shown by the proximity of

oxidized and non oxidized fiber failure shown in many specimens.
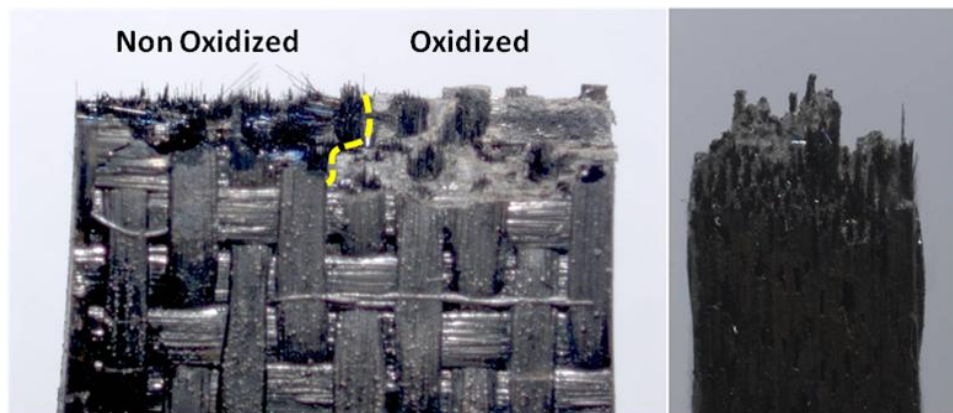
Figure 34: Optical micrograph of specimen P10-7 fracture surface.

Characteristics of oxidized and non-oxidized fracture surfaces can often be distinguished if the

degree of glass formation is severe enough. The optical micrograph in Figure 34 shows oxidation

and glass deposits associated with an advancing fatigue crack for a specimen tested a steam

environment. Specimen P10-7 also shows and a final failure surface of high fiber pull out

characteristic of non oxidized material.

5.8.1 Microstructure of Specimens Tested in Tension to Failure

The fracture surfaces of specimens that were tested in monotonic tension to failure

examined with the optical microscope and SEM. Figure 35 through Figure 37 show the optical

micrographs of the fracture surfaces. Fiber pull-out is evident in all the fracture surfaces.

Specimens P5-7 and P10-8 show some localized delamination occurring in the fracture surface. This could be due to a weak lamina or poor lamina bonding brought on as a result of the CVI material processing.

Figure 35: Optical micrographs of specimen P5-7 tested in tension at 1200°C in air. UTS = 296.3 MPa.
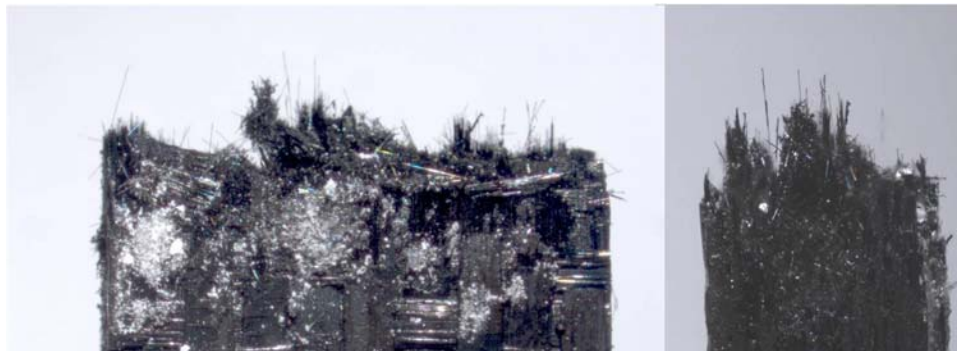
Figure 36: Optical micrographs of specimen P7-7 tested in tension at 1200°C in air. UTS = 406.9 MPa.

Figure 37: Optical micrographs of specimen P10-8 tested in tension at 1200°C in air. UTS = 391.9 MPa.

SEM micrographs of the tension to failure fracture surface of specimen P7-7 are presented in Figure 32. The SEM micrograph shows details of fiber pull-out and the absence of noticeable oxidation to the SiC matrix. Brittle fiber fracture is the accompanied with fiber pull-out is the dominant failure mechanism. The lack of any oxidation is due to the short time the specimen spent in the 1200°C air environment. The micrographs presented in Figure 32 are characteristic of non oxidized fracture surfaces seen throughout this testing effort.

5.8.2 Microstructure of Specimens Tested in Tension-Compression Fatigue

Specimens tested in tension-compression fatigue were examined with the optical microscope and SEM. Optical micrographs of the fracture surfaces for specimens tested with a maximum stress of 80 MPa in air and steam are presented in Figure 38 and Figure 39. The optical micrographs of fracture surfaces for specimens tested in fatigue with a maximum stress of 200 MPa in air and steam are given in Figure 40 and Figure 41 respectively.
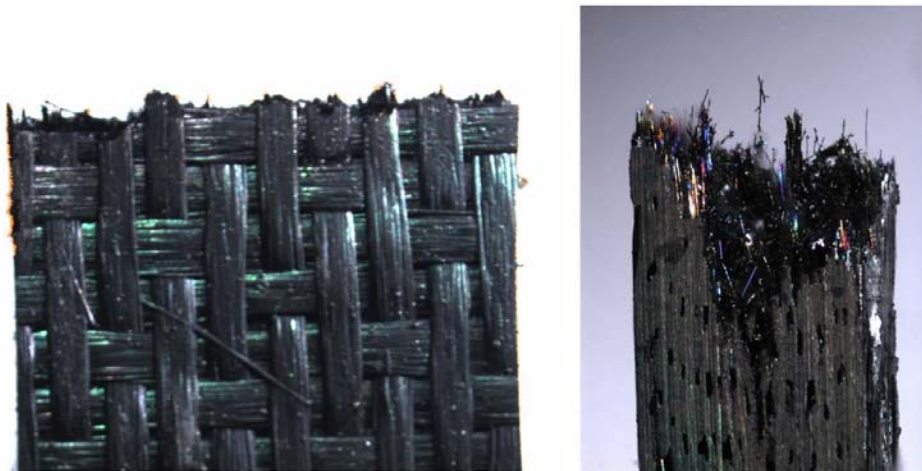
Figure 38: Optical micrograph of specimen P10-6 tested in fatigue at 1200°C in air. σ = 80 MPa, N_f =200000.

Specimen P10-6 reached run out and was then subjected to tension to failure. Its fracture surface is nearly identical to those observed for monotonic tension to failure specimens.

Significant fiber pull out and a nearly uniform fracture surface are evidence of little to no oxidation effects in the CMC.

Figure 39: Optical micrograph of specimen P5-2 tested in fatigue at 1200°C in steam. σ = 80 MPa, N_f =200000.

Figure 40: Optical micrograph of specimen P7-8 tested in fatigue at 1200°C in air. σ = 200 MPa, N_f =10656.

Figure 41: Optical micrograph of specimen P7-4 tested in fatigue at 1200°C in steam. σ = 200 MPa, N$_f$ =948.

Specimens tested in a steam environment formed glass (SiO$_2$) deposits on the fracture surface. Longer exposure to the oxidizing environment typically corresponded to higher amounts of glass. Specimen P5-2 having reached run-out at $2x10^5$ cycles has significant SiO$_2$ formations on the specimen surface, as well as on the fracture surface as evident in Figure 39. Specimen P7-4 given in Figure 41 does not display glass formations characteristic of fatigue testing in steam at 1200°C due to the relatively short (N$_f$ =948 cycles) exposure time. Specimens tested at maximum stress levels of 80MPa and 200MPa in air and steam environments demonstrated fiber pull-out as well as tensile failure modes.

Composite SEM micrograph images of the fracture surfaces of specimens tested in fatigue at 1200°C in air and steam with a maximum stress ranging from 80 MPA to 200 MPa are given in Figure 42 through Figure 52. The fracture surface was divided into relative areas of oxidized and non oxidized fracture. Specimens P10-6 and P5-2 given in Figure 42 and Figure 43 reached run out and were subsequently tested in tension to failure. Their fracture surfaces are characteristic of tension to failure specimens seen in section 5.8.1 with minimal oxidation and

primarily fiber pull out failure. Specimen P5-2 developed glass deposits along an isolated

environmental attack pathway originating from the left of the fracture surface.
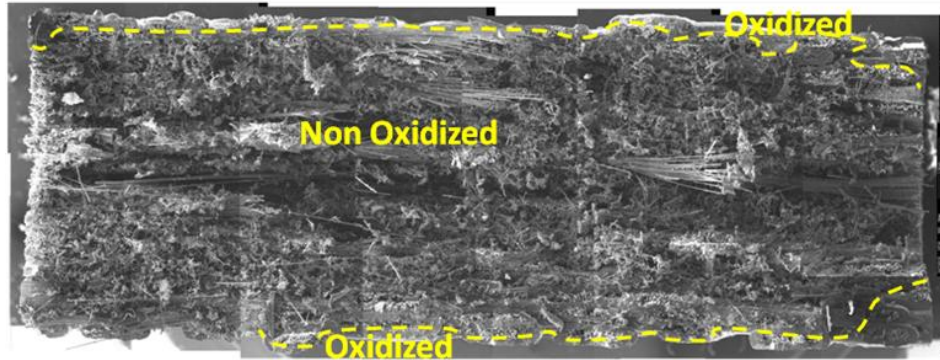
Figure 42: SEM micrograph specimen P10-6 fracture surface tested in fatigue at 1200°C in air. σ = 80 MPa, N_f =200000.
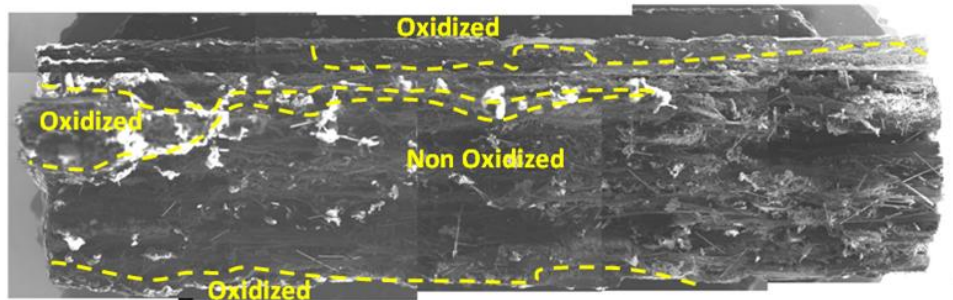
Figure 43: SEM micrograph specimen P5-2 fracture surface tested in fatigue at 1200°C in steam. σ = 80 MPa, N_f =200000.

Fatigue testing carried out at maximum stress levels greater than 100 MPa show much

more extensive oxidized regions. Small matrix cracks combine forming a dominant unbridged

crack providing a pathway for the oxidizing environment to enter the CMC. For testing in both

air and steam the extent of oxidation is approximately inversely proportional to the maximum

stress. At lower maximum stress levels the fatigue life of the specimen is greater, allowing for

longer matrix exposure times and subsequent oxidation.
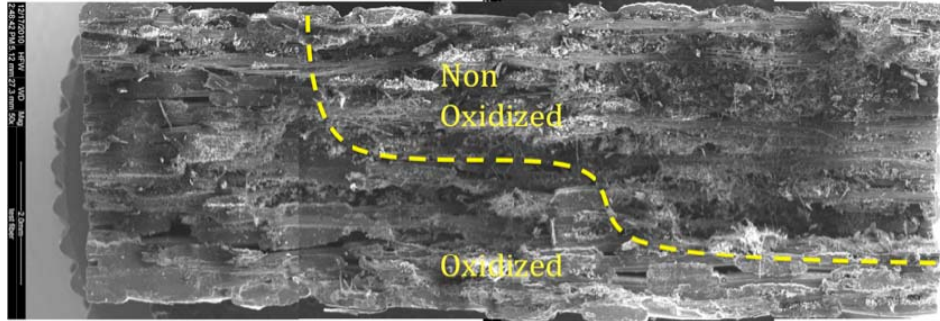
Figure 44: SEM micrograph specimen P10-3 fracture surface tested in fatigue at 1200°C in air. σ = 100 MPa, N_f =161110.
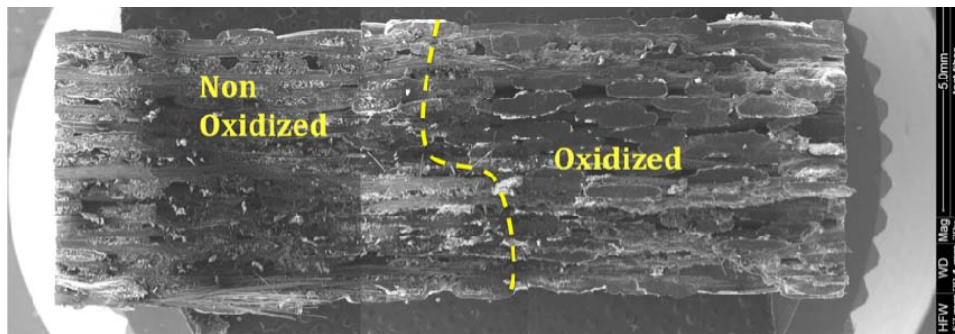
Figure 45: SEM micrograph of specimen P10-7 fracture surface, tested in fatigue at 1200°C in steam. σ = 100 MPa, N_f =144519.
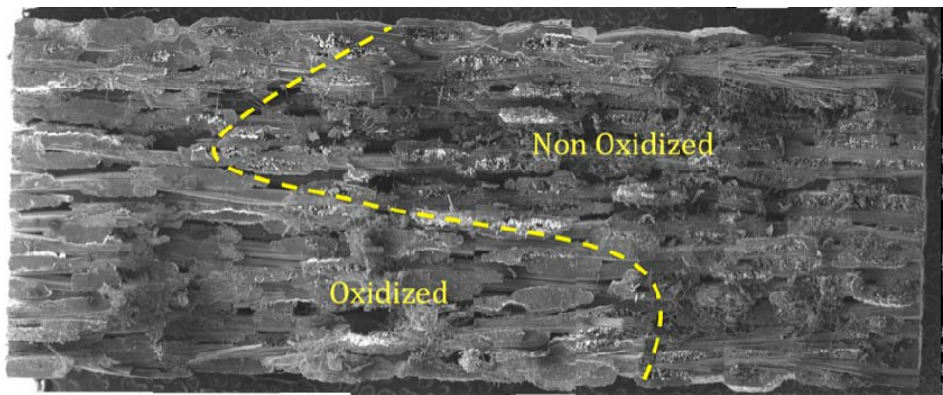
Figure 46: SEM micrograph of specimen P10-5 fracture surface, tested in fatigue at 1200°C in air. σ = 120 MPa, N_f =83799.
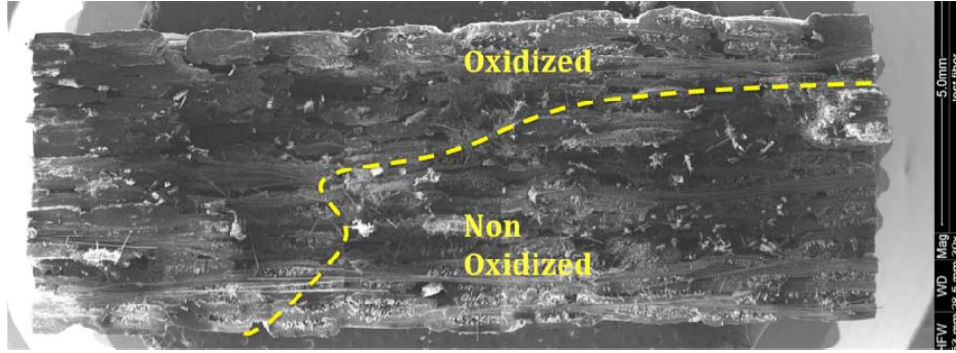
Figure 47: SEM micrograph of specimen P10-1 fracture surface, tested in fatigue at 1200°C in steam. σ = 120 MPa, N_f =50499.
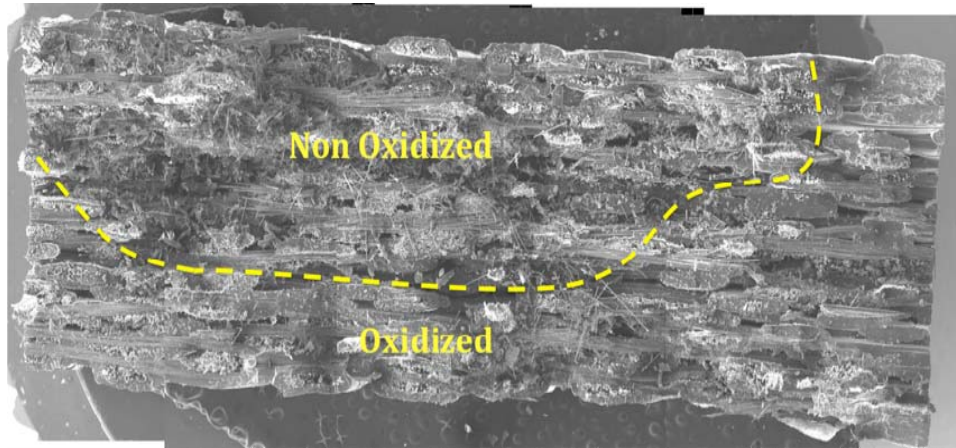
Figure 48: SEM micrograph of specimen P10-2 fracture surface, tested in fatigue at 1200°C in air. σ = 140 MPa, N_f =23277.
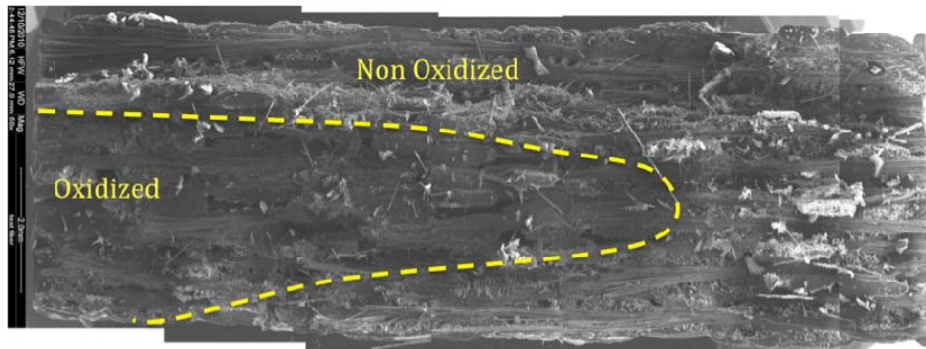
Figure 49: SEM micrograph of specimen P5-4 fracture surface, tested in fatigue at 1200°C in steam. σ = 140 MPa, N_f =12784.
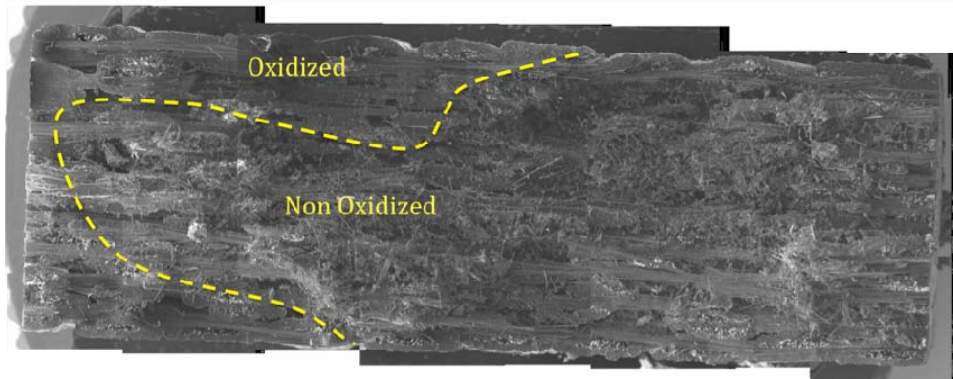
Figure 50: SEM micrograph of specimen P7-1 fracture surface, tested in fatigue at 1200°C in air. σ = 160 MPa, N_f =6914.
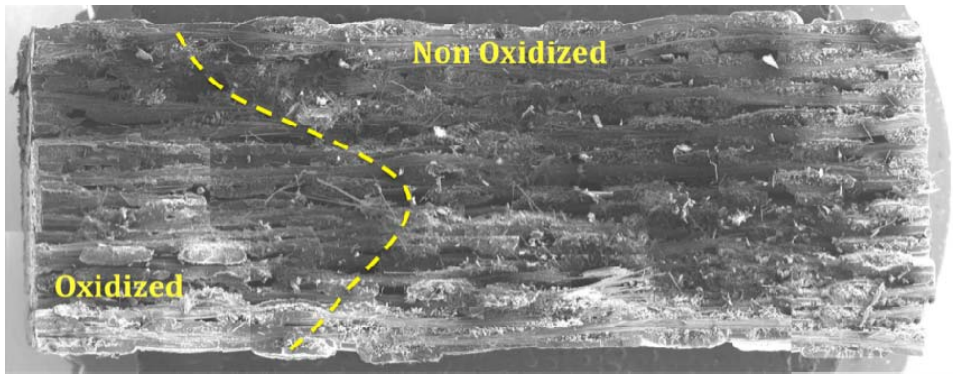
Figure 51: SEM micrograph of specimen P7-2 fracture surface, tested in fatigue at 1200°C in steam. σ = 160 MPa, N_f =2214.
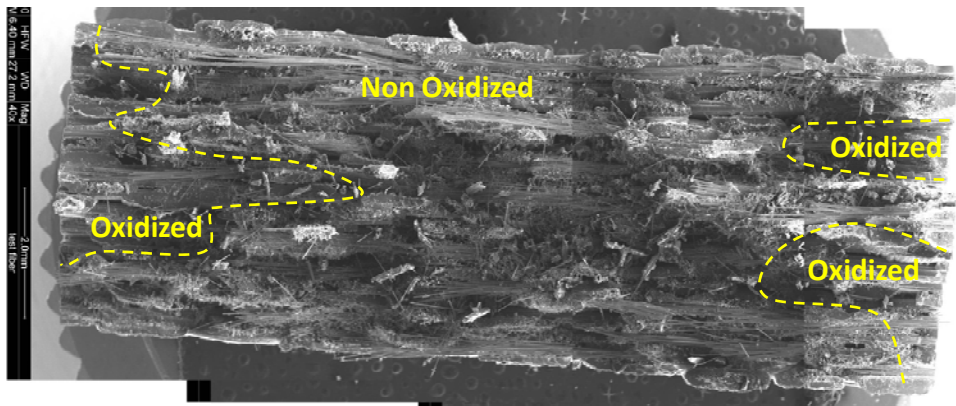
Figure 52: SEM micrograph of specimen P7-4 fracture surface, tested in fatigue at 1200°C in steam. σ = 200 MPa, N_f =948.

The boundaries of the oxidized regions of the fracture surfaces extend inward along the direction of the transverse fibers. This behavior is readily seen in Figure 52, Figure 50, and Figure 49. Voids created by the transverse fibers provide the initial avenues from which the oxidizing environment can enter the specimen. As the test is prolonged at lower maximum stress levels the oxidized surface spreads interlaminarly through the thickness of the test specimen.

A SEM micrograph of a polished section of specimen P10-6 oriented normal to the loading direction is shown in Figure 53. Fibers oriented in the loading direction are denoted as being in the material's 1 co-ordinate direction. Fibers in the same lamina, oriented transverse to the loading direction are in the 3 direction. The through thickness of the specimen, completing the right hand co-ordinate system is the 2 direction. Figure 53 shows longitudinal cracks in the 1-2 and 1-3 plane of the specimen. These longitudinal cracks were typical of those observed for all polished specimens investigated by the SEM. The cracks originate from stress concentrations brought on by voids in the matrix material. As the crack progresses though the matrix it is deflected at the fiber matrix interface and does not propagate through the fiber. This is due to the B_4C PyC fiber coating that has not been affected by oxidation. These longitudinal cracks are brought on by the Poisson's effect of the material when it is loaded in compression. Compressive testing done on a CMC with a similarly dense matrix as Hi-Nicalon/ PyC/HyprSiC displayed the same effect [12].
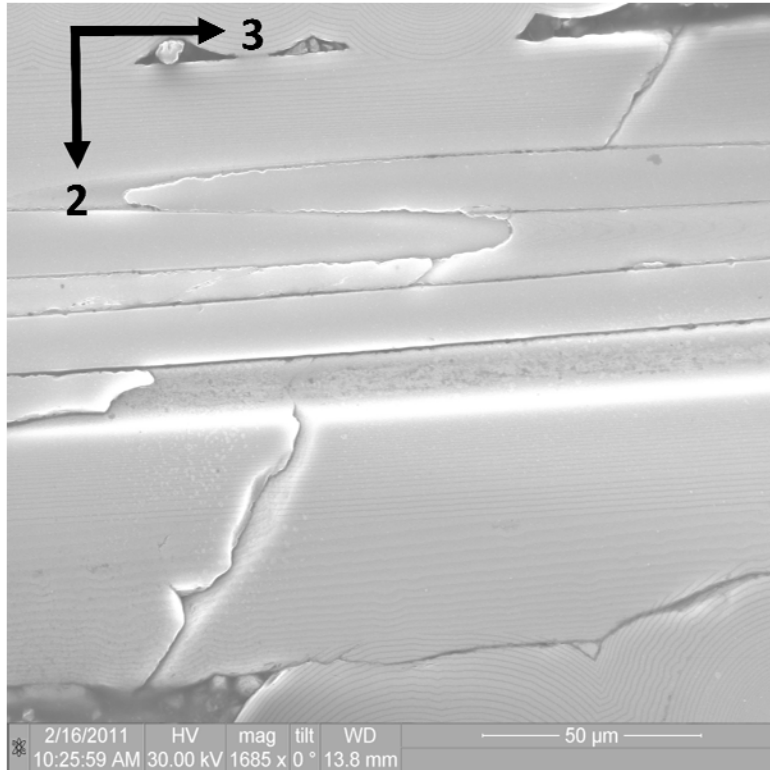
Figure 53: Longitudinal crack in 1-2 and 1-3 planes of specimen P10-6.

Matrix cracking orientations relative to loading condition are presented in Figure 54.
Previous work done in tension-tension by Delapasse [7] showed only the mode 1 cracking
brought on by tension loading. The presence of a compressive stroke in the fatigue cycle for the
testing carried out in this effort introduced crack surfaces parallel to the loading direction. For
equivalent maximum stress levels, specimens tested in fully reversed fatigue developed more
matrix cracking than those tested in tension-tension fatigue. Further the orientation of voids in
the lamina of the CMC served to promote the formation of cracks brought on by the compressive
loading portion. Cracks parallel to the loading direction originating from a matrix void in the
CMC are visible in Figure 53.
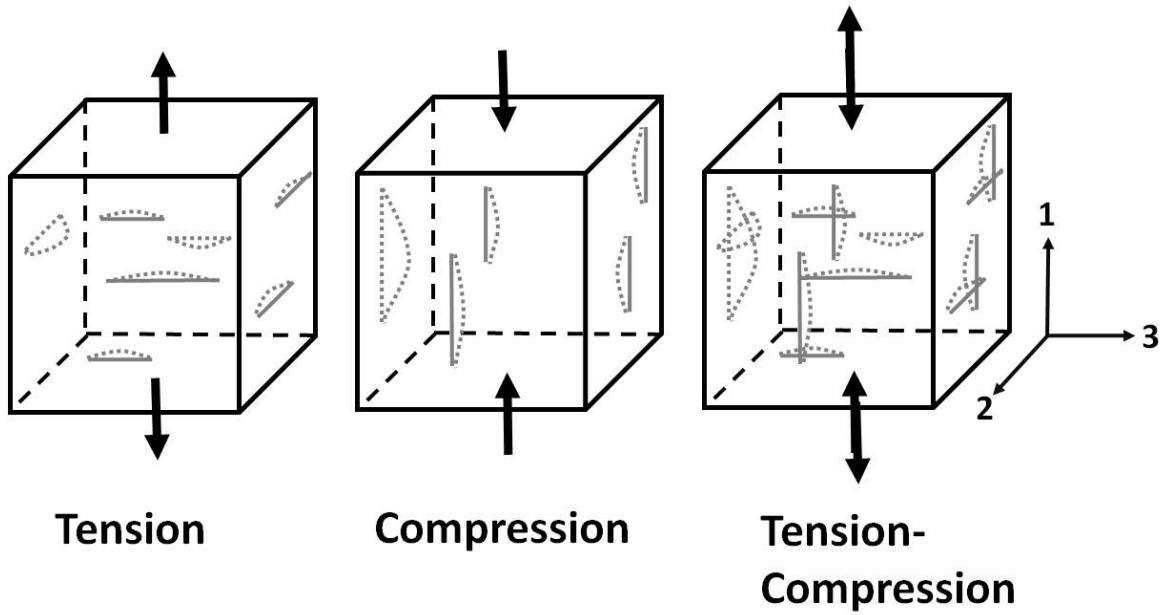
Figure 54: Material element crack development for tension, compression, and tension-compression loading for mode 1.

Specimens tested in this effort reached shorter fatigue lives than those tested in tension-tension due to the development of more matrix cracks caused by compression. The oxidizing test environment had a more pronounced reduction for testing conducted in steam as shown in Figure 20.

V1. Conclusion and Recommendations

6.1 Conclusion

Hi-Nicalon/PyC/HyprSiC demonstrated encouraging response to fully reversed cyclic fatigue at 1200°C in air and steam. The fatigue life of the composite decreased with increasing magnitude of fatigue stress. Fatigue run-out was achieved in both air and steam at 80 MPa. The presence of steam in the test environment further reduced resistance of the CMC to fatigue. Hi-Nicalon/PyC/HyprSiC did not experience strain ratcheting due to the presence of the compressive load in the fatigue cycle. The material did exhibit a reduction in tensile modulus with increasing cycle number, however the reduction was independent of the stress level or presence of steam.

The CMC's response to compressive loads was found to contribute to shorter fatigue lives due to the development of additional cracking. The compressive response during fatigue is identical to that of the as-processed material. Retained tensile properties showed little influence of prior fatigue, retaining 100% of their strength and stiffness. This contrasts with previous tension-tension testing that demonstrated a large effect on the retained tensile strength of Hi-Nicalon/PyC/HyprSiC [7].

Optical examination of the fracture surfaces under SEM revealed higher amounts of oxidation and silicon dioxide formations on specimens tested in steam. Typically oxidation existed only on the outer edge of the fracture surface. In some specimens a dominant crack formed, and led to a large area of the fracture surface becoming highly oxidized. Outside of the dominant crack surface, and away from the edges failure exhibited fiber pullout.

6.2 Recommendations

Characterization of the effects of compressive loads during fatigue response of Hi-Nicalon/PyC/HyprSiC should be further investigated. Compression-compression testing at various mean stress values in air and steam would provide data to complete the fatigue envelope of this material. Additionally the fatigue history effects of varying the R ratio during a fatigue test would give insight into the material behavior.

Appendix A
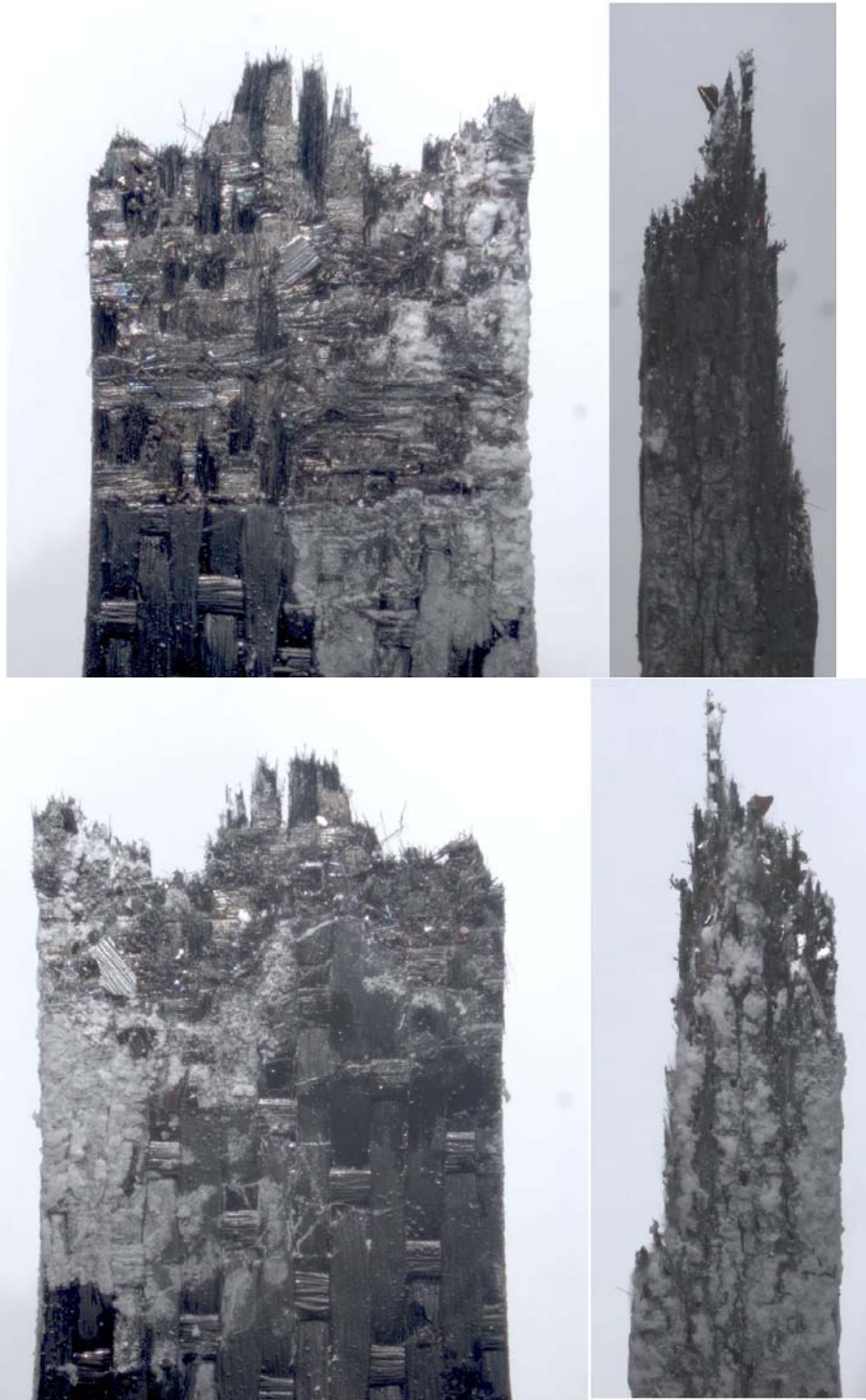
Figure 55: Optical micrographs of specimen P5-2 tested in fatigue at 1200°C in steam . σ = 80 MPa, N$_f$ =200000.

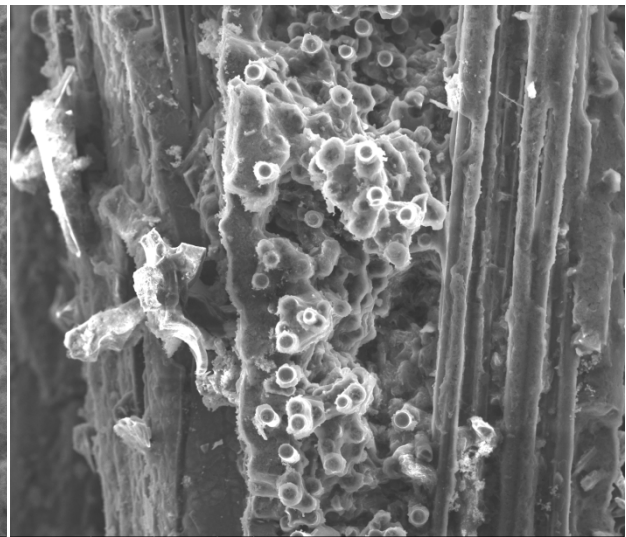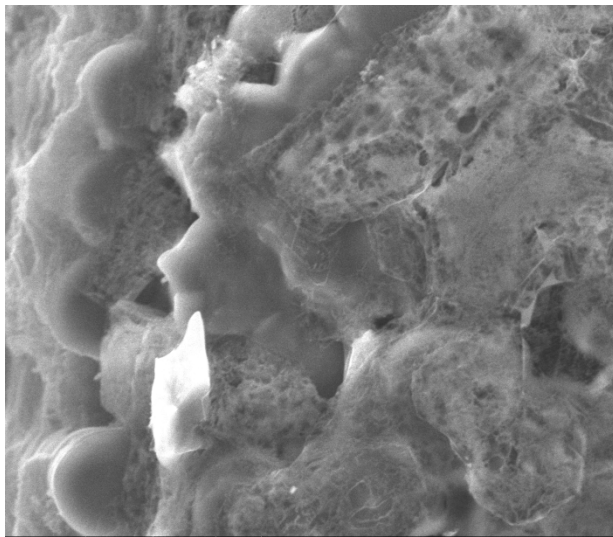**Figure 56: Optical micrographs of specimen P5-3 tested in fatigue at 1200°C in air. σ = 160 MPa, N_f =29988.**

Figure 57: Optical micrographs of specimen P5-4 tested in fatigue at 1200°C in steam. σ = 140 MPa, N_f =12784.

Figure 58: Optical micrographs of specimen P5-7 tested in tension at 1200°C in air. UTS = 296.3 MPa.

Figure 59: Optical micrographs of specimen P7-1 tested in fatigue at 1200°C in air. σ = 160 MPa, N_f =6914.

Figure 60: Optical micrographs of specimen P7-2 tested in fatigue at 1200°C in steam. σ = 160 MPa, N_f =2214.
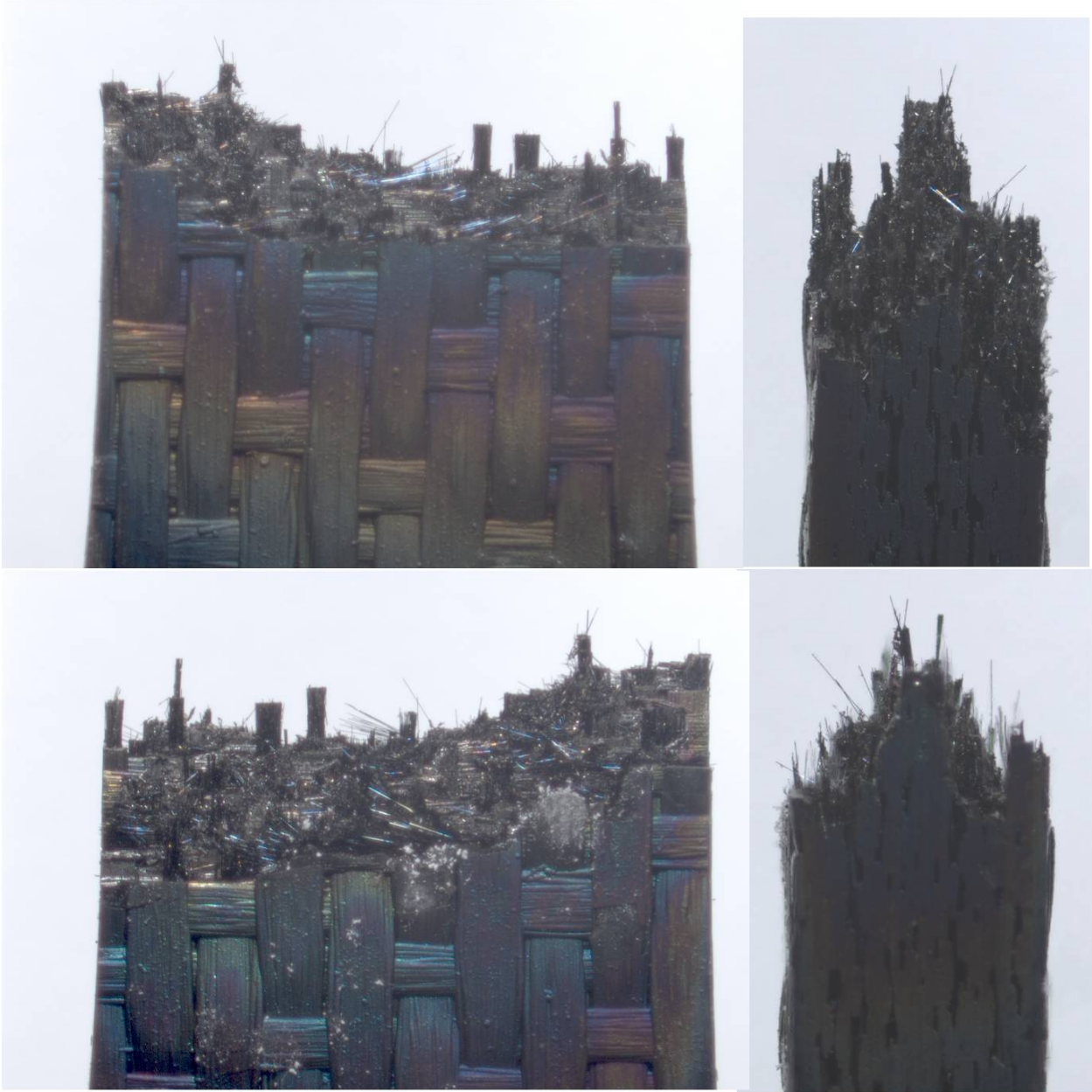
Figure 61: Optical micrographs of specimen P7-4 tested in fatigue at 1200°C in steam. σ = 200 MPa, N_f =948.

Figure 62: Optical micrographs of specimen P7-7 tested in tension at 1200°C in air. UTS = 406.9 MPa.
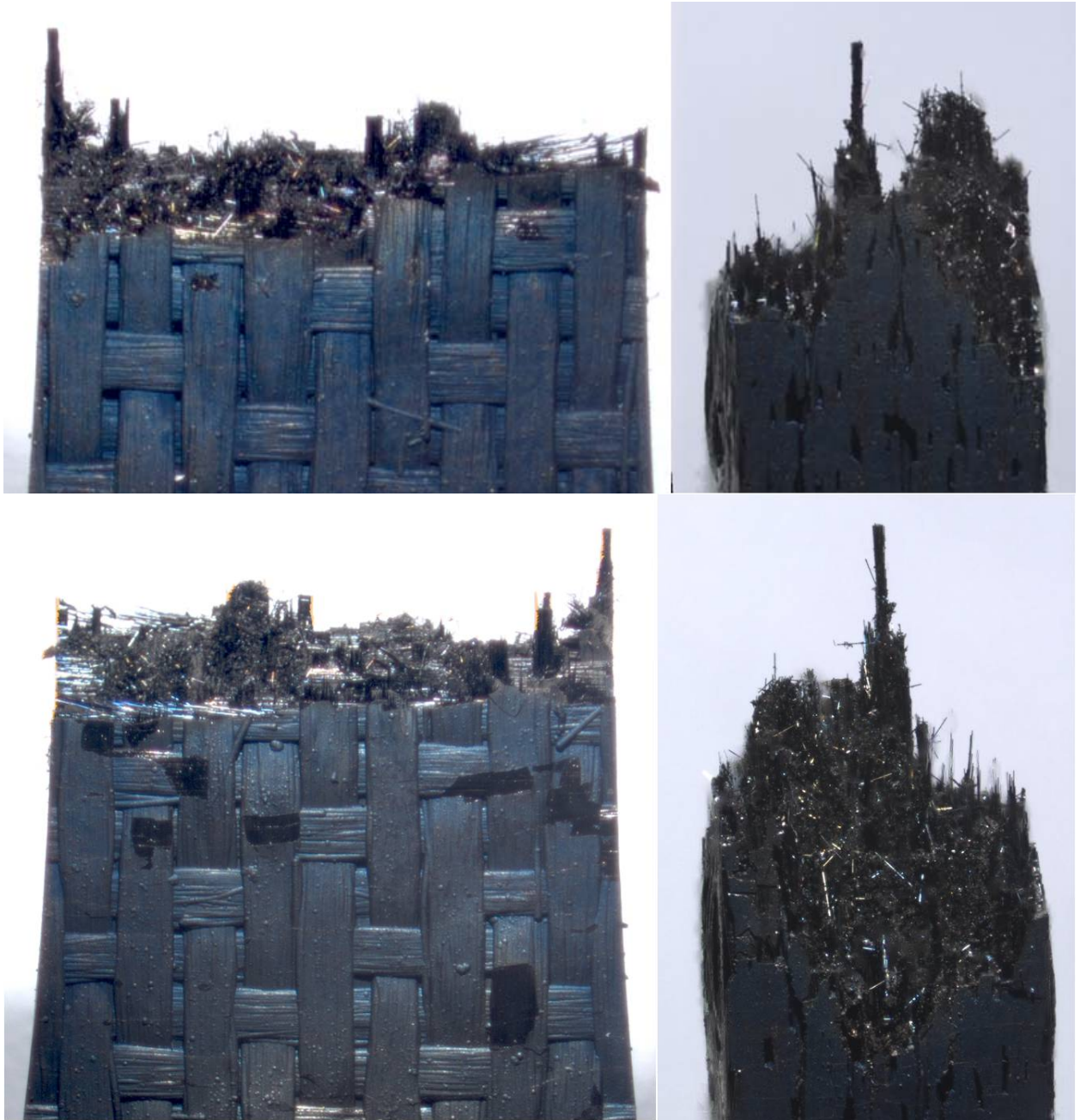
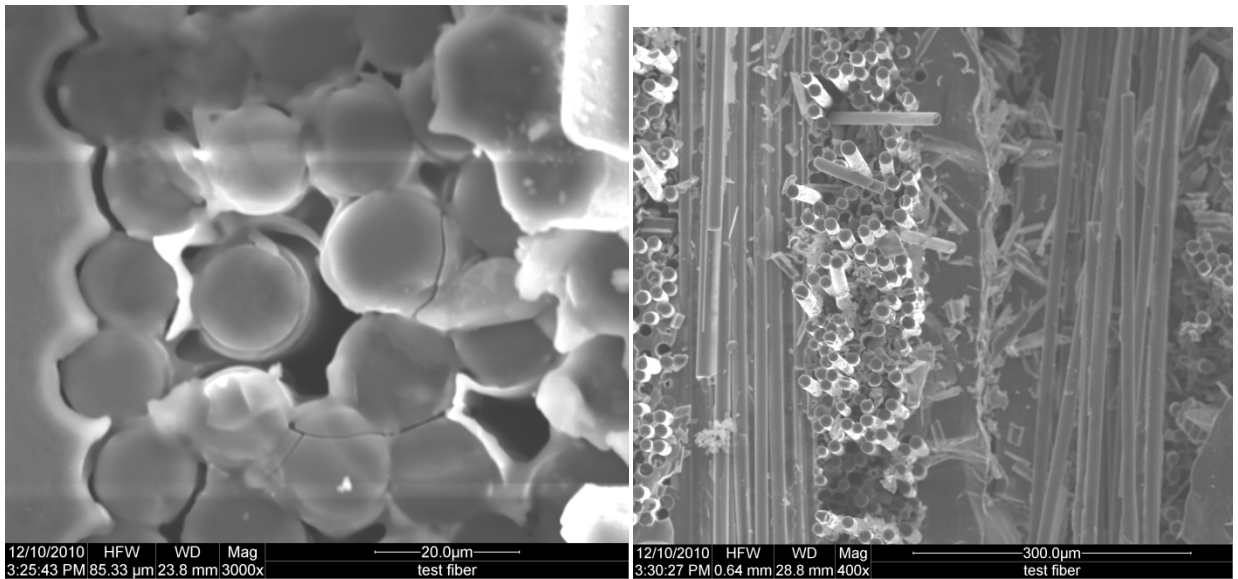**Figure 63: Optical micrographs of specimen P7-8 tested in fatigue at 1200°C in air. σ = 200 MPa, N_f =10656.**
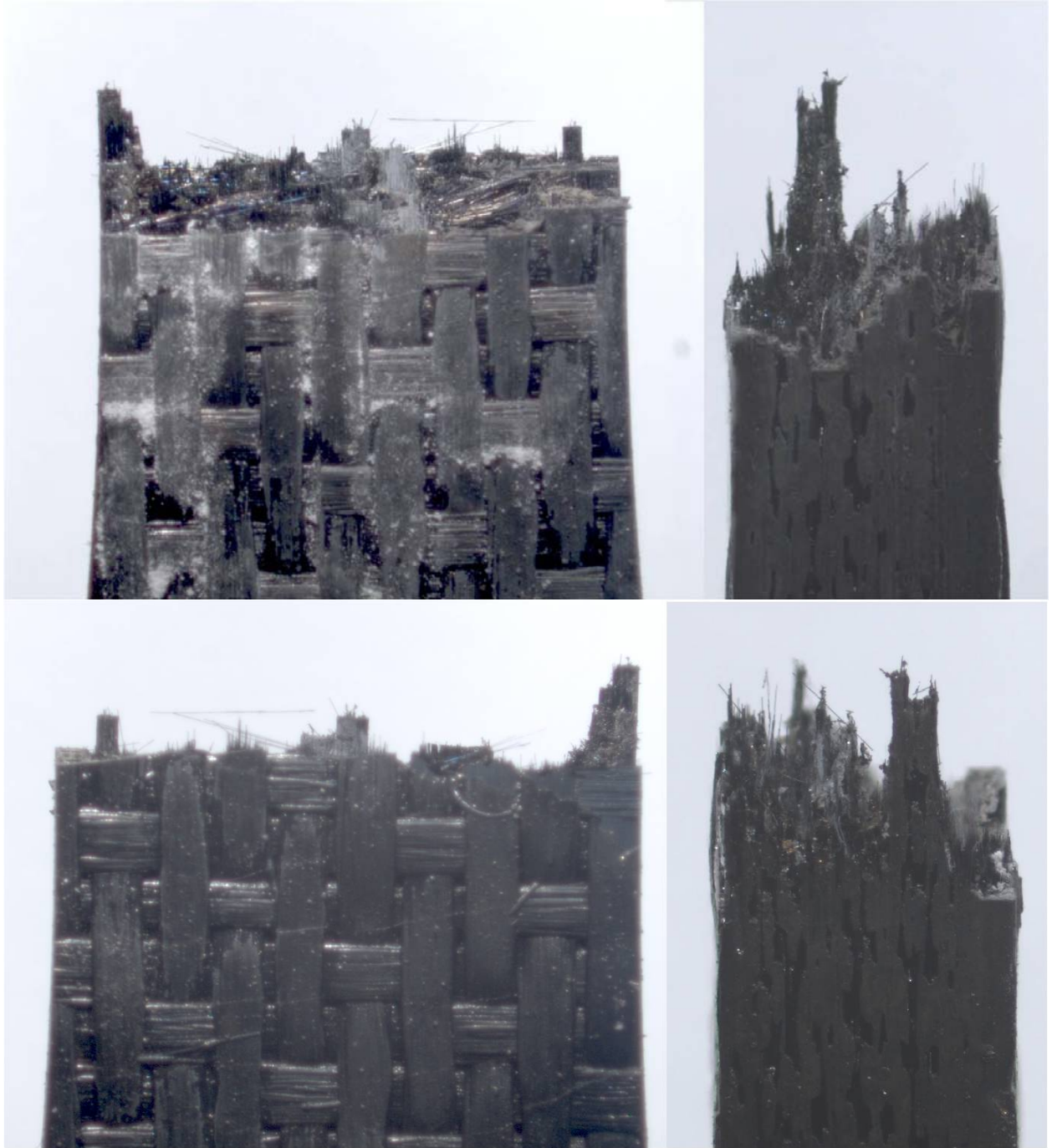
Figure 64: Optical micrographs of specimen P10-1 tested in fatigue at 1200°C in steam. σ = 120 MPa, N_f =50499.
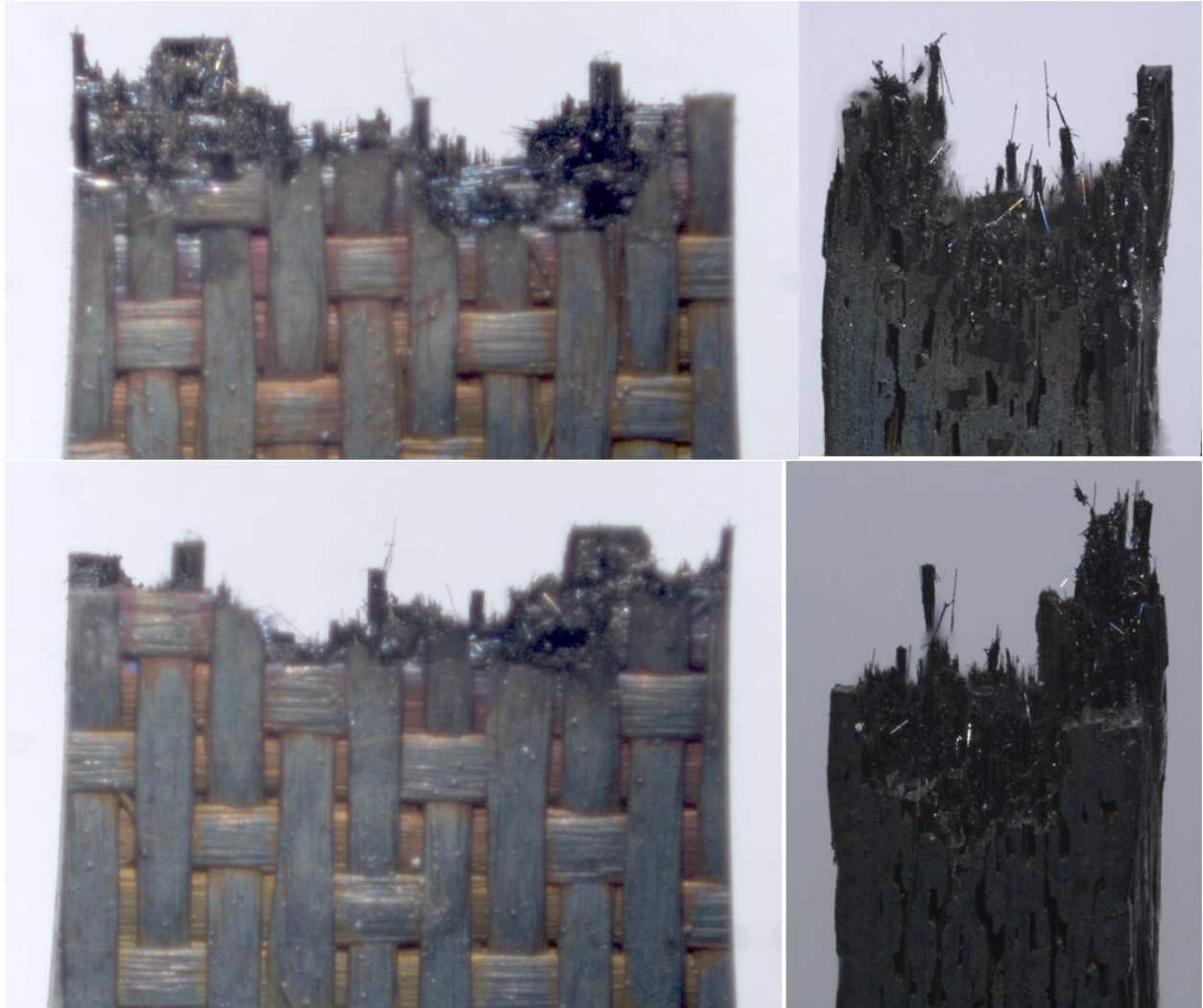
Figure 65: Optical micrographs of specimen P10-2 tested in fatigue at 1200°C in air. σ = 140 MPa, N_f =23277.
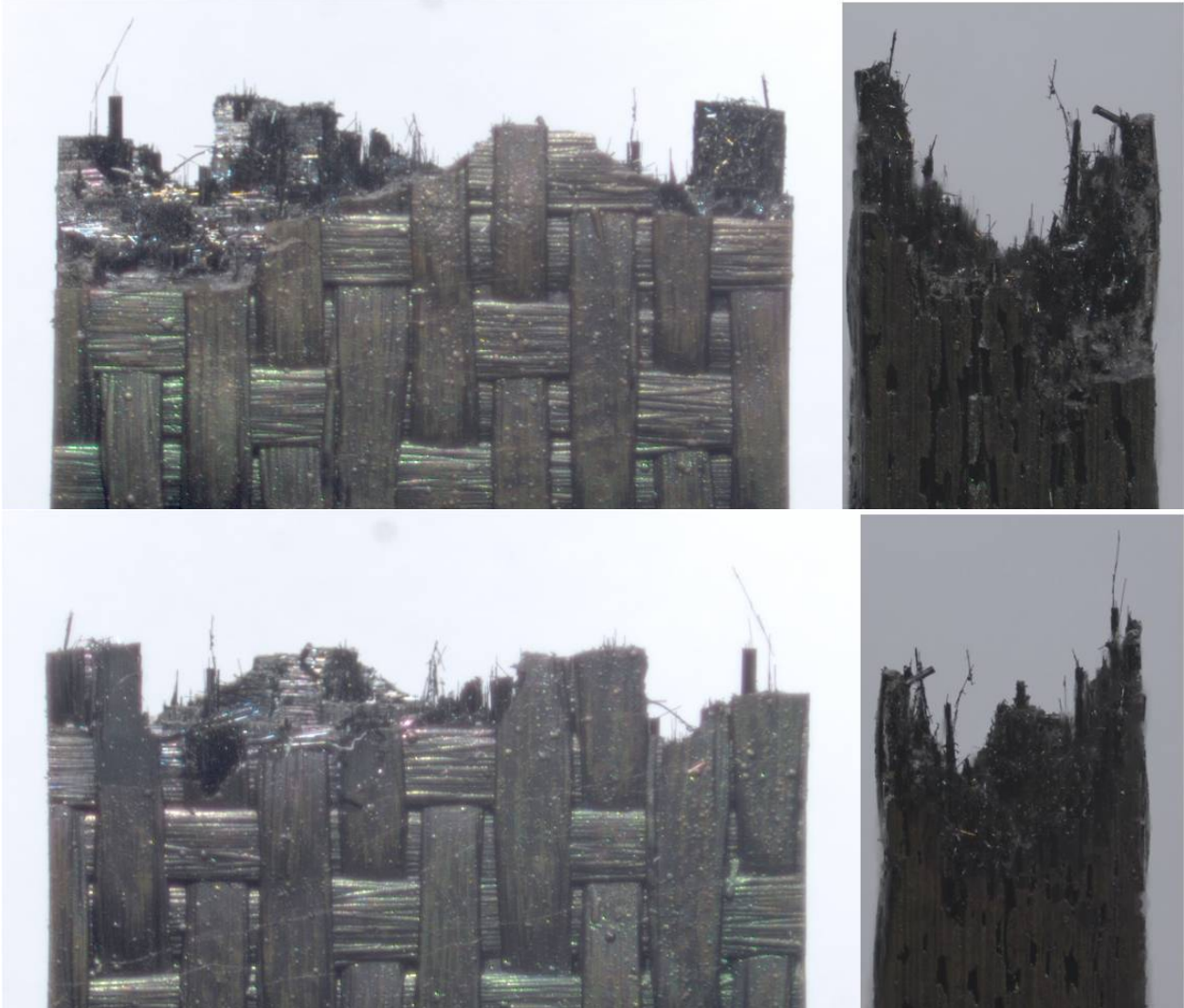
Figure 66: Optical micrographs of specimen P10-3 tested in fatigue at 1200°C in air. σ = 100 MPa, N_f =161110.
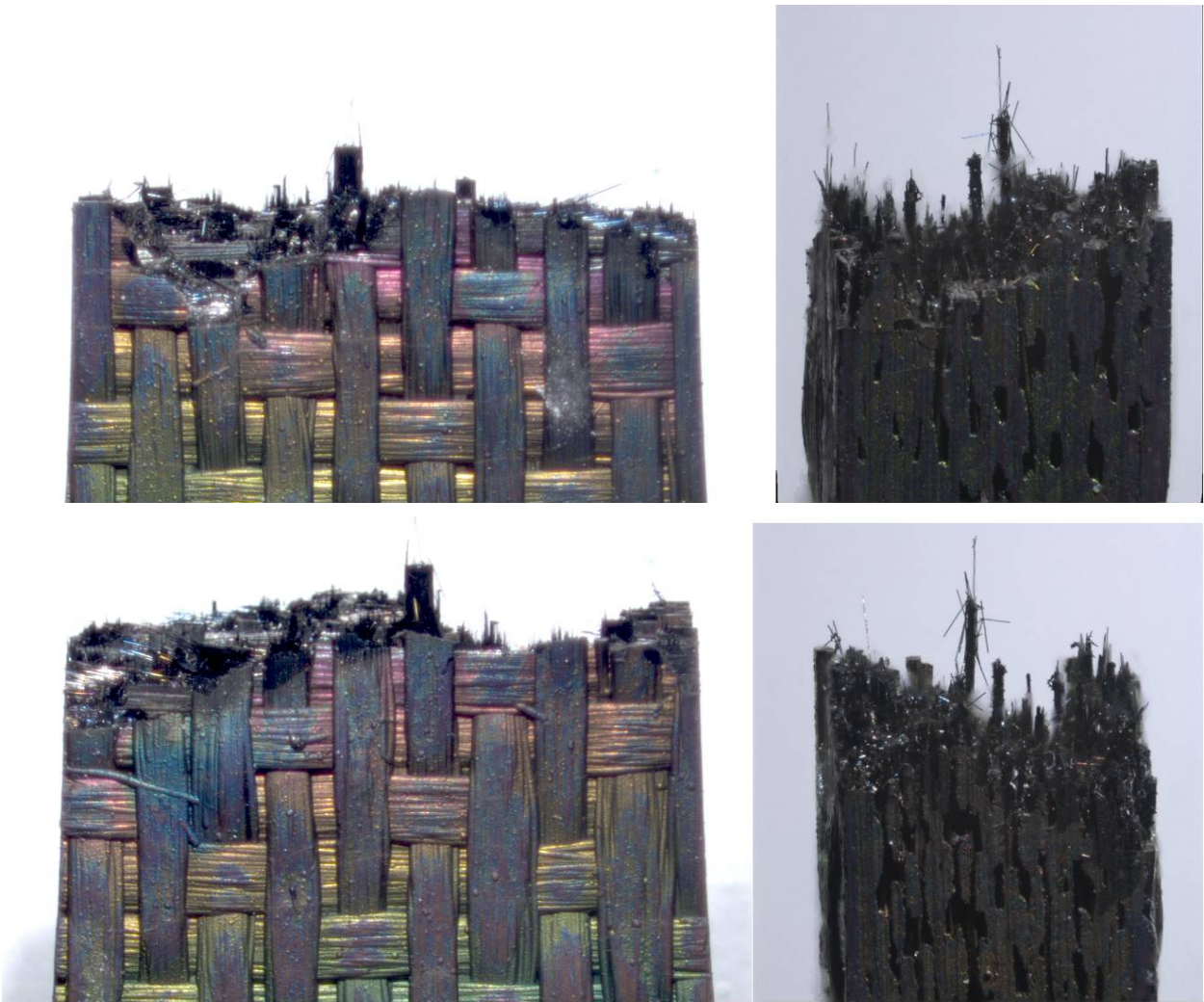
Figure 67: Optical micrographs of specimen P10-5 tested in fatigue at 1200°C in air. σ = 120 MPa, N_f =83799.

Figure 68: Optical micrographs of specimen P10-6 tested in fatigue at 1200°C in air. σ = 80 MPa, N_f =200000.
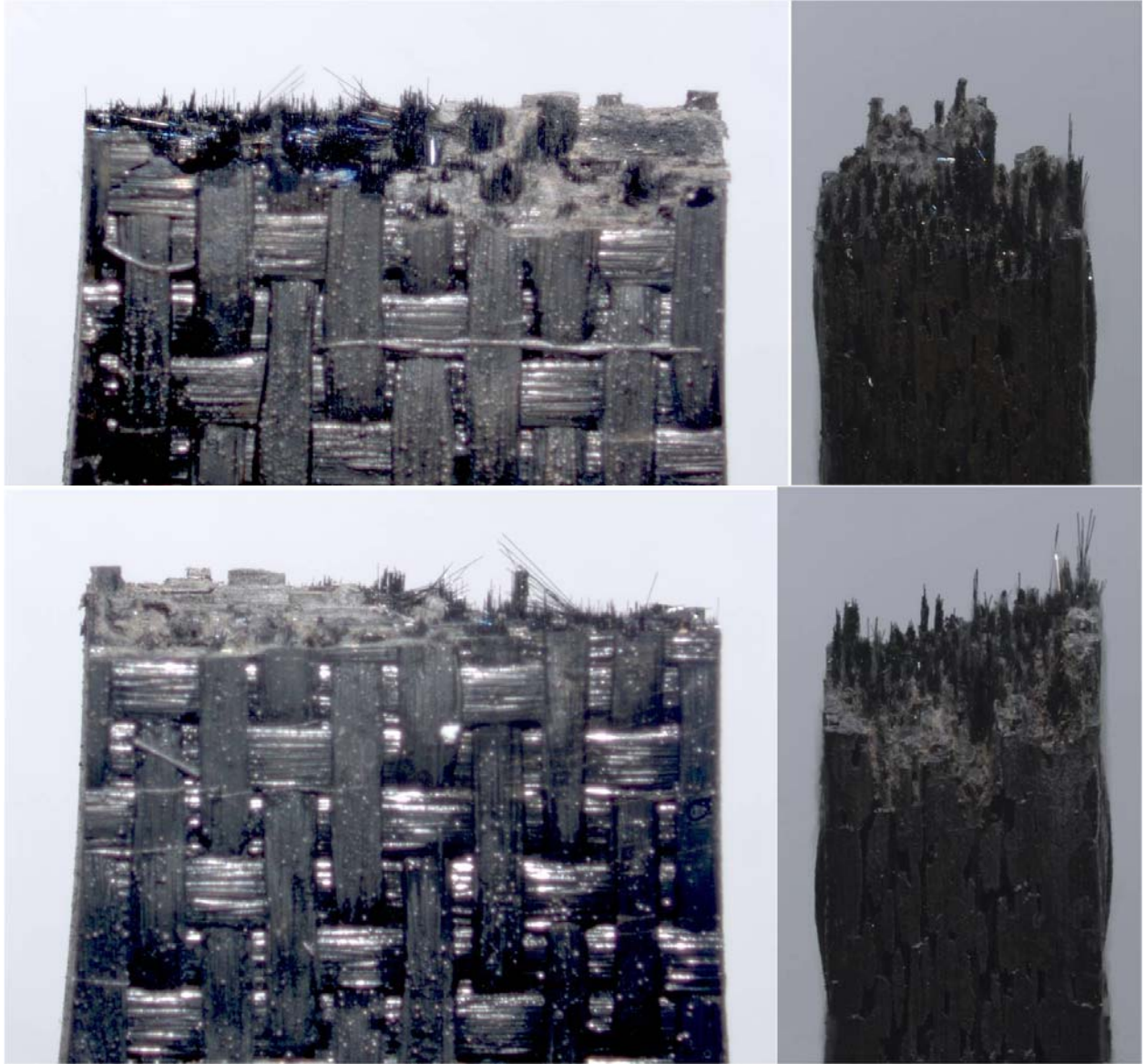
Figure 69: Optical micrographs of specimen P10-7 tested in fatigue at 1200°C in steam. σ = 100 MPa, N_f =144519.
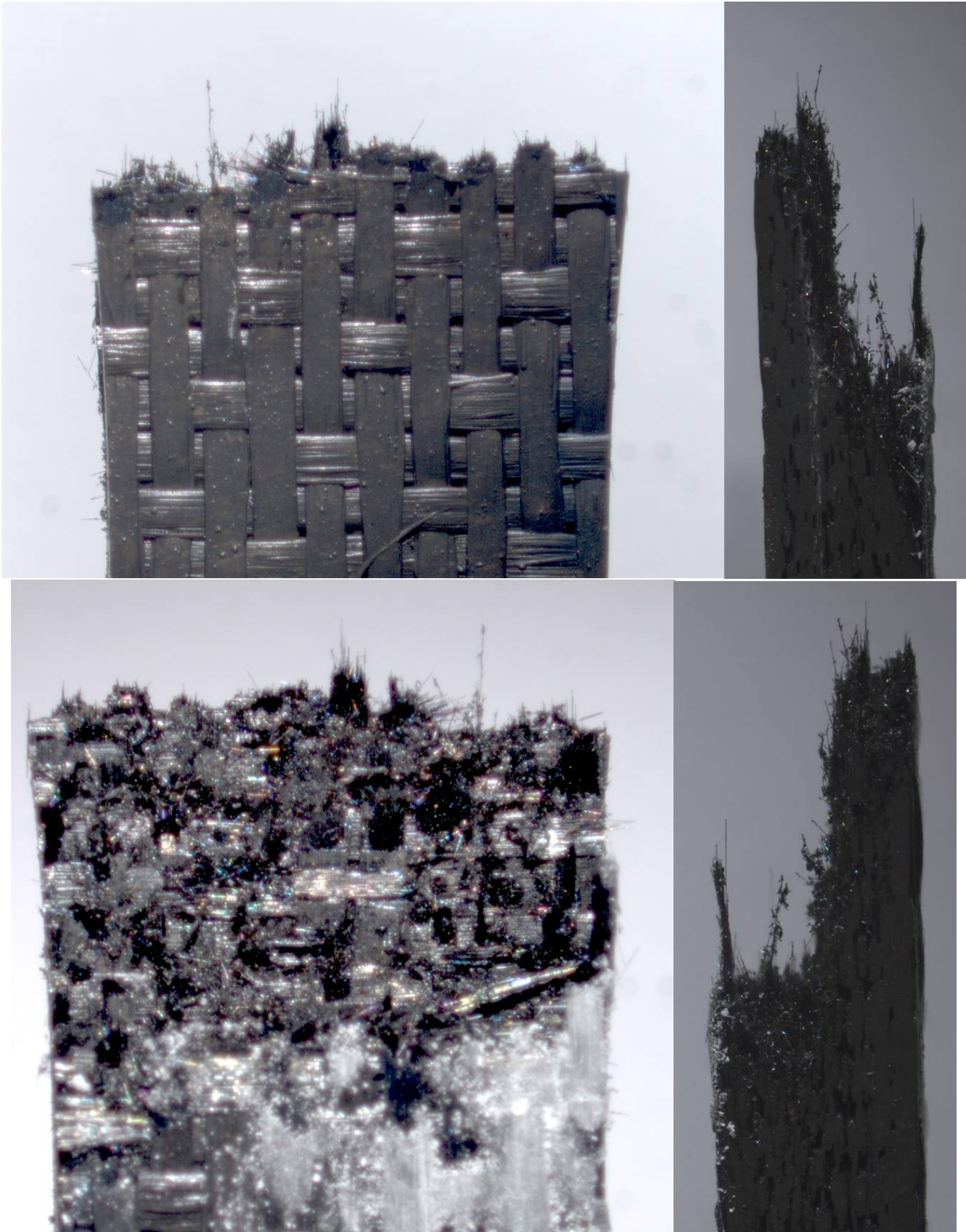
Figure 70: Optical micrographs of specimen P10-8 tested in tension at 1200°C in air. UTS = 391.9 MPa.
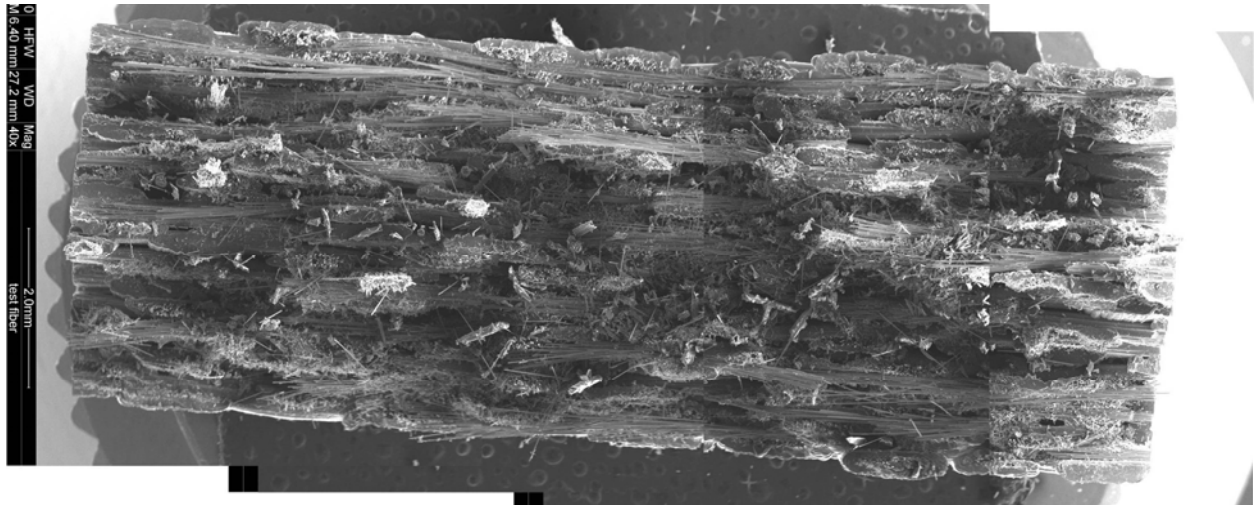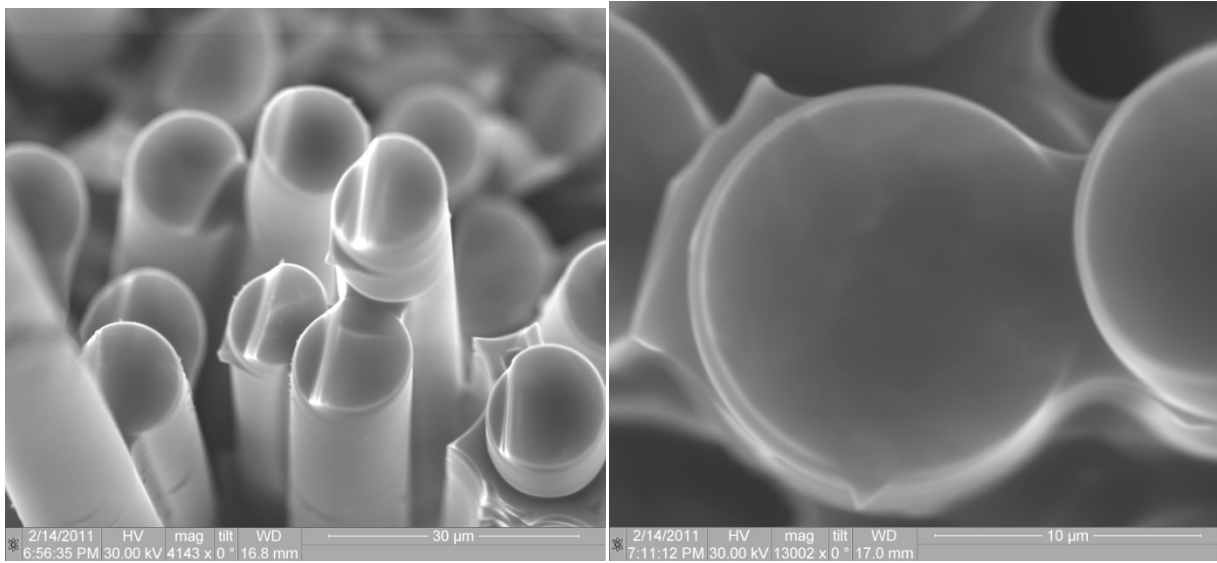
Appendix B
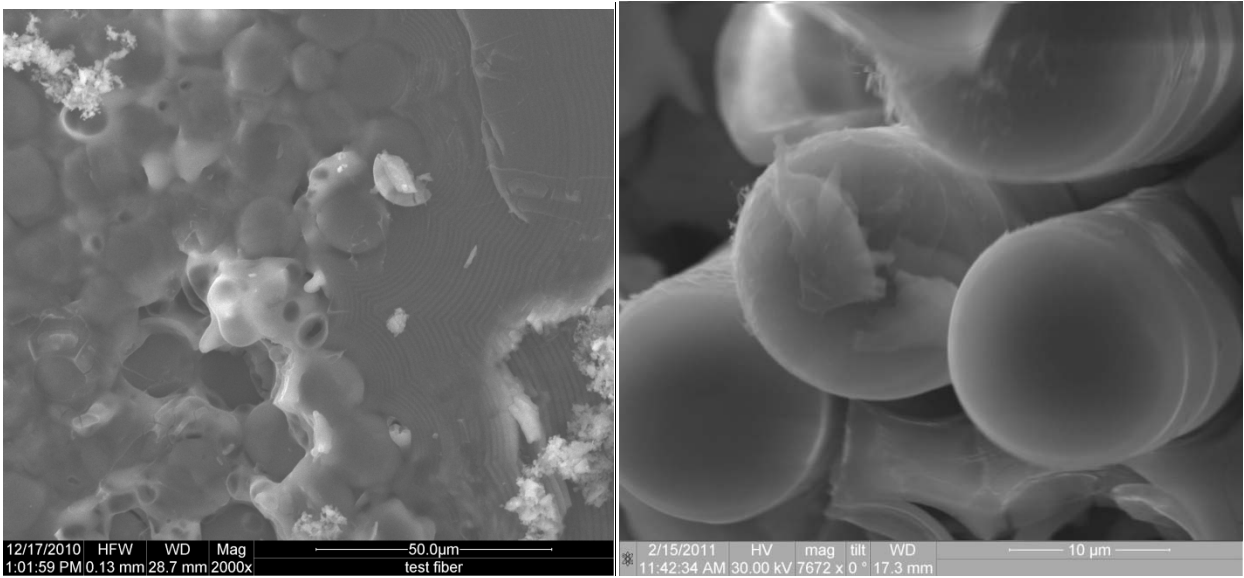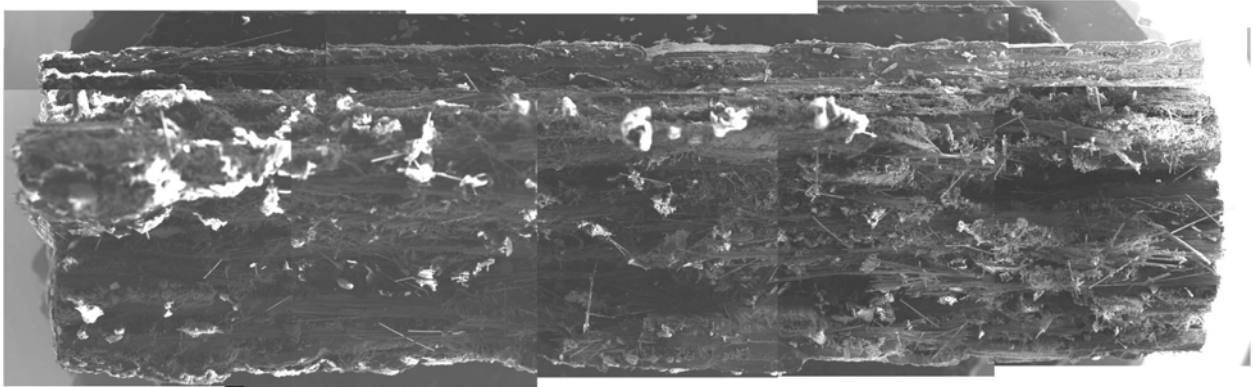
Figure 71: Scanning Electron Micrographs of specimen P5-2 tested in fatigue at 1200°C in steam. σ = 80 MPa, N_f =200000.
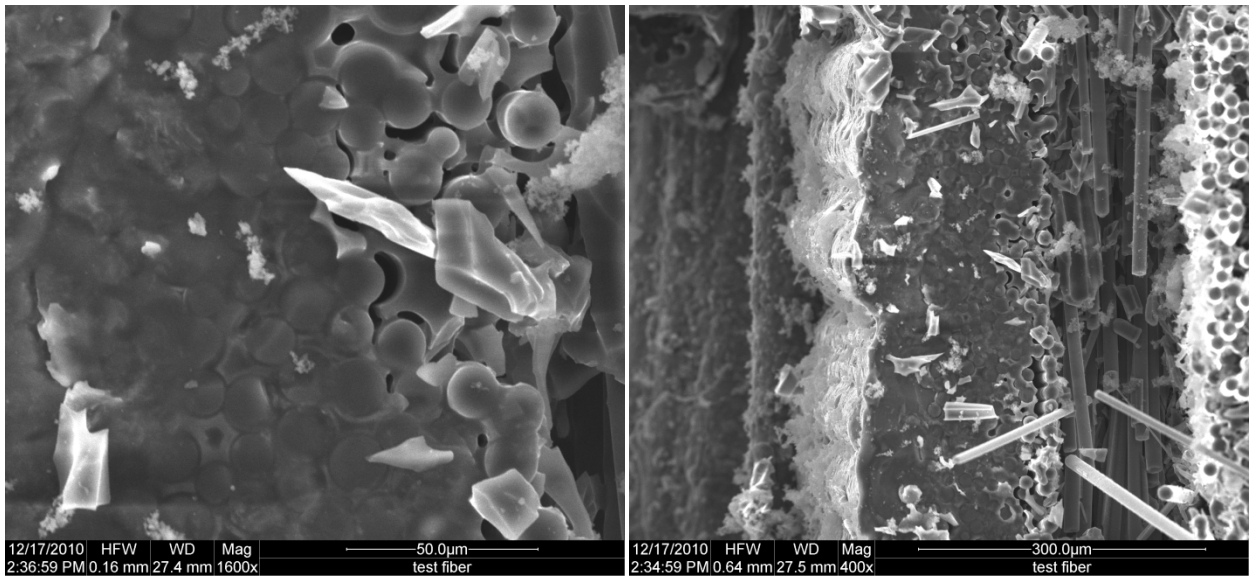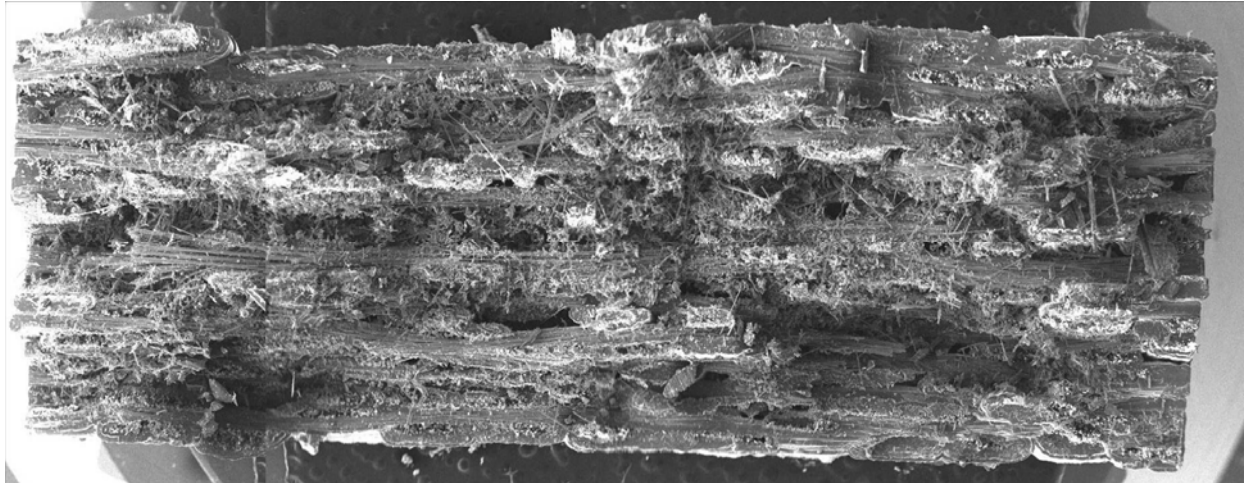
Figure 72: Scanning Electron Micrographs of specimen P5-3 tested in fatigue at 1200°C in air. σ = 160 MPa, N_f =29988.
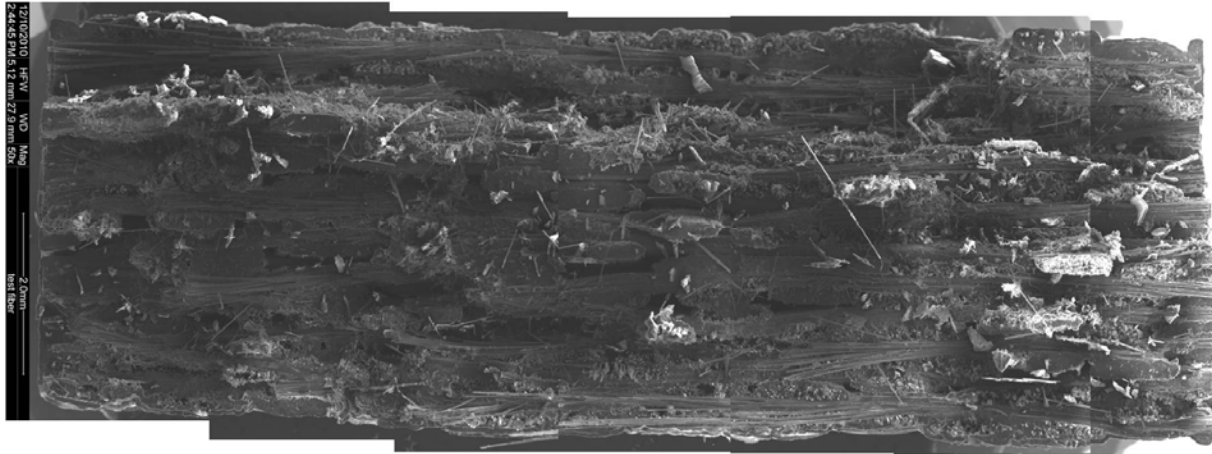
Figure 73: Scanning Electron Micrographs of specimen P5-4 tested in fatigue at 1200°C in steam. σ = 140 MPa, N_f =12784.
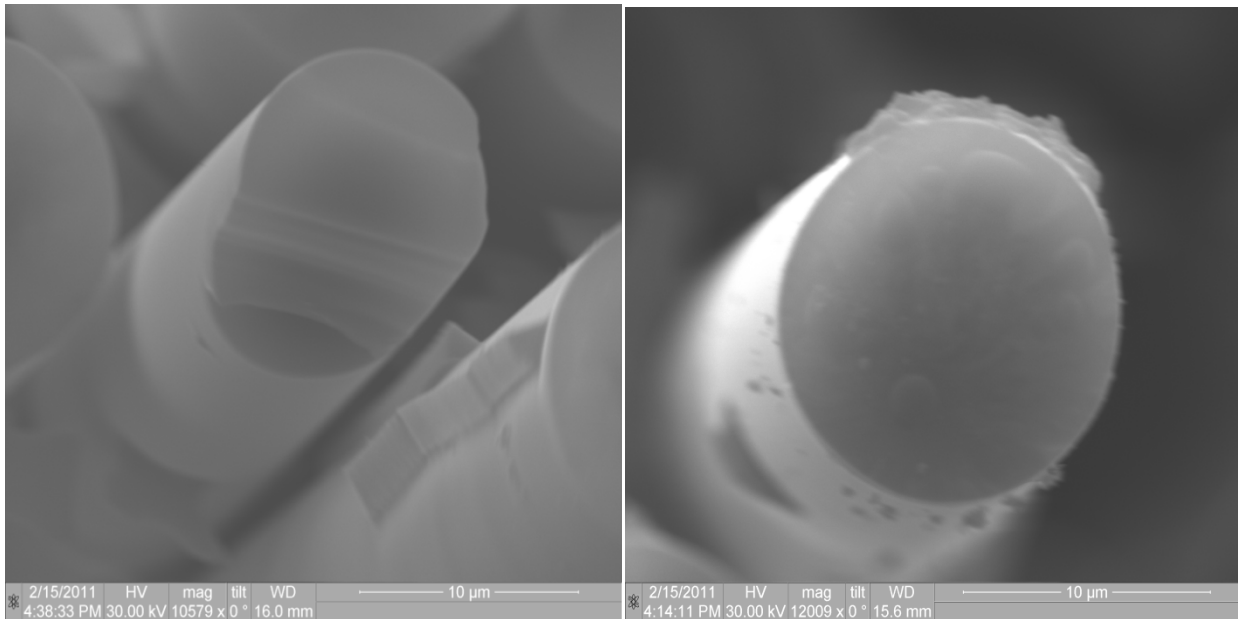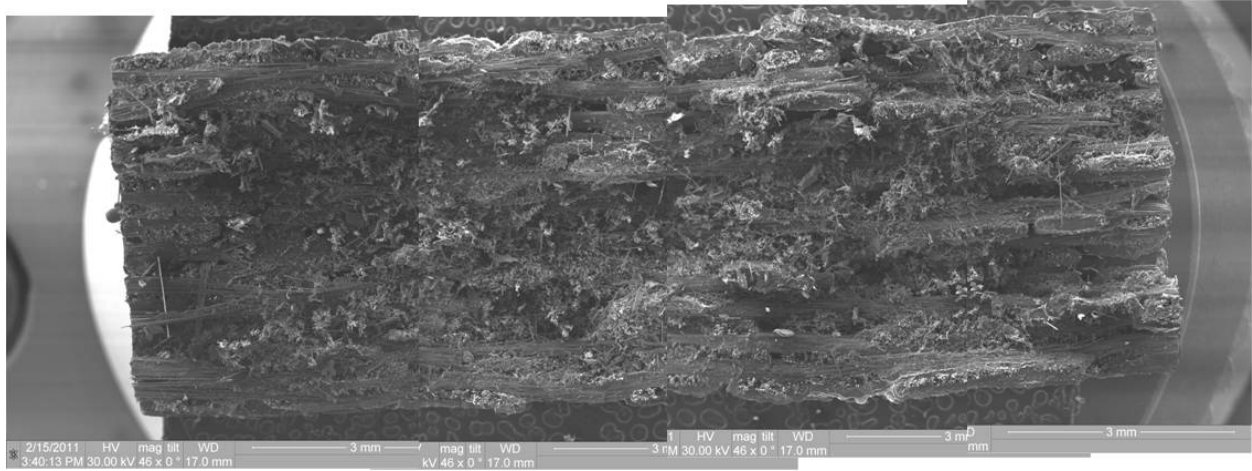
Figure 74: Scanning Electron Micrographs of specimen P5-5 tested in fatigue at 1200°C in steam. σ = 200 MPa, N_f =9612.
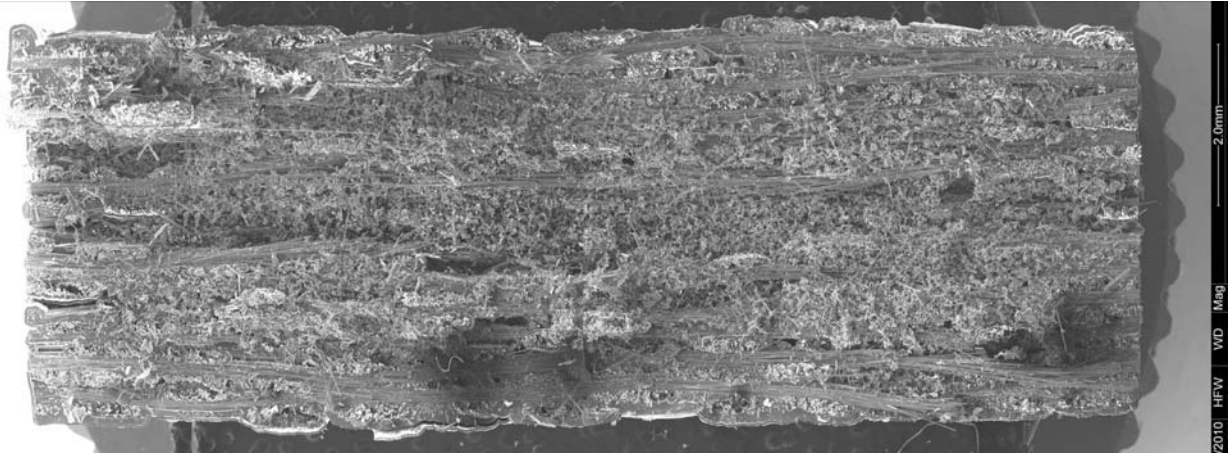
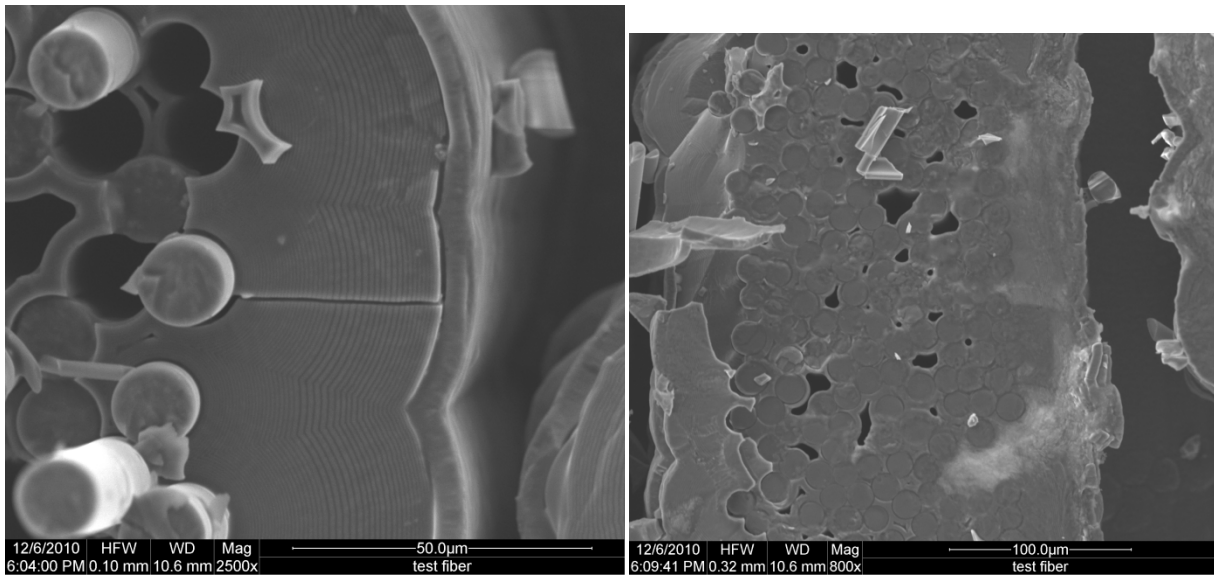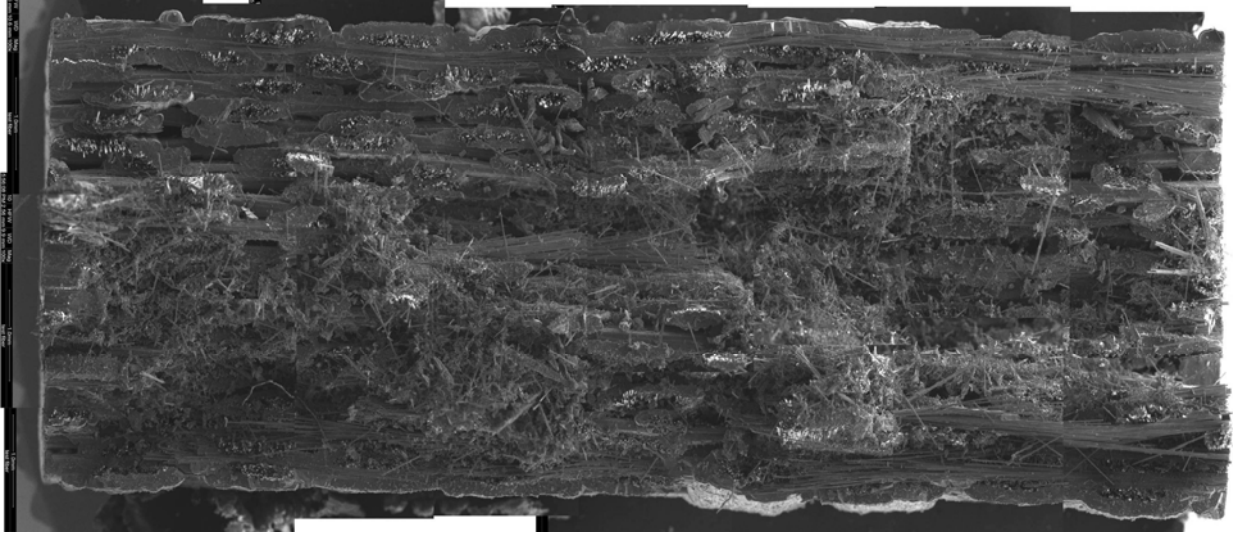**Figure 75: Scanning Electron Micrographs of specimen P5-7 tested in tension at 1200°C in air. UTS = 296.3 MPa.**

12/7/2010 | HFW | WD | Mag | 500.0µm
12:06:51 PM | 0.85 mm | 12.7 mm | 300x | test fiber

12/7/2010 | HFW | WD | Mag | 100.0µm
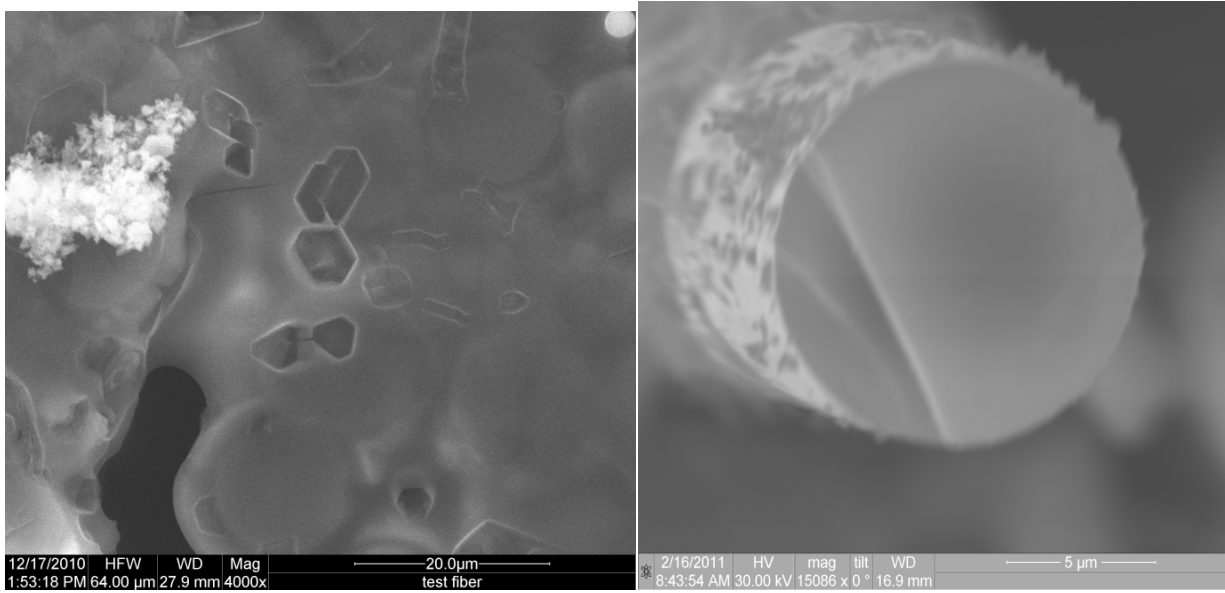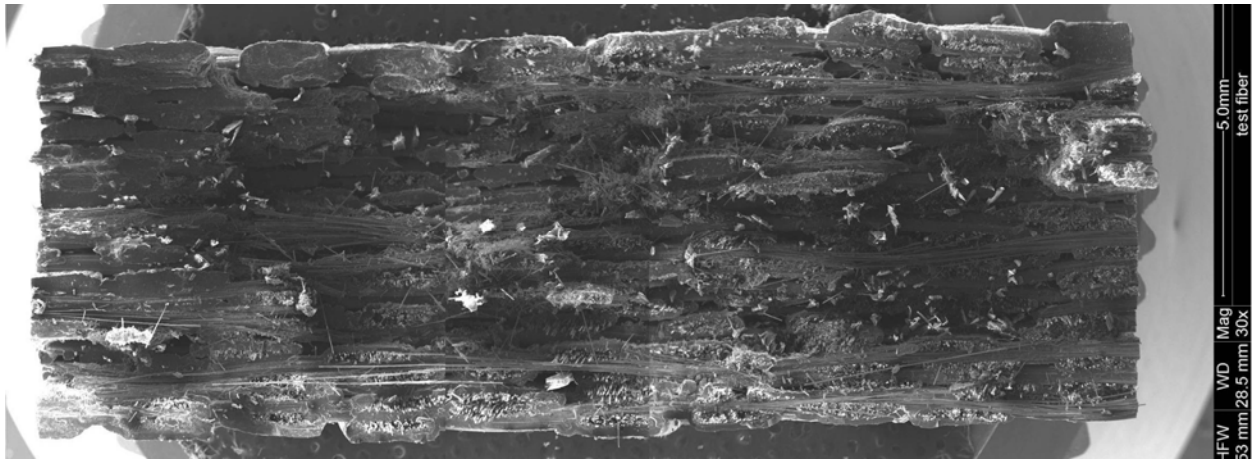12:04:00 PM | 0.21 mm | 12.8 mm | 1200x | test fiber
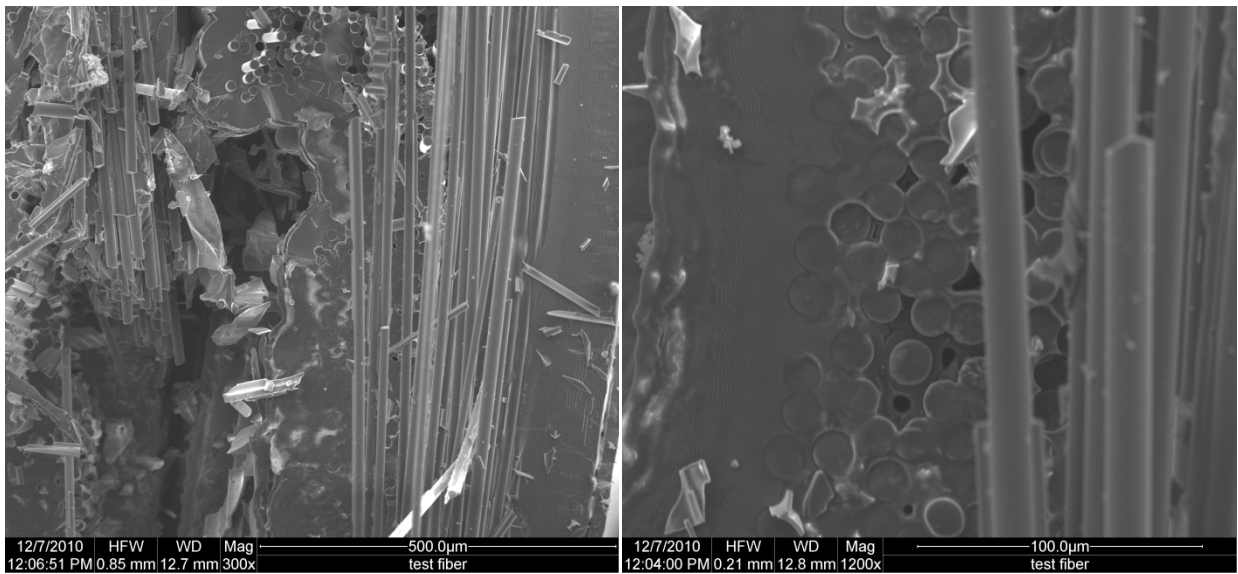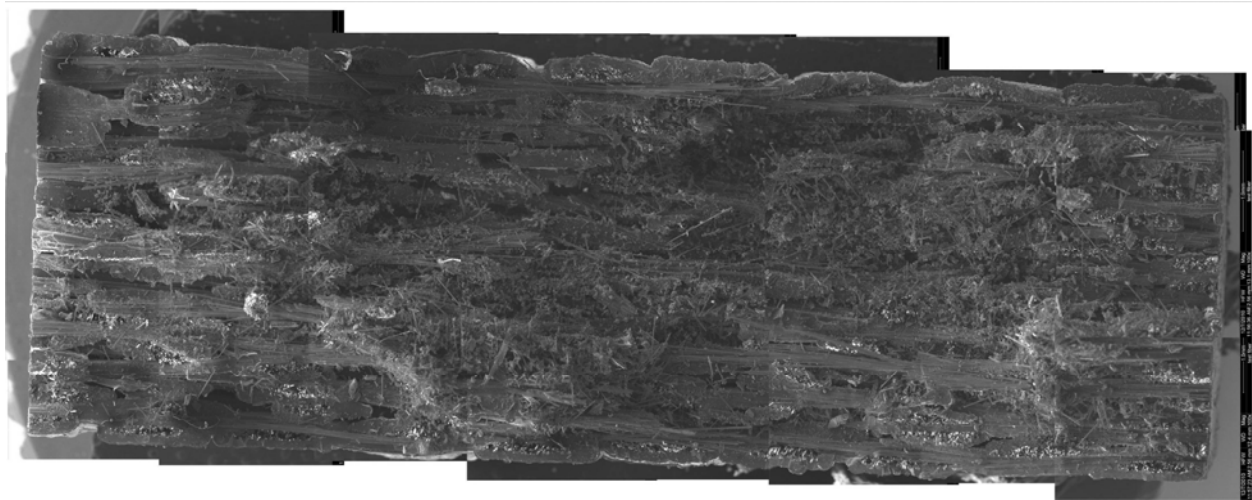
Figure 76: Scanning Electron Micrographs of specimen P7-1 tested in fatigue at 1200°C in air. σ = 160 MPa, N_f =6914.

12/10/2010 | HFW | WD | Mag | 20.0μm
3:25:43 PM | 85.33 μm | 23.8 mm | 3000x | test fiber

12/10/2010 | HFW | WD | Mag | 300.0μm
3:30:27 PM | 0.64 mm | 28.8 mm | 400x | test fiber
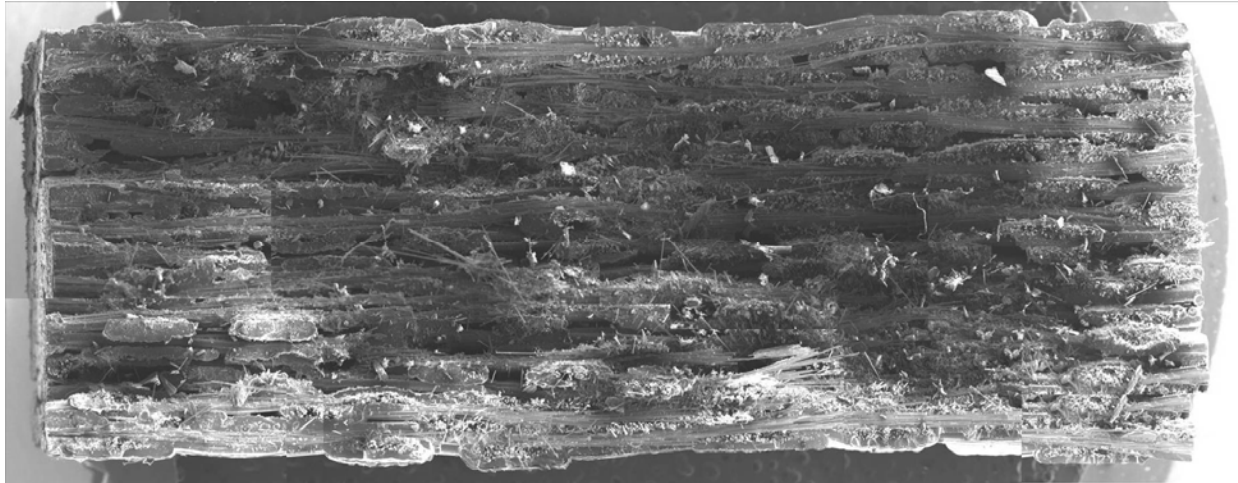
Figure 77: Scanning Electron Micrographs of specimen P7-2 tested in fatigue at 1200°C in steam. σ = 160 MPa, N_f =2214.
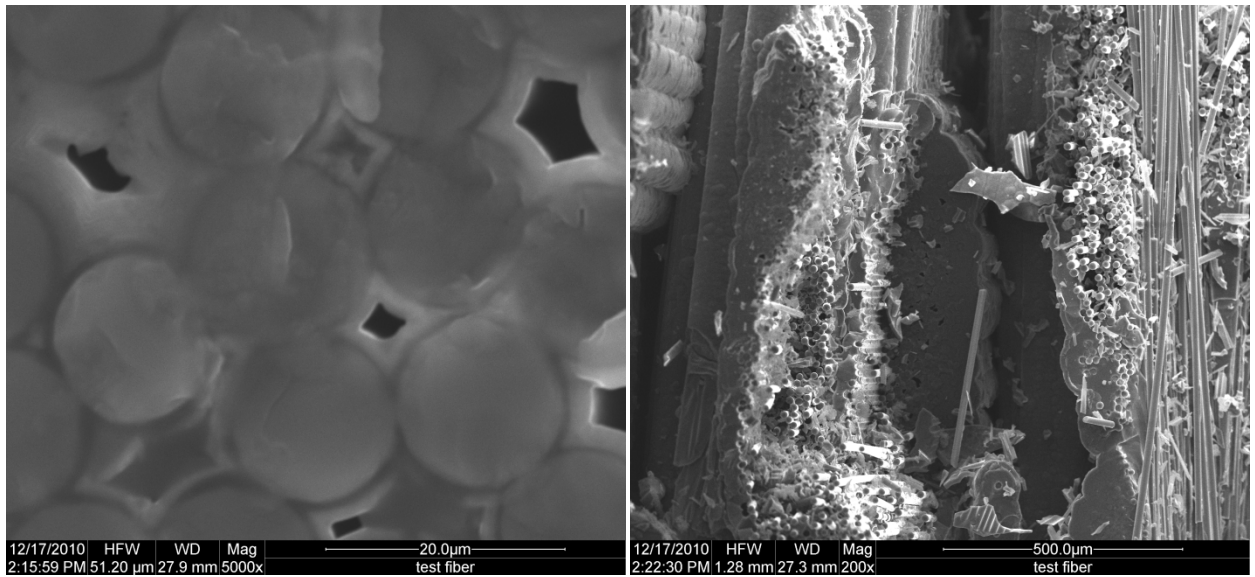
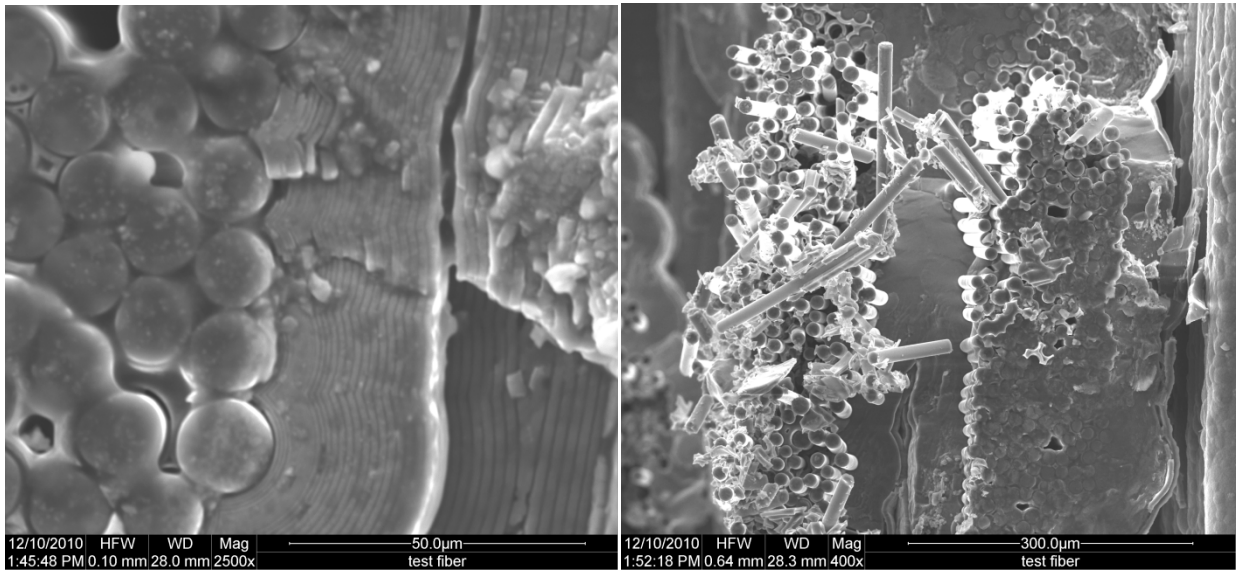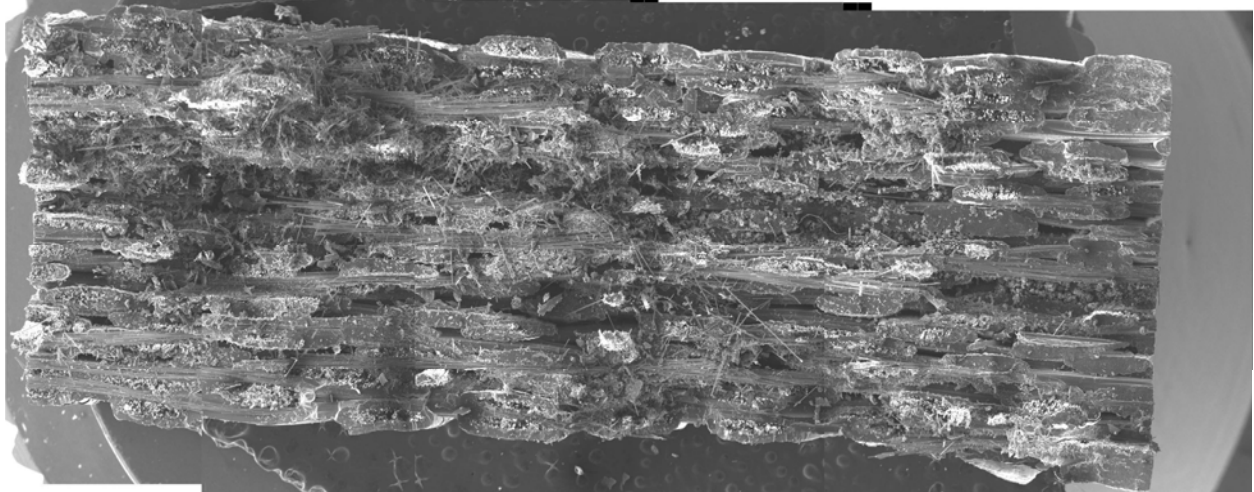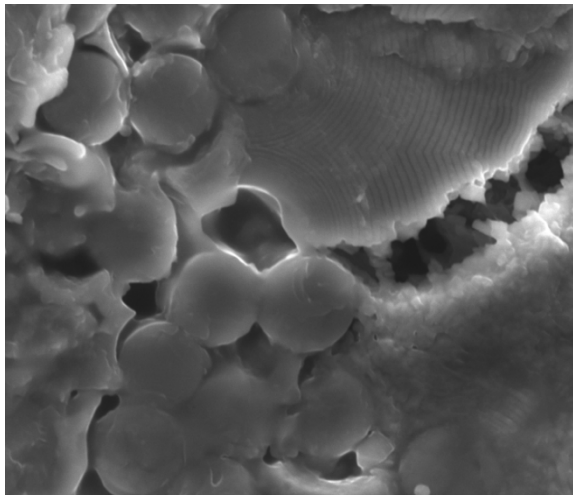**Figure 78: Scanning Electron Micrographs of specimen P7-4 tested in fatigue at 1200°C in steam. σ = 200 MPa, N_f =948.**
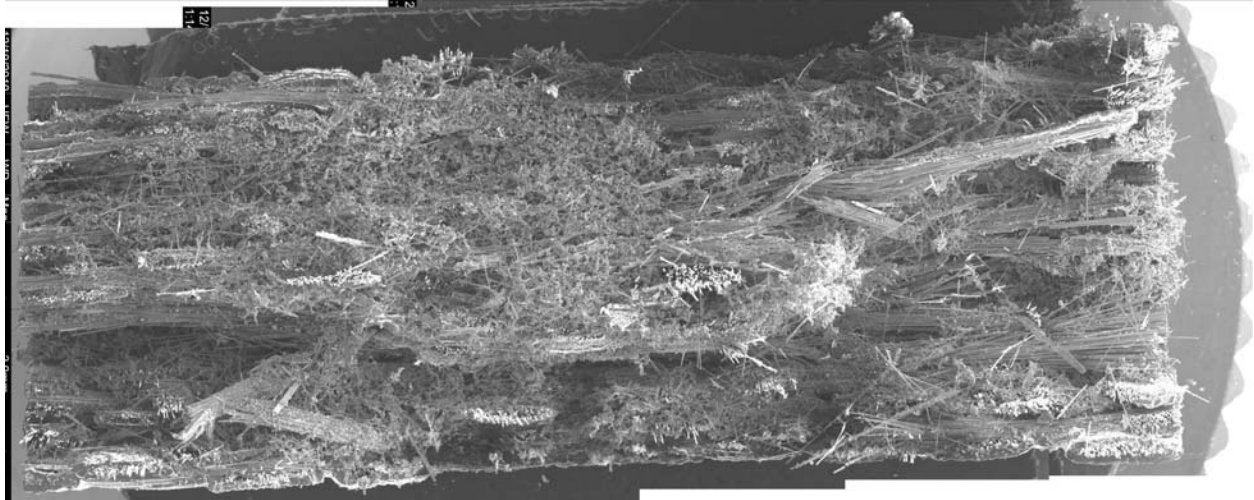
Figure 79: Scanning Electron Micrographs of specimen P7-7 tested in tension at 1200°C in air. UTS = 406.9 MPa.

Figure 80: Scanning Electron Micrographs of specimen P7-8 tested in fatigue at 1200°C in air. σ = 200 MPa, N_f =10656.

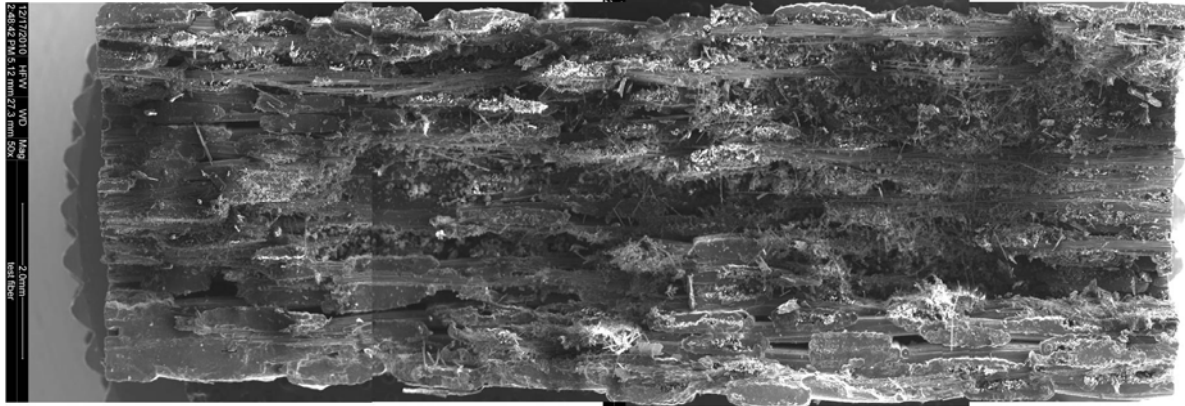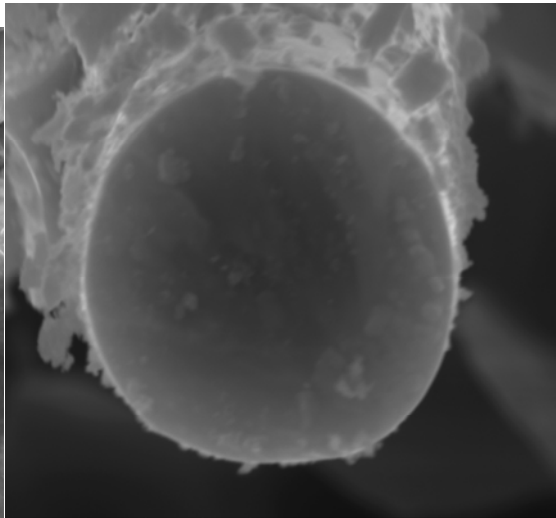**Figure 81: Scanning Electron Micrographs of specimen P10-1 tested in fatigue at 1200°C in steam. σ = 120 MPa, N_f =50499.**

Figure 82: Scanning Electron Micrographs of specimen P10-2 tested in fatigue at 1200°C in air. σ = 140 MPa, N_f =23277.
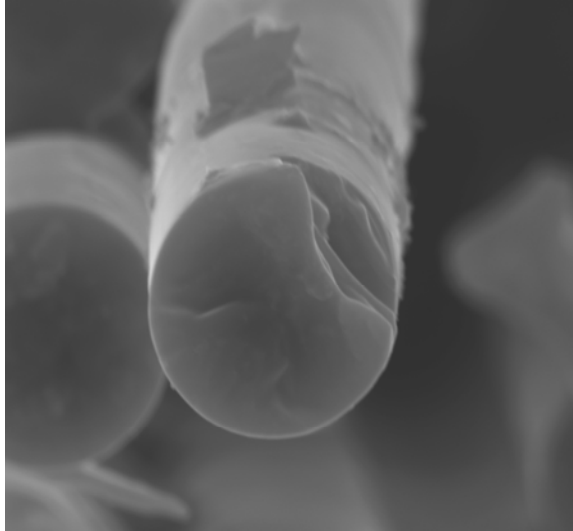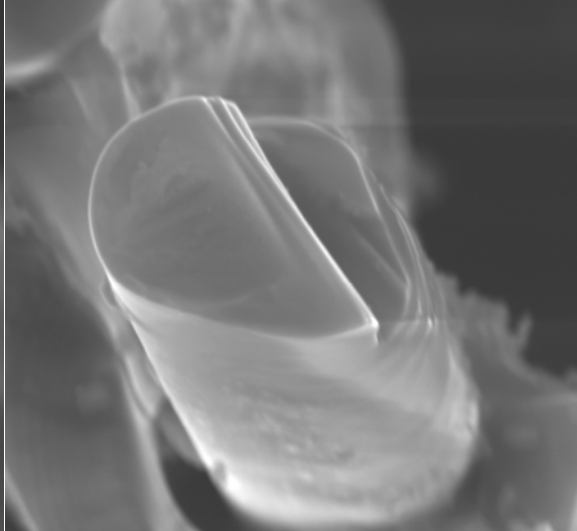
Figure 83: Scanning Electron Micrographs of specimen P10-3 tested in fatigue at 1200°C in air. σ = 100 MPa, N_f =161110.

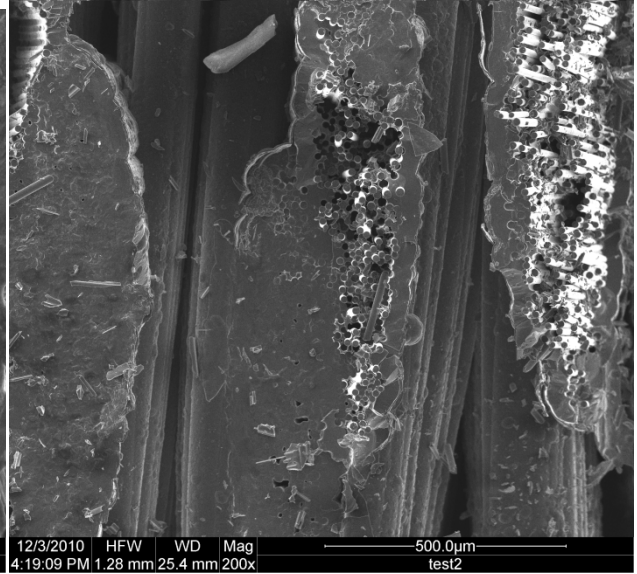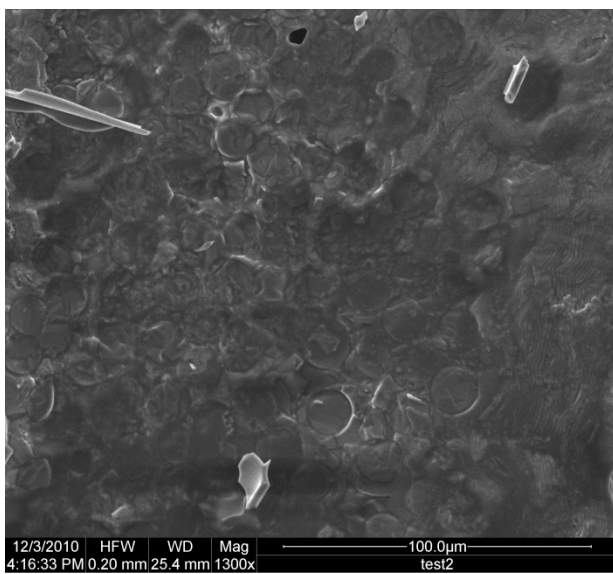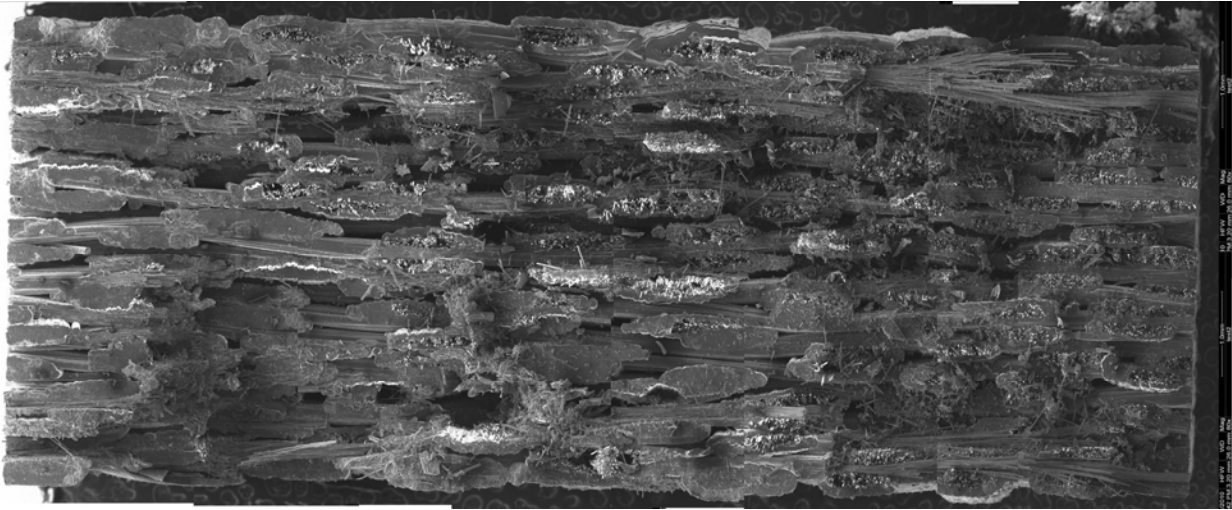**Figure 84: Scanning Electron Micrographs of specimen P10-5 tested in fatigue at 1200°C in air. σ = 120 MPa, N_f =83799.**
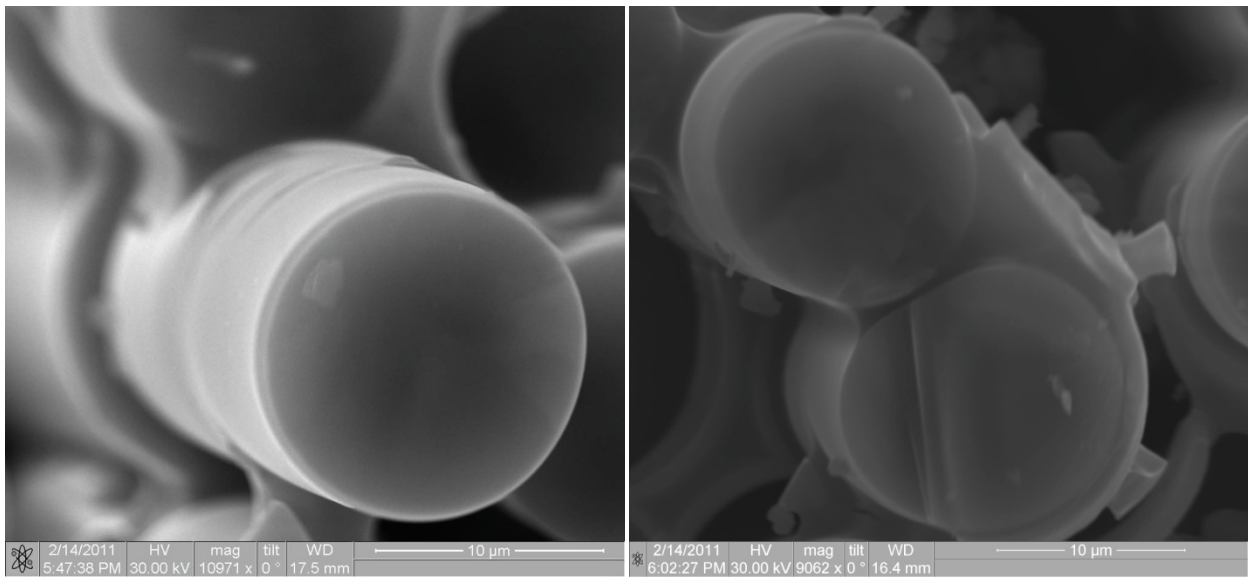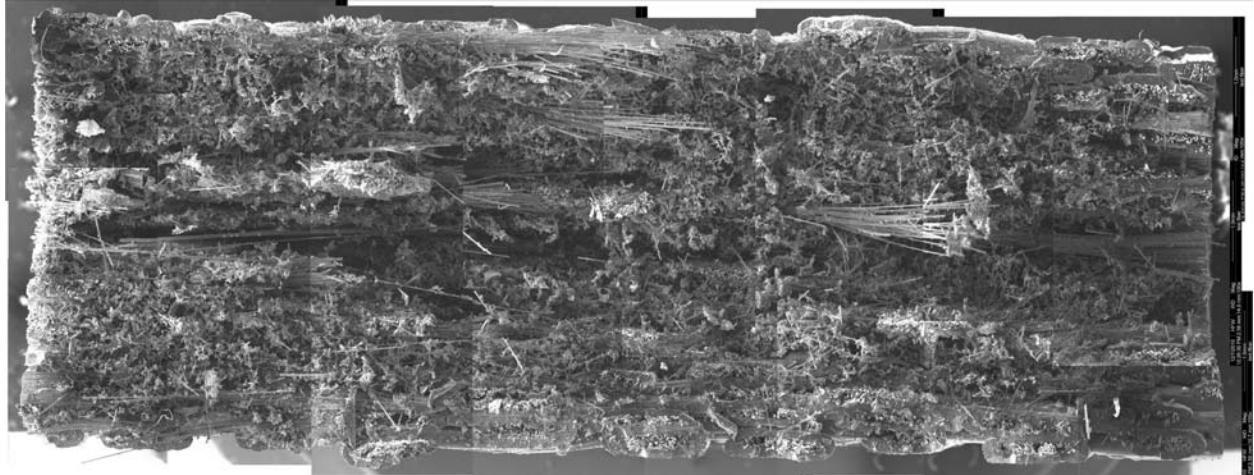
Figure 85: Scanning Electron Micrographs of specimen P10-6 tested in fatigue at 1200°C in air. σ = 80 MPa, N_f =200000.

Figure 86: Scanning Electron Micrographs of specimen P10-7 tested in fatigue at 1200°C in steam. σ = 100 MPa, N$_f$ =144519.

12/10/2010 | HFW | WD | Mag | 100.0µm
12:56:31 PM | 0.21 mm | 18.8 mm | 1200x | test fiber

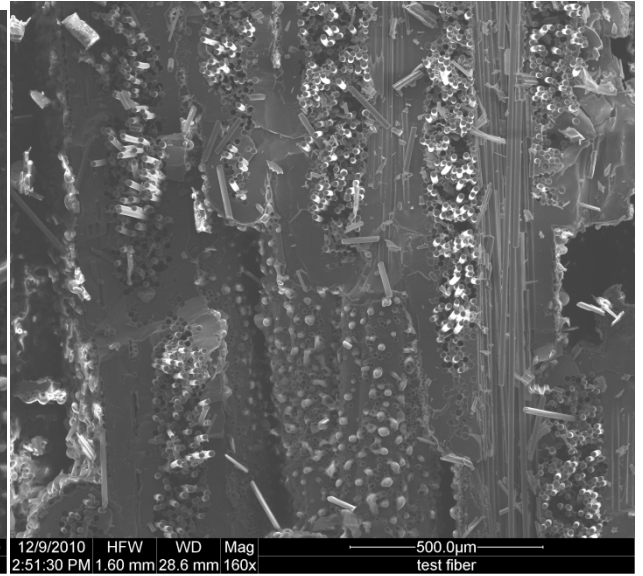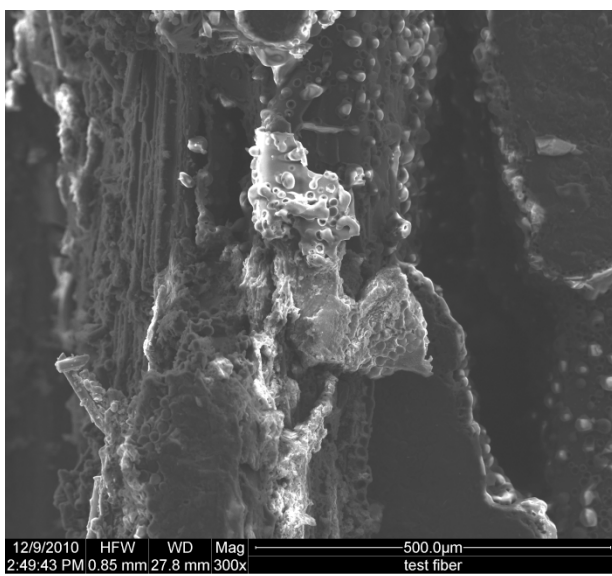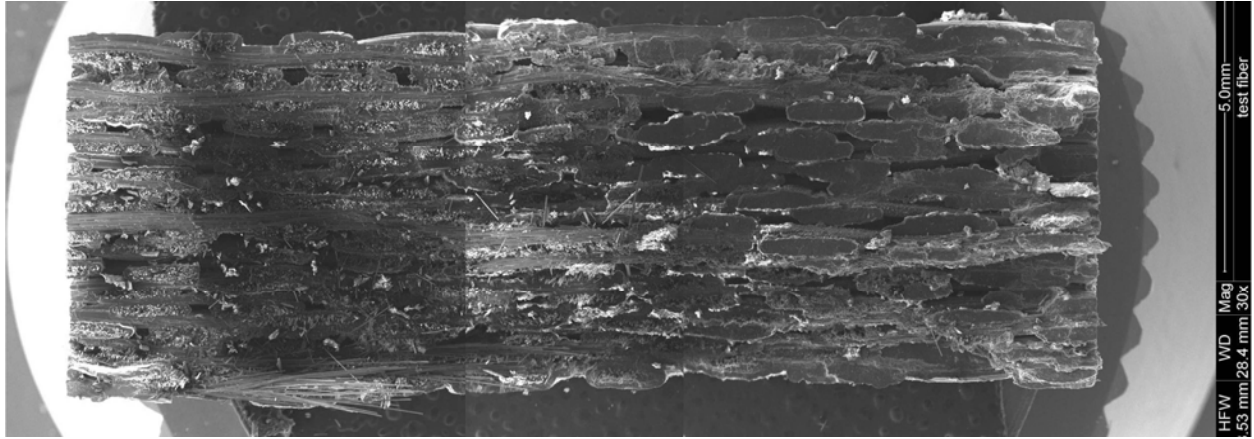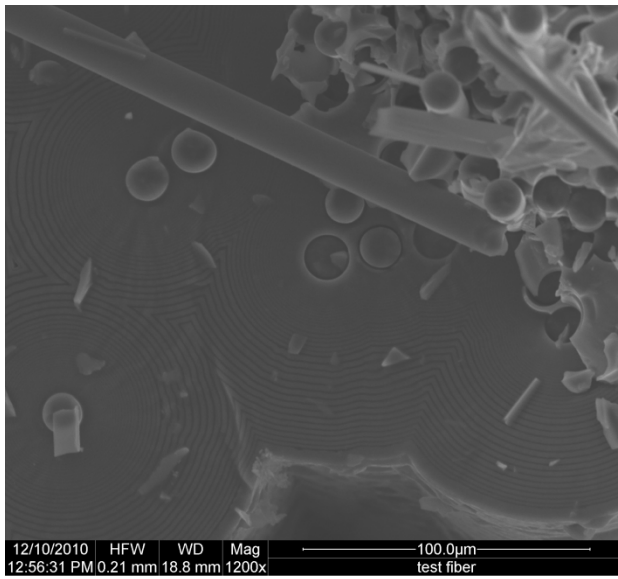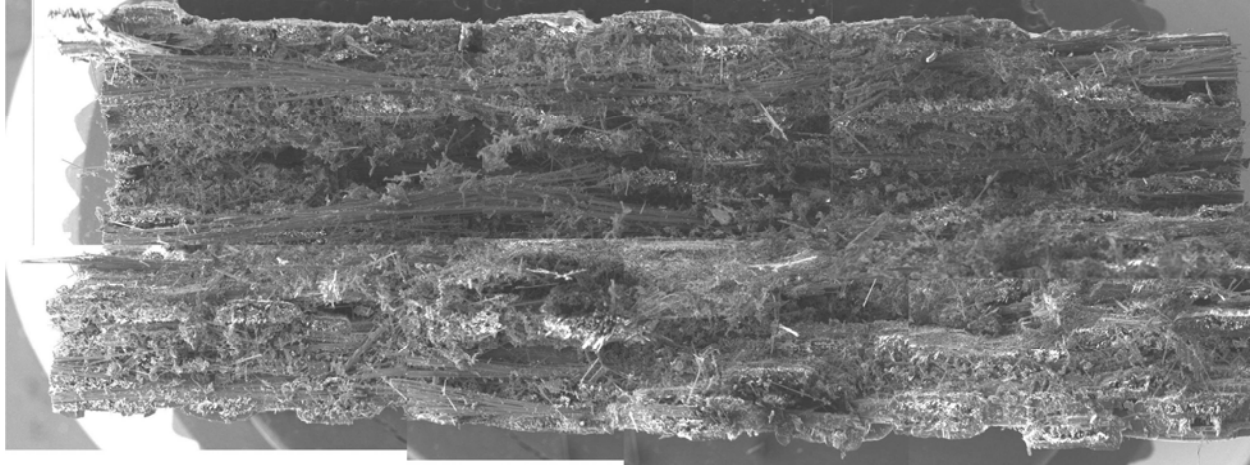**Figure 87: Scanning Electron Micrographs of specimen P10-8 tested in tension at 1200°C in air. UTS = 391.9 MPa.**

End of line.

Bibliography

1. AIAA Air Breathing Propulsion Technical Committee, *"The Versatile Affordable Advanced Turbine Engines (VAATE) Initiative."* American Institute of Aeronautics and Astronautics, January 2006.

2. Aveston, J., Cooper, G.A., and Kelly, A., *The properties of Fibre Composites, National Physical Laboratory Conference Proceedings*, IPC Science and Technology Press Ltd., Surry, England, 15-26 (1971).

3. Baker, A. A., "Composite Materials for Aircraft Structures" Second Edition. American Institute of Aeronautics and Astronautics, 2004.

4. Brewer D. HSR/EPM combustor materials development program. Master Sci Eng A 1999; A261:284-91.

5. Brewer D, Ojard G, Gibler M. *"Ceramic matrix composite combustor liner rig test."* ASME Turbo Expo 2000, Munich Germany, May 8-11, 2000 ASME Paper 2000-GT-0670.

6. Chawla, K. K. *Ceramic Matrix Composites.* Vol. Second Edition. Boston: Kluwer Acadmic Publishers, 2003.

7. Delapasse, Jacob. *"Fatigue Behavior of an Advanced SiC/SiC Composite with an Oxidation Inhibited Matrix at 1200°C in Air and Steam."* MS Thesis, AFIT/GAE/ENY/06-J05. School of Engineering and Management, Air Force Institue of Technology (AU), Wright-Patterson Air Force Base, OH, March 2010.

8. Hill, Philip and Peterson, Carl *Mechanics and Thermodynamics of Propulsion* Second Edition. Addison-Wesley Publishing Company, 1992.

9. Howe, R. J. and Owen, M. J., "Cumulative Damage in Chopped Strand Mat/Polyester Resin Laminates," 8th International R. P. Conference, British Plastics Federation, Brighton, Oct 1972: Paper 21.

10. J.M. Corum et al., Durability-Based Design Properties of Reference Crossply Carbon-Fiber Composite, ORNL/TM-200/322, Oak Ridge National Laboratory, Oak Ridge, Tenn., April 2001.

11. Knauf, Michael, *"Fatigue Behavior of a SiC/SiC Composite at 1000°C in Air and Steam."* MS Thesis, AFIT/GAE/ENY/10-D01. School of Engineering and Management, Air Force Institue of Technology (AU), Wright-Patterson Air Force Base, OH, December 2010.

12. Mall, S. and Weidenaar, W.A. *"Tension-compression fatigue behavior of fibre-reinforced ceramic matrix composite with circular hole."* Composites: 26, 1995: 631-636.

13. Mazdiyasni, K.S., "Fiber Reinforced Ceramic Composites." Park Ridge, New Jersey: Noyes Publications, 1990.

14. McNulty JC, He MY, Zok FW. *"Notch sensitivity of fatigue life in a SylramicTM/SiC composite at elevated temperature."* Composites Science and Technology 2004;64:155-170.

15. More KL, Tortorelli PF, Feber MK, Keiser JR. *"Observations of accelerated silicon carbide recession by oxidation at high water-vapor pressures."* J Am Cer Soc 2000; 83(1):211-213.

16. Ogata, Takashi, "Life Prediction Method of CC and DS Ni Base Superalloys Under High Temperature Biaxial Fatigue Loading." Journal of Engineering for Gas Turbines and Power: Vol 132, November 2010.

17. Ohnabe, H., S. Masaki, M. Onozuka, K. Muyahara, and T. Sasa. "Potential Applications of Cermic Matrix Compsites to Aero-engine Components." *Composites: Part A, 30*, 1999: 489-496.

18. Owen, MJ and Smith, T.R. "Plastics and Polymers." Vol. 36, Feb. 1968: 33-44

19. Rotem, A., Nelson, H.G. "Failure of a Laminated Composite Under Tension-Compression Fatigue Loading." *Composites Science and Technology* 36, 1989: 45-62.

20. Ruggles-Wrenn, M.B., Christensen, D.T., Chamberlain, A., Lane, J., Cook, T., *"Effect of frequency and envirionment on fatigue behavior of a CVI SiC/SiC ceramic matrix composite at 1200°C."* Composites Science and Technology 2010; doi: 10.1016/jcompscitech.2010.11.008.

21. Schmidt, S., H. Knabe, H. Immich, R. Mestring, and A. Gessler. "Advanced Ceramic Matrix Composite Material fo Current and Future Propulsion Technology Applications." *Acta Astronautica, 55*, 2004: 409-420.

REPORT DOCUMENTATION PAGE

Form Approved
OMB No. 0704–0188

1. REPORT DATE (DD–MM–YYYY)	2. REPORT TYPE	3. DATES COVERED (From — To)
24 03 2011	Master's Thesis	SEP 09 – MAR 11

4. TITLE AND SUBTITLE
Tension-Compression Fatigue of Hi-Nicalon/SiC Ceramic Matrix Composite at 1200°C in Air and Steam

5a. CONTRACT NUMBER

5b. GRANT NUMBER

5c. PROGRAM ELEMENT NUMBER

6. AUTHOR(S)

Jones, Tyler P.

5d. PROJECT NUMBER

5e. TASK NUMBER

5f. WORK UNIT NUMBER

7. PERFORMING ORGANIZATION NAME(S) AND ADDRESS(ES)
Air Force Institute of Technology
Graduate School of Engineering and Management (AFIT/ENY)
2950 Hobson Way
WPAFB OH 45433-7765

8. PERFORMING ORGANIZATION REPORT NUMBER

AFIT/GA/ENY/11-M09

9. SPONSORING / MONITORING AGENCY NAME(S) AND ADDRESS(ES)

This space intentionally left blank

10. SPONSOR/MONITOR'S ACRONYM(S)

11. SPONSOR/MONITOR'S REPORT NUMBER(S)

12. DISTRIBUTION / AVAILABILITY STATEMENT
APPROVED FOR PUBLIC RELEASE; DISTRIBUTION UNLIMITED

13. SUPPLEMENTARY NOTES
This material is declared the work of the U.S. Government and is not subject to copyright protection in the United States

14. ABSTRACT
The tension-compression fatigue of a Hi-Nicalon /Silicon Carbide ceramic matrix composite (CMC) was studied at 1200°C in laboratory air and in steam environment. The CMC investigated in this effort consisted of an oxidation inhibited HyprSiC matrix reinforced with laminated woven Hi-Nicalon fibers. Fiber preforms had pyrolytic carbon fiber coating with boron carbide overlay applied were then densified with the HyprSiC oxidation inhibited matrix through chemical vapor infiltration (CVI). The tensile stress-strain behavior was evaluated and the tensile properties measured at 1200°C. Tension-compression fatigue tests were conducted at a frequency of 1.0 Hz with a ratio of minimum stress to maximum stress of R = -1.0. Tension-compression fatigue behavior was studied for fatigue stresses ranging from 80 to 300 MPa in air and in steam. Fatigue run-out was defined as 2×10^5 cycles. Fatigue limit (based on a run-out condition of 2×10^5 cycles) was 80 MPa in air and in steam. The presence of steam decreased the fatigue life of specimens tested above the fatigue limit. Specimens that achieved fatigue run-out were subjected to tensile tests to failure to characterize the retained tensile properties. The material retained 100% of its tensile strength. Reduction in tensile modulus was 68% while the change in compressive modulus was negligible.

15. SUBJECT TERMS
Ceramic matrix composite, fatigue, tension, compression, steam, HyprSiC, high temperature

16. SECURITY CLASSIFICATION OF:			17. LIMITATION OF ABSTRACT	18. NUMBER OF PAGES	19a. NAME OF RESPONSIBLE PERSON
a. REPORT	b. ABSTRACT	c. THIS PAGE	UU	118	Dr. Marina Ruggles-Wrenn
U	U	U			19b. TELEPHONE NUMBER (Include Area Code) (937)255-3636, ext 4641 Email: marina.ruggles-wrenn@afit.edu

Standard Form 298 (Rev. 8–98)
Prescribed by ANSI Std. Z39.18